

# Advanced BroScience

---

Investigating Lifting Technique with Trajectory Optimization



Presented by:  
Liyana Singh

Prepared for:  
Dr Stacey Shield  
Dept. of Electrical and Electronics Engineering  
University of Cape Town

Submitted to the Department of Electrical Engineering at the University of Cape Town  
in partial fulfilment of the academic requirements for a Bachelor of Science degree in  
Mechatronics

**October 27, 2025**



## Declaration

---

1. I know that plagiarism is wrong. Plagiarism is to use another's work and pretend that it is one's own.
2. I have used the IEEE convention for citation and referencing. Each contribution to, and quotation in, this report from the work(s) of other people has been attributed, and has been cited and referenced. Any section taken from an internet source has been referenced to that source.
3. This report is my own work, and is in my own words (except where I have attributed it to others).
4. **I have not paid a third party to complete my work on my behalf. My use of artificial intelligence software has been limited to none.**
5. I have not allowed and will not allow anyone to copy my work with the intention of passing it off as his or her own work.
6. I acknowledge that copying someone else's assignment or essay, or part of it, is wrong, and declare that this is my own work.



Signed:

Word Count: 13 927

## Acknowledgments

---

I would like to express my deepest gratitude to my supervisor, Dr. Stacey Shield, for her guidance, expertise, and unwavering passion for bioengineering. Her enthusiasm and insight were a constant source of inspiration and played a vital role in shaping this project.

To my family, thank you for your endless love and belief in me. You have always made me feel that I could achieve anything and the only reason I truly can is because of your support. A special thank you to my mom, my greatest role model, whose strength and kindness guide me in everything I do.

To my best friends, Alexa and Kiyura, thank you for always being there for me, even from across the country. Your encouragement and love kept me grounded through every stressful moment.

To the UCT Tour Guides, thank you for keeping me smiling through all the late-night lab sessions. My university experience has been filled with so much laughter, support, and love because of you. I truly couldn't have done this degree without you.

Lastly, to my cats, KitKat and Chai, for keeping me company through countless hours of coding at the dining room table. As shown in Figure 1, KitKat took his role as research assistant very seriously, overseeing the animation of the planar 3DoF arm motion with great dedication.

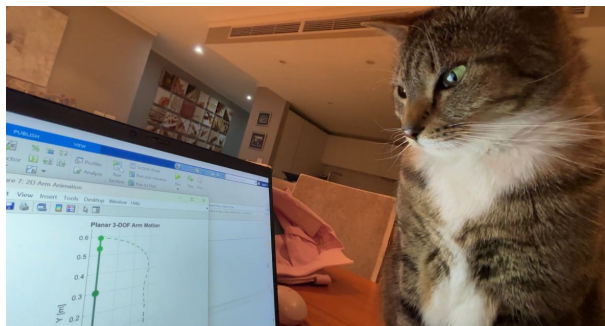


Figure 1: KitKat overseeing the animation of the planar 3DoF arm motion.

## Abstract

---

This study investigates how joint conditions and anthropometric factors influence optimal bench press technique, focusing on bar path and grip width. A trajectory optimisation framework was developed and applied to biomechanical models of increasing complexity to identify movement strategies that minimise joint torque. Two-dimensional (Stage 1) and three-dimensional (Stage 2) models were designed and validated through a series of tests addressing four key research questions related to shoulder and elbow protection, grip width, and brachial index.

Results showed that protecting the shoulder produced a J-shaped bar path, while protecting the elbow led to a straighter path. Grip width adapted accordingly, narrower when prioritising shoulder protection and wider when protecting the elbow. Variations in brachial index affected joint effort but not bar path shape, with longer upper arms requiring higher torque for the same movement. A narrow grip width was found to be optimal for larger brachial indices, while a wider grip width was optimal for smaller brachial indices. These findings align with existing literature and confirm the reliability of the developed optimisation framework.

A final case study demonstrated the model's clinical relevance, showing how individual anatomy and joint condition influence optimal bench press form. The framework provides a foundation for personalised exercise analysis and potential applications in sports science, rehabilitation, and intelligent gym equipment design. Recommendations include extending the skeletal model to four degrees of freedom, integrating muscle dynamics, and expanding the research to other upper-body exercises.

# Contents

<b>1</b>	<b>Introduction</b>	<b>1</b>
1.1	Background to the study . . . . .	1
1.2	Objectives of this study . . . . .	1
1.2.1	Problems to be investigated . . . . .	1
1.2.2	Purpose of the study . . . . .	1
1.3	Scope and Limitations . . . . .	2
1.4	Plan of development . . . . .	2
<b>2</b>	<b>Literature Review</b>	<b>3</b>
2.1	Introduction . . . . .	3
2.2	Fundamentals of the Bench Press . . . . .	4
2.3	Variables Influencing Bench Press Biomechanics . . . . .	5
2.3.1	Lifting Speed . . . . .	5
2.3.2	Bar Path . . . . .	5
2.3.3	Grip Width . . . . .	6

2.3.4	Elbow Flare Angle . . . . .	6
2.3.5	Body Proportions . . . . .	6
2.4	Biomechanical Modelling of the Human Body . . . . .	7
2.4.1	Skeletal Model . . . . .	7
2.4.2	Musculoskeletal Model . . . . .	8
2.4.3	Available Software Models . . . . .	9
2.5	Trajectory Optimization in Resistance Training . . . . .	9
2.5.1	Background . . . . .	9
2.5.2	Trajectory Optimization Techniques . . . . .	10
2.5.3	Examples in Resistance Training . . . . .	11
2.6	Conclusion . . . . .	11
<b>3</b>	<b>Theory Development</b>	<b>13</b>
3.1	Modelling . . . . .	13
3.1.1	Components of Models . . . . .	13
3.1.2	Degrees of Freedom and Coordinate System . . . . .	14
3.1.3	Dynamics of Motion . . . . .	15
3.1.4	State-Space Representation . . . . .	16
3.2	Trajectory Optimization . . . . .	16
3.2.1	Overview . . . . .	16
3.2.2	The Trajectory Optimization Problem . . . . .	17

3.2.3	Direct Collocation Method . . . . .	17
3.2.4	Nonlinear Programming Formulation . . . . .	19
3.2.5	Practical Considerations . . . . .	19
<b>4</b>	<b>Method</b>	<b>20</b>
4.1	Overview . . . . .	20
4.2	Approach . . . . .	21
4.3	Development Stages . . . . .	21
4.3.1	Stage 1: Model A . . . . .	21
4.3.2	Stage 2: Model B . . . . .	22
4.3.3	Stage 3: Model C . . . . .	23
4.4	Clinical Application . . . . .	23
<b>5</b>	<b>Problem Formulation</b>	<b>24</b>
5.1	Fixed Components . . . . .	25
5.1.1	Model Choice . . . . .	25
5.1.2	Software Choice . . . . .	25
5.1.3	Coordinate System . . . . .	27
5.1.4	Trajectory Optimization Method . . . . .	28
5.2	Variable Components . . . . .	28
5.2.1	Model Design . . . . .	28

5.2.2	Anthropometric Parameters . . . . .	29
5.2.3	Boundary Conditions . . . . .	30
5.2.4	Control and Path Constraints . . . . .	31
5.2.5	Objective Function Design . . . . .	31
5.2.6	Initial Guess . . . . .	32
<b>6</b>	<b>Stage 1: 2D Arm Motion</b>	<b>33</b>
6.1	Test A1.1 . . . . .	34
6.1.1	Iteration 1: Problem Formulation . . . . .	34
6.1.2	Iteration 1: Results and Discussion . . . . .	36
6.1.3	Iteration 2: Problem Formulation . . . . .	37
6.1.4	Iteration 2: Results and Discussion . . . . .	39
6.2	Test A1.2 . . . . .	39
6.2.1	Problem Formulation . . . . .	39
6.2.2	Results and Discussion . . . . .	40
6.3	Test A1.3 . . . . .	40
6.3.1	Problem Formulation . . . . .	41
6.3.2	Results and Discussion . . . . .	41
6.4	Test A2.1 . . . . .	42
6.4.1	Problem Formulation . . . . .	42
6.4.2	Results and Discussion . . . . .	43

<b>7 Stage 2: 3D Arm Motion</b>	<b>44</b>
7.1 Test B1.1 . . . . .	44
7.1.1 Problem Formulation . . . . .	44
7.1.2 Results and Discussion . . . . .	47
7.2 Test B1.2 . . . . .	48
7.2.1 Problem Formulation . . . . .	48
7.2.2 Results and Discussion . . . . .	48
7.3 Test B1.3 . . . . .	49
7.3.1 Problem Formulation . . . . .	49
7.3.2 Results and Discussion . . . . .	49
7.4 Test B1.4 . . . . .	50
7.4.1 Iteration 1: Problem Formulation . . . . .	50
7.4.2 Iteration 1: Results and Discussion . . . . .	51
7.4.3 Iteration 2: Problem Formulation . . . . .	51
7.4.4 Iteration 2: Results and Discussion . . . . .	52
7.5 Test B1.5 . . . . .	52
7.5.1 Problem Formulation . . . . .	53
7.5.2 Results and Discussion . . . . .	53
7.6 Test B1.6 . . . . .	54
7.6.1 Problem Formulation . . . . .	54

7.6.2	Results and Discussion . . . . .	54
7.7	Test B2.1 . . . . .	55
7.7.1	Problem Formulation . . . . .	55
7.7.2	Results and Discussion . . . . .	56
7.8	Test B2.2 . . . . .	57
7.8.1	Problem Formulation . . . . .	57
7.8.2	Results and Discussion . . . . .	57
7.9	Test B3.1 . . . . .	58
7.9.1	Problem Formulation . . . . .	58
7.9.2	Results and Discussion . . . . .	59
7.10	Test B3.2 . . . . .	60
7.10.1	Problem Formulation . . . . .	60
7.10.2	Results and Discussion . . . . .	60
7.11	Test B3.3 . . . . .	61
7.11.1	Problem Formulation . . . . .	61
7.11.2	Results and Discussion . . . . .	61
7.12	Test B4.1 . . . . .	62
7.12.1	Problem Formulation . . . . .	62
7.12.2	Results and Discussion . . . . .	63
<b>8</b>	<b>Clinical Application</b>	<b>64</b>

8.1	Test Subject: Josh . . . . .	64
8.1.1	Problem Formulation . . . . .	64
8.1.2	Results and Discussion . . . . .	65
8.2	Test Subject: Lee . . . . .	66
8.2.1	Problem Formulation . . . . .	66
8.2.2	Results and Discussion . . . . .	67
<b>9</b>	<b>Conclusion</b> . . . . .	<b>68</b>
9.1	Question 1 . . . . .	68
9.2	Question 2 . . . . .	68
9.3	Question 3 . . . . .	69
9.4	Question 4 . . . . .	69
9.5	Clinical Application . . . . .	69
9.6	Recommendations . . . . .	70
<b>A</b>	<b>Graduate Attributes</b> . . . . .	<b>77</b>
<b>B</b>	<b>Ethics Clearance</b> . . . . .	<b>78</b>
B.1	Ethics Pre-screening Questionnaire Outcome Letter . . . . .	79
<b>C</b>	<b>Additional Information</b> . . . . .	<b>80</b>
C.1	GitHub Link . . . . .	80
C.2	Stage 1 Figures . . . . .	80

C.2.1	Test A1.1	80
C.2.2	Test A1.2	82
C.2.3	Test A1.3	83
C.2.4	Test A2.1	84
C.3	Stage 2 Figures	85
C.3.1	Test B1.1	85
C.3.2	Test B1.2	86
C.3.3	Test B1.3	87
C.3.4	Test B1.4	88
C.3.5	Iteration 1	88
C.3.6	Iteration 2	89
C.3.7	Test B1.5	90
C.3.8	Test B1.6	91
C.3.9	Test B2.1	92
C.3.10	Test B2.2	94
C.3.11	Test B3.1	95
C.3.12	Test B3.2	97
C.3.13	Test B3.3	98
C.3.14	Test B4.1	100

# **Chapter 1**

## **Introduction**

### **1.1 Background to the study**

Optimal lifting technique is a critical consideration in resistance training as it directly affects both performance and injury risk. Defining a universally “correct” technique is challenging due to the variability in limb proportions, shoulder and elbow weakness, and specific training goals for individuals. The optimal bench press technique is often debated because it is widely practised yet has a high incidence of shoulder and elbow injuries. This study focuses on identifying bench press lifting techniques to reduce injury risk using trajectory optimization.

### **1.2 Objectives of this study**

#### **1.2.1 Problems to be investigated**

The main problem to be investigated is determining the optimal technique for performing the bench press to reduce injury. This involves finding the best bar path and grip width for different brachial indices (forearm divided by upper arm) and to minimize shoulder or elbow exertion.

#### **1.2.2 Purpose of the study**

The purpose of this study is to investigate lifting technique and provide a personal optimal lifting technique for the bench press. The aim is to develop a reliable program that collects relevant personal data, such as body weight, upper arm and forearm lengths, shoulder width, past injuries and persistent pain. Using this information, the program can determine the optimal bar path and grip width for each individual. Therefore, providing a reliable tool for lifters to find the best lifting technique to prevent injury.

## 1.3 Scope and Limitations

The study includes a basic rigid body model of the arm, but does not include advanced biomechanical simulations. It focuses only on the path of the bar and grip width but elbow flare and other joint kinematics are not considered. It investigates the flat back bench press exercise specifically, without extending to other upper body movements. It only considers the concentric (upward) phase of the lift and models a single arm, assuming symmetry between the left and right sides. While it considers safety and performance in terms of technique (bar path and grip width), it does not consider strength (load) or endurance (sets and repetitions). Lastly, experimental validation with human subjects is outside the scope of this project.

Time constraints prevent expanding the model to include additional upper body exercises such as shoulder press, incline bench, dumbbell press, or chest flies. The simplified rigid body model does not capture soft tissue dynamics, joint stability, or muscle activation patterns meaning that the results cannot fully capture the complexity of human movement. The model assumes idealized motion and does not capture compensatory strategies lifters may use under heavy loads or when fatigued.

## 1.4 Plan of development

In Chapter 1, the basic outline of the project is presented. Chapter 2 provides a literature review on biomechanical modelling and trajectory optimisation for identifying an optimal bench press technique, focusing on chest hypertrophy and injury risk minimisation. Chapter 3 gives an overview of the theoretical background relevant to this project. Chapter 4 details the approach to the problem, while Chapter 5 presents the problem formulation and major design decisions. In Chapter 6, the research questions are explored using a basic 2D model, focusing on bar path through a series of iterative tests. Chapter 7 expands this analysis with a 3D model, examining bar path and grip width. Chapter 8 applies the developed model to determine the optimal bar path and grip width for two test subjects. Finally, Chapter 9 presents the conclusions for each research question, discusses the clinical application, and provides recommendations for future work.

# Chapter 2

## Literature Review

### Biomechanical Modelling and Trajectory Optimization Approaches to Identifying an Optimal Bench Press Technique for Chest Hypertrophy and Injury Risk Minimization

### 2.1 Introduction

”What do you bench?” is one of the most common questions heard among gym-bros and lifters, and with good reason [1]. The bench press is widely considered a fundamental exercise in strength training and bodybuilding, serving not only as a key indicator of upper-body strength but also as a movement that enhances everyday functionality and athletic performance [2]. As a compound pressing movement, it primarily engages the pectoralis major, anterior deltoid, and triceps brachii muscles. It is traditionally performed on a flat bench with the bar just resting on the chest before pressing upward over the shoulders [3].

Yet beneath its apparent simplicity, the bench press is a complex biomechanical lift that engages multiple joints and muscle groups working in harmony. This very complexity makes it one of the lifts to cause the most injuries, alongside the squat and deadlift. The bench press causes shoulder, elbow, and upper-limb injuries [4, 5]. Because so many variables can influence bench press mechanics, guidance on proper form is difficult to generalize so there is a lot of uncertainty about the safest and most effective way to perform the lift.

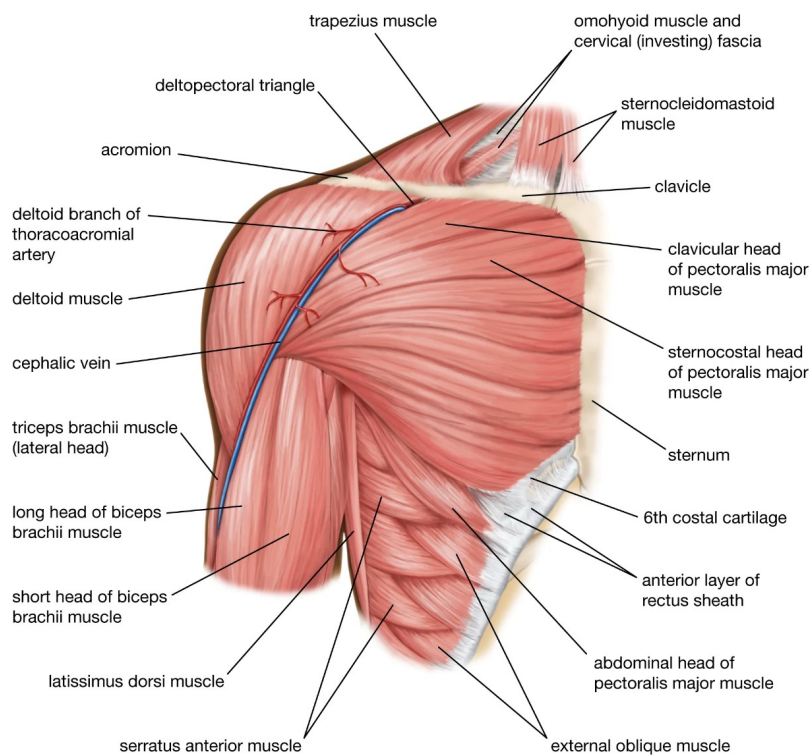
This literature review investigates the fundamental biomechanics of the bench press and the key variables that influence its execution. It then reviews current methods for modelling the human body, which can be integrated with trajectory optimization. Various trajectory optimization techniques are assessed for their applicability and effectiveness in providing guidance to lifters aiming to maximize performance while minimizing injury risk.

## 2.2 Fundamentals of the Bench Press

The bench press is one of the most practised resistance exercises. To provide a consistent basis for biomechanical analysis, this review focuses on the flat-back bench press technique, which is the most commonly adopted and standardized variation.

The flat-back bench press is performed on a horizontal bench with a bar rack. Proper setup is characterized by five points of contact: the head, shoulder blades, thoracic trunk, buttocks, and feet. Lifters must maintain the natural lordotic curvature of the lumbar spine without intentionally exaggerating it [6]. This position establishes a stable foundation for the lift and ensures reliable force transfer from the body into the bar.

During the movement, several muscles are activated, including the triceps lateral head, triceps long head, anterior deltoid, pectoralis clavicular head, pectoralis sternocostal head, pectoralis abdominal head, and biceps brachii [7]. Figure 2.1 illustrates the muscle groups to aid readers without anatomical knowledge. The main joints involved are the shoulder, elbow, and wrist, which collectively coordinate the pressing motion and bear the majority of the mechanical load.



© Encyclopædia Britannica, Inc.

Figure 2.1: Muscles in Upper Body [8]

## 2.3. VARIABLES INFLUENCING BENCH PRESS BIOMECHANICS

Other biomechanical variables, such as lifting speed, bar path, grip width, elbow flare angle, and body proportions, can alter which muscles and joints are emphasized. These factors will be discussed in Section 2.3, where their influence on hypertrophy and injury risk is examined in detail.

## 2.3 Variables Influencing Bench Press Biomechanics

### 2.3.1 Lifting Speed

The bench press is often performed slowly and with control in studies, with lifts typically lasting around two seconds [9, 10]. However, high-speed lifting at the same load has been shown to promote greater muscle growth over time [11]. In general, lifting speed is highly correlated with the percentage of one-repetition maximum (1RM), with lighter loads allowing faster movements. This means that increasing lifting speed for a given load can enhance muscle development [12].

### 2.3.2 Bar Path

The start and end positions of the bench press are widely recognized as beginning with the bar lowered just below the pectoralis major, with the forearms perpendicular to the bar, and ending with the bar positioned directly above the shoulders [13, 14, 15]. The bar must remain horizontal throughout the lift to ensure balanced force distribution and minimize injury risk [16, 17].

Elite powerlifters typically guide the bar closer to the shoulders compared to amateur lifters [16, 17]. Kinematic analyses indicate that the bar path often follows a curved, parabolic trajectory: beginning above the lower chest, drifting slightly back toward the shoulders, and finishing with a vertical press to lockout [13]. This “J-curve” pattern has been associated with improved mechanical efficiency and reduced shoulder stress, and some authors conclude that it enhances lifting performance by decreasing the moment generated by the bar about the shoulder joint [17].

### 2.3.3 Grip Width

Performing the bench press with a narrow grip increases activation in the triceps brachii, the clavicular portion of the pectoralis major and the anterior deltoid [10, 7, 18]. The narrow grip reduces shoulder abduction, keeping the arms closer to the torso and thereby minimizing stress on the shoulder joint. This makes it a suitable variation for individuals trying to manage shoulder discomfort [15]. However, narrow grips increase elbow joint loading at deeper flexion angles, so those with elbow pain may benefit from wider grips [7].

Conversely, wider grips shift the emphasis toward the pectoralis major, especially the abdominal head, while reducing triceps activity [7, 19]. Maximal strength is generally observed with hand spacing around 165-200% of biacromial width [10]. However, this grip increases shoulder muscular load and joint stress due to greater abduction [7]. While advantageous for maximizing force output, the wide grip should be applied cautiously in populations with a history of shoulder pain.

### 2.3.4 Elbow Flare Angle

Elbow flare alters both triceps recruitment and joint loading in the bench press. With a close grip and elbows flared outward, the hand aligns over the shoulder, creating a larger moment arm at the elbow and greater triceps brachii activation. Therefore, it enhances triceps strength and hypertrophy, particularly in the lateral head, and increases elbow joint loading at high flexion angles [7, 18]. In contrast, keeping the elbows tucked (less than 45° abduction) shifts the elbow under the hand, reducing torque and minimizing triceps involvement [18]. For lifters with elbow discomfort, wider grips with no elbow flare may be preferable to reduce joint stress while maintaining chest activation [7].

### 2.3.5 Body Proportions

The bench press involves coordinated movement of the shoulder, elbow, and wrist. It is known that upper and forearm lengths can influence performance. The brachial index has been shown to be strongly associated with bench press performance, with a longer upper arm negatively correlated with strength. A greater brachial index may enhance mechanical efficiency by reducing the load's moment arm [20]. There are also descriptive statistics of upper and forearm lengths for women and men [21]. However, there is a lack

of literature on how this ratio specifically influences bar path, grip width, and elbow flare for optimal lifting technique.

## 2.4 Biomechanical Modelling of the Human Body

Biomechanical modelling has been developed since the 1970s as a way to represent the human body in simplified form [22]. Human movement comes from the interaction of neural, muscular, and skeletal systems, and modelling provides a framework to analyse this complexity, predict new trends, and estimate variables that are difficult to measure directly during motion [23]. The choice of modelling approach depends on the purpose of the study, the required level of anatomical detail, and the type of motion being investigated [24]. This review will focus on three main approaches to biomechanical modelling: skeletal models, musculoskeletal models, and available software models.

### 2.4.1 Skeletal Model

A skeletal model represents the human body as a rigid body system of segments connected by joints that allow movement under mechanical constraints [24, 25]. In these models, the size and shape of each segment are kept constant, meaning deformation of the body is not included. Only the degrees of freedom (DoF) linked to translations and rotations are considered [24]. This makes it possible to describe complex human motion in a simplified and structured way.

The structure of a skeletal model is built from segments and joints. Each segment needs to have its geometry, dimensions, inertial properties, origin, and orientation defined [26, 27]. Joints are then added to connect these segments, and they are usually given one, two, or three DoF depending on the biological joint being represented [26]. For instance, the neck, hip, and shoulder are often modelled as ball-and-socket joints with three DoF, the elbow and wrist as universal joints with two DoF, and the knee and ankle as hinge joints with one DoF [24]. To make models simpler, some studies reduce complexity. For example, one approach fixes the scapula to the clavicle and models the shoulder with only two DoFs, which still produces reasonable upper arm movement [28]. The skeletal model does not consider skin motion artifacts which may cause unrealistic joint movements or inconsistencies during analysis [24].

## 2.4. BIOMECHANICAL MODELLING OF THE HUMAN BODY

The purpose of skeletal models is to provide a simplified way to study human movement while still capturing important dynamics. These models are often used in injury prevention to highlight dangerous joint positions, in equipment design to improve ergonomics and safety, and in sport and rehabilitation to refine movement techniques [24].

### 2.4.2 Musculoskeletal Model

Musculoskeletal models simulate the interaction between bones, muscles, tendons, and ligaments. Unlike simpler skeletal models that only describe joint motion and torques, musculoskeletal models consider internal forces such as muscle activations and joint loads [24]. In both models, motion can be driven by joint actuators, which apply prescribed torques at the joints. However, in musculoskeletal models, motion can also be generated by muscle actuators, which simulate the pulling action of muscles on bones to produce movement [29].

The main components of a musculoskeletal model are bones, joints, muscles, tendons, ligaments, and scaling parameters. Bones and joints form the rigid framework and define movement. Muscles and tendons are commonly modelled using the Hill-type model, which captures how muscles generate and transmit force. This model includes an active contractile element that represents the force produced by muscle fibres and passive elastic components that simulate the natural resistance and stretching behaviour of muscle and tendon tissues [24, 29]. In some musculoskeletal models, ligaments are also added. They connect bone to bone and are usually represented as non-linear springs. Scaling adjusts the model to match the individual's anatomy giving the most accurate results [24].

The primary purpose of musculoskeletal models is to estimate biomechanical quantities that cannot be measured directly, including muscle forces, tendon forces, joint loads, and activation patterns. Similar to the skeletal model, the musculoskeletal model is used for injury prevention, in equipment design, and in sport and rehabilitation analysis. However, it provides a more detailed and accurate understanding of human movement because it accounts for muscle forces and activations [24].

### 2.4.3 Available Software Models

Human body models are no longer limited to those with the expertise to develop their own models. There are several commercial and open-source software packages such as OpenSim, AnyBody, Visual3D and SIMM that are available to all researchers and practitioners [23, 24].

OpenSim is the most widely used open-source platform for musculoskeletal modelling, offering comprehensive tools for kinematic, dynamic, and muscle-driven simulations. It supports motion capture data integration, optimal control, and detailed analysis of muscles, tendons, and joint mechanics, with APIs available in Python, MATLAB, and C++ [30, 31]. AnyBody is similar to OpenSim but focuses on inverse dynamics and has greater detailed anatomical models [32]. Visual3D is mainly used for clinical and performance motion analysis, integrating force and EMG data but it requires preprocessed video input [33]. SIMM, a commercial tool capable of forward and inverse simulations but is less user-friendly [33, 34].

The main purpose of such software is to simplify the construction and analysis of musculoskeletal models because creating custom-developed computational models remains time-consuming and costly [23]. These tools help further advancements in engineering and movement science.

## 2.5 Trajectory Optimization in Resistance Training

### 2.5.1 Background

The aim of trajectory optimization is to find an optimal path and control inputs that move a system from an initial state to a desired final state while minimizing a specified cost function. The system is typically described by its dynamics, for example  $\dot{x} = f(x, u)$ , where  $x$  represents the system state and  $u$  represents the control inputs [35, 36, 37].

To ensure the trajectory is feasible, several constraints must be satisfied. Boundary constraints specify the initial and final states of the system. System dynamics ensure that the trajectory follows the true physical behaviour of the system. Control input constraints limit the magnitude or rate of control actions according to actuator capabilities [37].

Trajectory optimization generally produces open-loop solutions, which are sequences of control inputs that change the system from a specific initial state to a desired final state. This defines a single trajectory through the state space. In contrast, closed-loop solutions, also called optimal policies, provide a control law that specifies the optimal action for every possible state. Closed-loop solutions can generate trajectories from any starting point but are usually more computationally expensive, often obtained via dynamic programming [37].

### 2.5.2 Trajectory Optimization Techniques

**Direct shooting** turns trajectory optimization into a nonlinear program by simulating the system forward. In single shooting, the whole trajectory is simulated as one segment. The decision variables are the initial state and control inputs. It works well for simple control and few constraints, such as spacecraft trajectories [35, 37, 38]. Multiple shooting divides the trajectory into segments. Each segment is simulated separately, improving robustness and convergence. Path constraints are still challenging to implement [35, 37].

**Collocation methods** approximate the trajectory with polynomials at discrete points. Low-order methods, like trapezoidal or Hermite-Simpson, are simple and efficient. High-order uses Chebyshev or Legendre polynomials. High-order methods achieve spectral convergence, reducing error quickly for smooth trajectories. Barycentric interpolation helps keep these high-order computations stable when taking derivatives or integrals [35, 37].

**Differential Dynamic Programming** is a shooting-based method that optimizes by propagating control backward along the trajectory. Unlike standard shooting, it exploits the time-dependent dynamics, improving convergence for nonlinear problems [37].

**Multiphase methods** are used when trajectories have multiple continuous phases separated by discrete events. Examples include multistage rockets and walking robots. Each phase is optimized separately while boundary constraints connect them. This simplifies computation and maintains accuracy [37].

No method is best for all problems. Direct methods are easier but can converge slowly for nonlinear systems. Indirect methods are more accurate but harder to implement [38]. Shooting works well for simple control. Collocation is best when dynamics and control need similar accuracy, and control structure is unknown, like robot joint torques. Multiphase optimization is practical for hybrid systems [37].

### 2.5.3 Examples in Resistance Training

Trajectory optimization can be applied in resistance training to improve lifting performance and reduce joint stress. In one study, the snatch lift was modelled using a five-link biomechanical system, where the bar path was treated as the performance index. The model minimized the sum of joint torques throughout the lift [39]. The optimized bar path aligned with experimental data, showing the model's accuracy and usefulness for performance improvement.

Another study used a six-link model including the shin, thigh, trunk, upper arm, forearm, and head to analyse the snatch lift. The control problem was designed to minimize the total work done by the lifter [40]. Again, the resulting optimal trajectories and joint torques aligned with experimental data, providing valuable insight for coaches and athletes.

Trajectory optimization has also been applied to robotic exercise machines. A model-free optimization method based on Extremum Seeking Control was used to adapt trajectory parameters in real time using muscle activation feedback. By adjusting the trajectory orientation to minimize or maximize specific muscle activity, the system could target or relax particular muscle groups [41]. This approach shows how optimal trajectory control can personalize resistance training for muscle activation.

## 2.6 Conclusion

The bench press typically lasts around 2 seconds, with velocity depending on the percentage of 1RM. Shoulder stress is reduced by a J-shaped bar path, narrow grip, or greater brachial index, and increased by a straight-line path, wide grip, or smaller brachial index. Elbow stress increases with a J-curve and narrow grip especially with flared elbows, and decreases with a straight-line path or wide grip. Muscle activation is also grip-dependent: narrow grips increase activation of the anterior deltoid, triceps brachii, and clavicular head of the pectoralis major, while wide grips increase activation of the abdominal head of the pectoralis major.

Biomechanical modelling represents the human body in simplified form to analyse movement, predict trends, and estimate variables that are hard to measure directly. Skeletal models treat the body as rigid segments connected by joints, capturing essential motion dynamics, while musculoskeletal models include muscles, tendons, and ligaments

## 2.6. CONCLUSION

to estimate internal forces and activations. Software platforms such as OpenSim, AnyBody, Visual3D, and SIMM provide tools for building and analysing models efficiently, supporting research in sports, rehabilitation, and ergonomics.

Trajectory optimization aims to find control inputs that move a system from an initial state to a desired final state while minimizing a cost function, subject to constraints. Solutions are typically open-loop, defining a single trajectory, while closed-loop solutions provide optimal actions for all states but are more computationally expensive. Techniques include direct and multiple shooting, collocation, differential dynamic programming, multiphase, and through-contact methods, each suited to different problem types. In resistance training, trajectory optimization has been applied to model lifts like the snatch using multi-link biomechanical systems and minimizing joint torques and total work. It has also been used in robotic exercise machines with model-free optimization, adapting trajectory parameters in real time to target specific muscle activity and personalize training.

Integrating biomechanics, modelling, and trajectory optimization can be used to investigate bench press techniques that enhances chest growth and reduces the risk of injury. In the bench press, many factors influence joint stress and muscle activation. Biomechanical modelling and trajectory optimization together provide a framework to vary these factors, simulate the lift and analyse the results. This literature review highlights that trajectory optimization offers a practical and promising approach to improving bench press technique and advancing future research.

# Chapter 3

## Theory Development

This chapter outlines the foundational theory required to understand the biomechanical modelling and trajectory optimization techniques used in this study. The purpose is not to present an exhaustive theoretical review, but rather to highlight key principles relevant to the development and control of multibody systems.

### 3.1 Modelling

In multibody system modelling, rigid links are used to represent physical bodies, connected by joints that constrain relative motion. This simple representation allows the study of kinematics and dynamics without modeling internal structures. A rigid-body diagram can illustrate the links, joints, and their relative motion.

#### 3.1.1 Components of Models

A basic model consists of:

- **Rigid links:** Representing segments of the system, each with mass  $m$ , length  $L$ , and moment of inertia  $I$ . These properties determine the link's response to forces and torques.
- **Joints:** Define how links are connected and constrain relative motion. Common joint types include:
  - Revolute (hinge) joint: 1 rotational DoF.
  - Universal joint: 2 rotational DoF.
  - Spherical joint: 3 rotational DoF.

### 3.1.2 Degrees of Freedom and Coordinate System

The motion of a single link connected with a spherical joint ( 3 DoF) is described by the generalized coordinates:

$$\mathbf{q} = [\lambda, \beta, \alpha]^T$$

where each one represents a joint rotation.

In modelling, a global coordinate system defines positions and orientations relative to a fixed external reference frame. A local coordinate system is connected to each link, describing motion and orientation relative to that link's own axes.

Rotations of the axis in a local coordinate system can be represented using Euler angles. For example, the  $x$ - $y$ - $z$  Euler angles define orientation via sequential rotations about the  $x$ ,  $y$ , and  $z$  axes as seen in 3.1.

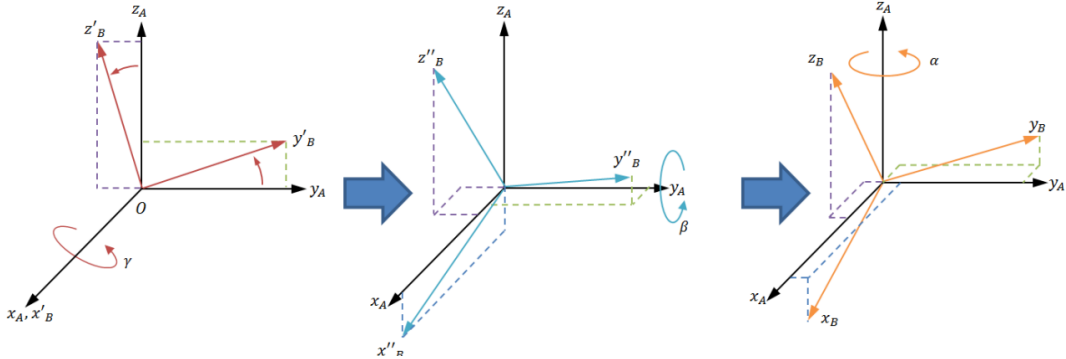


Figure 3.1: Euler angle rotations, where the black axis represents the global frame and the coloured axes represent the local frames after successive rotations [42].

Transformation from the local frame to the global frame is performed using a rotation matrix  $R$ , which defines the orientation of the local frame relative to the global frame. The position of a link, represented by the vector  $\mathbf{r}$ , can be expressed in the global frame as:

$$\mathbf{r}_{\text{global}} = R \mathbf{r}_{\text{local}} + \mathbf{p}_0$$

where  $\mathbf{p}_0$  denotes the position of the local axes origin defined in the global coordinate system. In this case,  $\mathbf{p}_0 = 0$ .

### 3.1.3 Dynamics of Motion

The dynamics of a rigid-body system describe how it moves under forces and torques. Two main formulations are typically used:

- **Lagrange's Method:** Based on energy principles, the system's dynamics are derived from the Lagrangian  $L = T - V$ , with  $T$  as kinetic energy and  $V$  as potential energy:

$$\frac{d}{dt} \left( \frac{\partial L}{\partial \dot{q}_i} \right) - \frac{\partial L}{\partial q_i} = Q_i$$

where  $Q_i$  is the generalized force or torque for coordinate  $q_i$ .

- **Newton-Euler Method:** Applies Newton's second law to each link individually:

$$\sum \mathbf{F} = m\mathbf{a}, \quad \sum \boldsymbol{\tau} = I\boldsymbol{\alpha}$$

where  $\mathbf{F}$  and  $\boldsymbol{\tau}$  are the net forces and torques on the link, and  $\mathbf{a}$  and  $\boldsymbol{\alpha}$  are linear and angular accelerations.

Both formulations result in the standard multibody dynamic equation, commonly known as the *Manipulator Equation*:

$$M(q)\ddot{q} + C(q, \dot{q})\dot{q} + G(q) = \boldsymbol{\tau}$$

where:

- $M(q)$  is the **mass (or inertia) matrix**, which depends on the configuration  $q$  and represents how mass is distributed across the system. It determines how applied torques or forces produce accelerations.
- $C(q, \dot{q})$  is the **Coriolis and centrifugal matrix**, which captures velocity-dependent forces that arise due to the motion of the links.
- $G(q)$  is the **gravity vector**, accounting for the torques or forces caused by gravitational acceleration.
- $\boldsymbol{\tau}$  is the **vector of applied joint torques or forces**, representing actuator inputs to the system.

This equation forms the foundation for analysing and controlling the motion of multibody systems.

### 3.1.4 State-Space Representation

For control purposes, the dynamics of a rigid-body system are often expressed in state-space form. The system state consists of the generalized coordinates  $\mathbf{q}$  and their time derivatives  $\dot{\mathbf{q}}$ :

$$\mathbf{x} = \begin{bmatrix} \mathbf{q} \\ \dot{\mathbf{q}} \end{bmatrix} \in \mathbb{R}^{2n}$$

where  $n$  is the number of generalized coordinates. The state-space formulation allows the second-order dynamics

$$M(q)\ddot{\mathbf{q}} + C(q, \dot{\mathbf{q}})\dot{\mathbf{q}} + G(q) = \tau$$

to be written as a first-order system:

$$\dot{\mathbf{x}} = \begin{bmatrix} \dot{\mathbf{q}} \\ M^{-1}(\mathbf{q})(\tau - C(\mathbf{q}, \dot{\mathbf{q}})\dot{\mathbf{q}} - G(\mathbf{q})) \end{bmatrix}$$

This representation is particularly useful for trajectory optimization as it explicitly expresses the system evolution in terms of a state vector  $\mathbf{x}$  and its derivative  $\dot{\mathbf{x}}$ .

## 3.2 Trajectory Optimization

Trajectory optimization is the process of finding a feasible trajectory for a dynamic system that minimizes a performance criterion while satisfying physical and task-specific constraints.

### 3.2.1 Overview

In general, trajectory optimization seeks to determine the time evolution of system states and control inputs that minimize a cost functional of the form:

$$J = \phi(x(t_f), t_f) + \int_{t_0}^{t_f} L(x(t), u(t), t) dt$$

subject to dynamic constraints (from the model)

$$\dot{x} = f(x, u, t),$$

and boundary or path constraints such as

$$c(x(t), u(t), t) \leq 0, \quad x(t_0) = x_0, \quad x(t_f) = x_f.$$

Here,  $x$  represents the state vector,  $u$  the control vector,  $t_i$  the initial and  $t_f$  the final time. The functions  $L$  and  $\phi$  define the running and terminal costs respectively.

### 3.2.2 The Trajectory Optimization Problem

In general, the continuous-time problem described above is infinite-dimensional and cannot be solved analytically for most nonlinear systems. Therefore, it is converted into a finite-dimensional nonlinear programming (NLP) problem through a process called *direct transcription*. The state and control trajectories are discretized at a finite number of points (called *knots*), and the system dynamics are enforced approximately using numerical integration schemes.

### 3.2.3 Direct Collocation Method

Direct collocation is a transcription method that converts a continuous-time trajectory optimization problem into a finite-dimensional nonlinear program by enforcing the system dynamics at selected collocation points within each time interval. The continuous trajectory is approximated using piecewise polynomial splines. The dynamics are enforced through numerical integration formulas such as the Trapezoidal and Hermite-Simpson methods.

#### Trapezoidal Collocation

As shown in Figure 3.2, the trapezoidal collocation method approximates the system trajectory using a piecewise linear spline defined over discrete time segments connecting adjacent knot points. Between two knot points  $k$  and  $k + 1$ , the dynamics are integrated

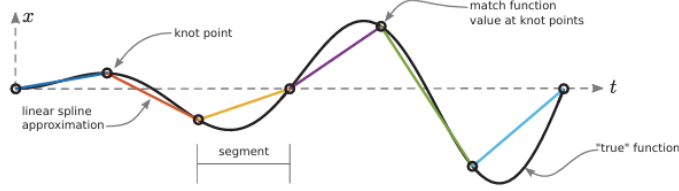


Figure 3.2: Trapezoidal collocation method: the system dynamics are approximated using the trapezoidal rule between consecutive knot points, forming a piecewise linear spline over each segment [37].

using the trapezoidal rule:

$$x_{k+1} = x_k + \frac{h}{2} [f(x_k, u_k) + f(x_{k+1}, u_{k+1})],$$

where  $h$  is the time step between knot points. This approach provides second-order accuracy and is relatively simple to implement. However, for stiff or highly nonlinear systems, integration errors may accumulate unless sufficiently small time steps are used.

### Hermite-Simpson Collocation

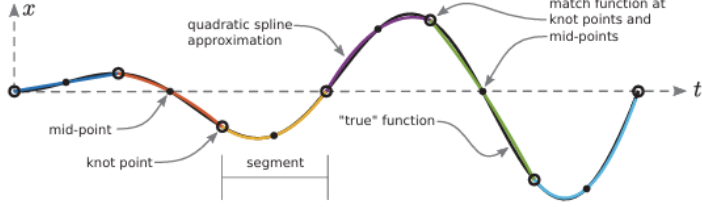


Figure 3.3: Hermite-Simpson collocation method: system dynamics are enforced at both knot points and midpoints, forming a smooth cubic spline across each segment for improved accuracy [37].

As illustrated in Figure 3.3, the Hermite-Simpson collocation method refines the trajectory representation by introducing a midpoint within each time segment between adjacent knot points. This allows the state trajectory to be modelled as a smooth cubic spline, resulting in improved accuracy and stability.

The state at the midpoint is approximated using Hermite interpolation:

$$x_{k+\frac{1}{2}} = \frac{1}{2}(x_k + x_{k+1}) + \frac{h}{8} [f(x_k, u_k) - f(x_{k+1}, u_{k+1})],$$

and the dynamics are enforced by the Simpson integration rule:

$$x_{k+1} = x_k + \frac{h}{6} \left[ f(x_k, u_k) + 4f(x_{k+\frac{1}{2}}, u_{k+\frac{1}{2}}) + f(x_{k+1}, u_{k+1}) \right].$$

This third-order accurate method provides smoother trajectories and greater numerical stability compared to the trapezoidal approach, making it well-suited for trajectory optimization applications.

### 3.2.4 Nonlinear Programming Formulation

After transcription, all state and control variables at each knot are collected into a single decision vector  $z$ . The problem is then formulated as a standard nonlinear program:

$$\begin{aligned} \min_z \quad & J(z) \\ \text{subject to} \quad & g(z) = 0, \\ & h(z) \leq 0, \end{aligned}$$

where  $g(z)$  represents the discretized dynamics and boundary conditions, and  $h(z)$  enforces inequality constraints such as control limits or joint bounds. This finite-dimensional problem can then be solved using standard optimization solvers.

### 3.2.5 Practical Considerations

In practice, the success of trajectory optimization depends heavily on:

- **Initialization:** Providing good initial guesses for the states and control inputs helps the nonlinear program converge to a feasible and optimal solution.
- **Mesh Refinement:** Adjusting the number and spacing of knot points for a finer or coarser mesh. A finer mesh can capture more complex dynamics while a coarser mesh reduces computational cost.
- **Error Analysis:** By finding the difference between the system dynamics and the collocation-based approximation, one can identify where the spline deviates from the true continuous dynamics and refine the mesh to improve accuracy.

# Chapter 4

## Method

### 4.1 Overview

This study investigates how joint conditions and anthropometric factors influence optimal bench press technique. Six key research questions were formulated:

1. How does the **bar path** change when protecting the shoulder versus the elbow (with grip width and elbow flare held constant)?
2. How does the **bar path** vary for different brachial indices (with grip width and elbow flare held constant)?
3. How does **grip width** change when protecting the shoulder versus the elbow (with bar path and elbow flare held constant)?
4. How does **grip width** vary for different brachial indices (with bar path and elbow flare held constant)?
5. How does **elbow flare** change when protecting the shoulder versus the elbow (with bar path and grip width held constant)?
6. How does **elbow flare** vary for different brachial indices (with bar path and grip width held constant)?

Due to time constraints, questions 5 and 6 were not experimentally investigated. The remaining questions were explored through a series of structured tests, followed by a case study illustrating the clinical applicability of the developed model and trajectory optimisation framework.

## 4.2 Approach

The study began with a problem formulation, where the constant components of the trajectory optimisation were defined, and the variable components, that would change across different tests, were outlined (see Chapter 5). The development process comprised three stages; however, only Stage 1 (see Chapter 6) and Stage 2 (see Chapter 7) were completed, followed by a clinical application (see Chapter 8). At each stage, tests were configured and conducted and the results verified to ensure that both the model and trajectory optimisation functioned correctly before proceeding further. With each stage, additional complexity was introduced, ultimately leading to the final model and optimisation framework applied in the clinical context. Finally, conclusions were drawn and recommendations for future work were proposed (see Chapter 9).

## 4.3 Development Stages

Development progressed in three stages, each introducing greater biomechanical detail. Model A established the foundation for two-dimensional bar path analysis, while Model B extended the representation to three dimensions, allowing grip width optimisation. A final model, Model C, was designed to further incorporate elbow flare as an additional degree of freedom; however, due to time constraints, it was not experimentally validated and is therefore excluded from this report.

### 4.3.1 Stage 1: Model A

After some adaptation through experimental design, 2 DoF 2D model was developed to study how bar path changes under different protective strategies and anthropometric conditions using trajectory optimisation.

The following tests were conducted to answer the key research questions:

#### **Question 1:**

- **A1.1:** Find bar path with narrow grip width and constant elbow flare.
- **A1.2:** Find bar path when protecting the shoulder with narrow grip width and constant elbow flare.

- **A1.3:** Find bar path when protecting the elbow with narrow grip width and constant elbow flare.

#### **Question 2:**

- **A2.1:** Find bar path variation for different brachial indices with narrow grip width and constant elbow flare.

The results were analysed and validated. Further complexity was added in Model B.

### **4.3.2 Stage 2: Model B**

After some adaptation through experimental design, a 3 DoF 3D model was developed to enable grip width analysis using trajectory optimisation.

The following tests were conducted to answer the key research questions:

#### **Question 1:**

- **B1.1:** Find bar path with narrow grip width and constant elbow flare.
- **B1.2:** Find bar path when protecting the shoulder with narrow grip width and constant elbow flare.
- **B1.3:** Find bar path when protecting the elbow with narrow grip width and constant elbow flare.
- **B1.4:** Find bar path with wide grip width and constant elbow flare.
- **B1.5:** Find bar path when protecting the shoulder with wide grip width and constant elbow flare.
- **B1.6:** Find bar path when protecting the elbow with wide grip width and constant elbow flare.

#### **Question 2:**

- **B2.1:** Find bar path variation for different brachial indices with narrow grip width and constant elbow flare.
- **B2.2:** Find bar path variation for different brachial indices with wide grip width and constant elbow flare.

#### **Question 3:**

- **B3.1:** Find grip width for a straight bar path with constant elbow flare.
- **B3.2:** Find grip width when protecting the shoulder for a straight bar path with constant elbow flare.
- **B3.3:** Find grip width when protecting the elbow for a straight bar path with constant elbow flare.

**Question 4:**

- **B4.1:** Find grip width variation for different brachial indices with a straight bar path and constant elbow flare.

The results were analysed and validated.

### 4.3.3 Stage 3: Model C

A 4 DoF 3D model was developed to extend motion representation and enable explicit elbow flare analysis through an additional rotation on the shoulder joint. The same trajectory optimisation framework was intended to be applied to this model to explore coordination between grip width, bar path, and elbow flare. However, due to time constraints, this model was not experimentally tested and is therefore excluded from this report.

## 4.4 Clinical Application

A final case study was conducted to demonstrate the clinical application of the model. Hypothetical test subjects with unique body proportions and specific joint discomfort (shoulder, elbow, or none) were simulated. The model was then used to determine the optimal grip width and bar path that minimized joint stress.

# Chapter 5

## Problem Formulation

The problem formulation is divided into fixed and variable components.

### Fixed components:

- Model Choice (Subsection 5.1.1)
- Software Choice (Subsection 5.1.2)
- Coordinate System (Subsection 5.1.3)
- Trajectory Optimisation Method (Subsection 5.1.4)

### Variable components:

- Model Design (Subsection 5.2.1)
- Anthropometric Parameters (Subsection 5.2.2)
- Boundary Conditions (Subsection 5.2.3)
- Control and Path Constraints (Subsection 5.2.4)
- Objective Function Design (Subsection 5.2.5)
- Initial Guess (Subsection 5.2.6)

The fixed components remain unchanged across all models and tests. The variable components follow a similar structure across the different models and tests but are modified as required. A complete overview of the variable components is provided in this chapter, while their specific configurations are detailed for each test in Stage 1 Chapter 6, Stage 2 Chapter 7, and in the final case study presented in the Clinical Application Chapter 8.

## 5.1 Fixed Components

### 5.1.1 Model Choice

The literature review provided descriptions of biomechanical models in Section 2.4, including skeletal, musculoskeletal and those available in pre-built software. Table 5.1 highlights key factors considered in the model selection process. Ultimately, the **skeletal model** was chosen for this study. It enabled the generation of fundamental bar trajectories and control of joint torques relevant to injury prevention. It was reasonable to design in the time frame. The model allowed efficient trajectory optimization while maintaining sufficient biomechanical realism for the specific research questions. In addition, the skeletal model is extendable to include muscles and activation dynamics in future work.

The design of the model, including number of links, DoF and dimensions, will change at each stage and is outlined in Subsection 5.2.1.

### 5.1.2 Software Choice

Table 5.2 summarizes the software and solver options considered for the skeletal model. Ultimately, **MATLAB** was chosen for this study because it provides a familiar and flexible environment which makes implementation and debugging easier. Its strong visualization capabilities allowed clear illustration of joint motions and bar trajectories which is beneficial for analysing and reporting. Coupled with **CasADi** and the IPOPT solver, MATLAB enabled symbolic modelling, automatic differentiation, and efficient solving of larger nonlinear optimization problems. It is set to solve until the error is smaller than  $10^{-6}$  or 5000 iterations are reached.

Table 5.1: Comparison of Model Choice Options

	Skeletal Model	Musculoskeletal Model	Available Software (e.g., OpenSim)
<b>Description</b>	Simplified rigid-body model representing bones and joints.	Includes muscles, tendons, and activation dynamics for realism.	Pre-built biomechanical models with integrated simulation tools.
<b>Computational Cost</b>	Low: efficient for trajectory optimization and control testing.	High: requires solving muscle redundancy and activation dynamics.	Moderate to high: depends on model complexity and solver.
<b>Model Complexity</b>	Simple structure; fewer parameters and equations.	Complex system with nonlinear muscle dynamics.	Varies: can be very complex depending on available model.
<b>Customizability</b>	Fully customizable; parameters can be tuned freely.	Customizable but requires detailed anatomical data.	Limited: depends on software capabilities and available datasets.
<b>Realism / Accuracy</b>	Moderate: approximates joint torques and kinematics.	High: accurately captures physiological forces.	High: validated models but some customization may still be needed.
<b>Development Effort</b>	Medium: requires formulation of rigid-body dynamics.	High: requires modeling muscles, activation, and force-length relations.	Low: uses existing framework and datasets.
<b>Use Case Suitability</b>	Ideal for studying joint trajectories and basic control.	Suitable for detailed injury and load analysis.	Useful for validation or rapid prototyping of biomechanics studies.

Table 5.2: Comparison of Software for Skeletal Model Trajectory Optimization

Software	Available Solvers	Strengths	Limitations
Python + CasADi [43]	IPOPT, SNOPT, KNITRO	Symbolic modelling, automatic differentiation, efficient NLP solving	Requires CasADi installation; solver licensing may apply
Python + SciPy [44]	SLSQP, trust-constr, L-BFGS-B	Easy to use, standard library, gradient-based optimization	Limited for highly constrained or very large-scale problems
MATLAB + fmincon [45]	Interior-point, SQP, trust-region-reflective	Supports nonlinear constraints and bounds; widely used in trajectory optimization applications	Limited for highly constrained or very large-scale problems; can become slow or may fail to converge
MATLAB + CasADi [43]	IPOPT, SNOPT, KNITRO	Symbolic modelling, automatic differentiation, efficient NLP solving	Requires CasADi installation; solver licensing may apply

### 5.1.3 Coordinate System

The global coordinate system is a fixed reference frame used to express positions and motions relative to the environment. In contrast, the local coordinate system is attached to each link, typically at a joint or link center, and moves with the link. Positions defined in local frames can be transformed to the global frame using rotation and translation.

For this project, due to the multiple links, varying degrees of freedom, and 3D models, a global coordinate system is impractical. Instead, a **local coordinate system** is defined for each link, with positions and orientations later transformed into the global frame. This is described in detail in the Theory Development Chapter 3 for readers seeking further understanding.

### 5.1.4 Trajectory Optimization Method

The Hermite-Simpson method is a higher-order collocation scheme that enforces dynamics at the start, midpoint and end of the interval using cubic interpolation. It has greater accuracy but is more computationally expensive than the trapezoidal method, which only enforces dynamics at the start and end with linear interpolation. A full explanation of the methods is provided in the Theory Development Chapter 3.

The **Hermite-Simpson direct collocation** method was selected for this project due to the high accuracy needed for biomechanical movement. The total motion time  $T$  is set to 2 seconds and divided into  $N = 100$  intervals, giving a time step  $\Delta t = T/N = 0.02$ . In the Hermite-Simpson collocation method, each interval is discretized at three points: the start ( $x_k$ ), the midpoint ( $x_m$ ), and the end ( $x_{k+1}$ ). A code snippet is shown in Figure 5.1. This approach was kept consistent across all stages, despite the different models and the various tests.

```
%% ----- Hermite-Simpson Collocation -----
for k = 1:N
    xk = X(:,k); xk1 = X(:,k+1);
    uk = U(:,k); uk1 = U(:,k+1);

    fk = f(xk, uk);
    fk1 = f(xk1, uk1);

    xm = (xk + xk1)/2 + (dt/8)*(fk - fk1);
    um = (uk + uk1)/2;
    fm = f(xm, um);

    opti.subject_to( xk1 == xk + dt/6*(fk + 4*fm + fk1) );
end
```

Figure 5.1: Code snippet implementing the Hermite-Simpson direct collocation method.

## 5.2 Variable Components

### 5.2.1 Model Design

The model consists of links (slender rods) and joints representing the arm segments (upper arm, forearm, and hand) and joints (shoulder, elbow, and wrist). The shoulder joint remains fixed in position but allows rotation, and all links are connected sequentially. The centre of mass (COM) of each link is assumed to be located at its midpoint. Only one arm is modelled, assuming symmetry between arms. For example, see Figures 5.2 and 5.3.

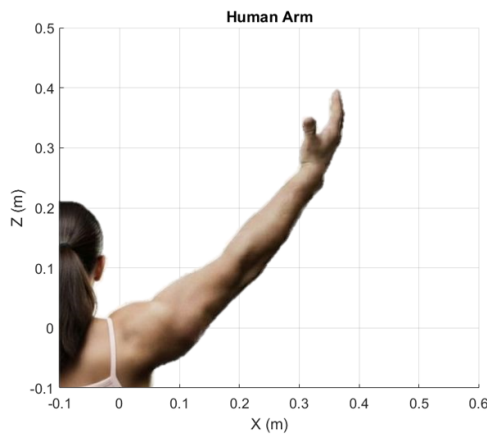


Figure 5.2: Human arm to be modelled.

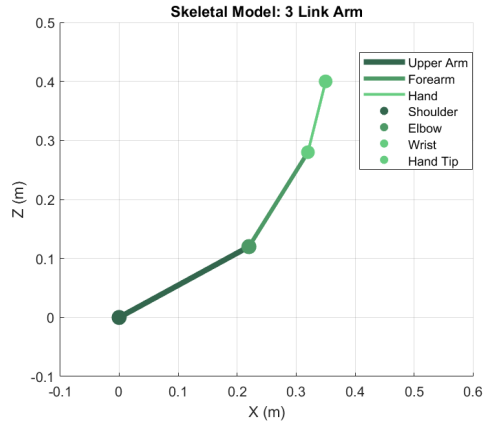


Figure 5.3: Individual links and joints of the arm model.

To obtain the equations of motion, the Newton-Euler method can be used but is often error-prone as it requires computing forces and moments for each link individually. Instead, this project uses the Lagrangian approach, which derives the equations from the system's kinetic and potential energy. Further details on model dynamics are provided in Chapter 3.

In Stage 1, the model evolves from a 2D 3DoF structure with three links and three joints to a simplified 2D 2DoF model with two links and two joints, each with one degree of freedom. The wrist and hand are removed for simplicity. The model design and development are discussed further in Chapter 6. In Stage 2, a 3D 3DoF model is developed, consisting of two links and two joints. The shoulder joint has two degrees of freedom, while the elbow joint has one. The model design and development are discussed further in Chapter 7. For the clinical application examples, the Stage 2 model is used.

### 5.2.2 Anthropometric Parameters

The anthropometric parameters are based on average female body proportions.

A total body mass of **67.8 kg** was selected based on South African population data [46]. Segmental mass distribution assigns **3.0695%** of body mass to the upper arm (Link 1), **1.7035%** to the forearm (Link 2), and **0.8065%** to the hand (Link 3) [47]. Segment lengths were taken as  $L_1 = 0.3012 \text{ m}$ ,  $L_2 = 0.2342 \text{ m}$ , and  $L_3 = 0.0586 \text{ m}$  [21]. Moments of inertia were estimated using the slender-rod approximation,  $I = \frac{1}{12}mL^2$ .

## 5.2. VARIABLE COMPONENTS

For body proportion tests, the forearm length ( $L_2$ ) and hand length ( $L_3$ ) must be kept constant, while the upper arm length ( $L_1$ ) is varied according to standard deviation:  $-2\sigma$ ,  $-1\sigma$ , mean,  $+1\sigma$ , and  $+2\sigma$ , defined as

$$L_{1,\text{values}} = L_{1,\text{mean}} + [-2, -1, 0, 1, 2] \cdot L_{1,\text{std.}}$$

For grip width tests, the biacromial diameter was taken as 0.35306 m [48]. Grip widths were calculated as percentages of the biacromial diameter, where 100% represents a narrow grip and 180% represents a wide grip.

### 5.2.3 Boundary Conditions

The motion begins with the forearm positioned perpendicular to the bar and stationary above the chest, and ends with the bar fully extended and held stationary above the shoulders. Figures 5.4 and 5.5 illustrate the general start and end positions. The initial and final angular velocities are always kept as zero. The initial and final angles for the shoulder pitch, elbow, and wrist are defined for each test.

Only the initial value of the shoulder yaw angle is specified. As the bar is lifted, the yaw angle is allowed to decrease to maintain a constant grip width throughout the motion. A constraint is included to enforce this condition; therefore, to avoid over-constraining the problem, the final shoulder yaw angle is left free and determined by the solver. This constraint is introduced in Stage 2 (Chapter 7) and will be explained in further detail there. It should also be noted that, for the grip width tests, the initial shoulder yaw angle is also determined by the solver.

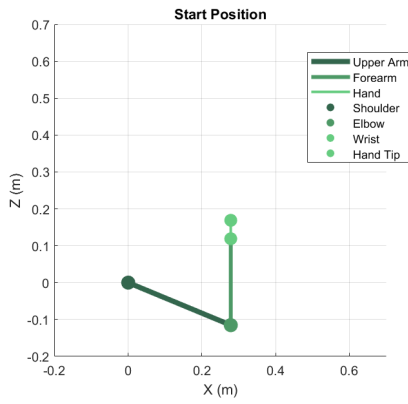


Figure 5.4: Start position: forearm perpendicular to the bar above the chest.

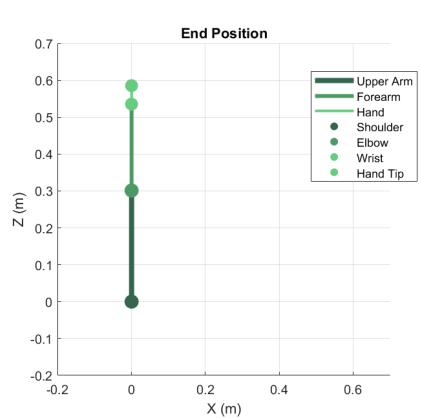


Figure 5.5: End position: bar extended above the shoulders.

However, not all models include every joint or DoF, so some boundary conditions are omitted where the corresponding joint or DoF is not present. The values used in each test are presented in Stage 1 Chapter 6, Stage 2 Chapter 7 and Clinical Application Chapter 8.

### 5.2.4 Control and Path Constraints

Joint angular velocities were limited to  $v_{\text{lim}} = 2 \text{ rad/s}$ , which closely resemble typical training speeds [49].

Joint torques were bounded by  $\tau_{\text{max}} = 40 \text{ Nm}$ . Although torque limits depend on individual strength (outside the scope of this project), a standard value of 40 Nm was chosen to allow the solver to fully utilize the torques if necessary. The optimization objective minimizes joint torques, with weighting factors which is discussed in Subsection 5.2.5.

For the different model configurations, joint rotation limits were defined to reflect realistic human arm motion. Although not all models include every joint or DoF, all possible constraints are listed for completeness. The shoulder allows two rotational axes, while the elbow and wrist each allow one. The specified ranges of motion are:

$$\begin{aligned} 0 &\leq \text{shoulder}_{yaw} \leq \frac{\pi}{2}, \\ -\frac{\pi}{8} &\leq \text{shoulder}_{pitch} \leq \frac{\pi}{2}, \\ 0 &\leq \text{elbow} \leq \pi, \\ -\frac{\pi}{2} &\leq \text{wrist} \leq \frac{\pi}{2}. \end{aligned}$$

To prevent the hand from moving behind the head, the horizontal position is constrained  $asx_{\text{hand}} \geq 0$ . An additional constraint is added in Stage 2 Chapter 7 to ensure that the hands remain fixed on the bar, maintaining a constant grip width throughout the lift.

### 5.2.5 Objective Function Design

The objective function minimises control effort while promoting smooth and realistic motion. For each interval  $k = 1, 2, \dots, N$ , it is defined as:

$$J = J + \frac{\Delta t}{6} (u_k^\top W u_k + 4u_m^\top W u_m + u_{k+1}^\top W u_{k+1}) + \lambda_1 \|u_{k+1} - u_k\|^2 + \lambda_2 (\dot{\theta}_{1,k}^2 + \dot{\theta}_{2,k}^2 + \dot{\theta}_{3,k}^2)$$

where  $u_k$ ,  $u_m$ , and  $u_{k+1}$  are the control inputs at the start, midpoint, and end of each interval. The objective function has three terms. **Term 1** minimises control effort using weighted joint torques. **Term 2** penalises rapid torque changes between intervals to encourage smooth control. **Term 3** penalises large joint angular velocities to maintain biomechanically realistic motion. For the grip width tests, a soft constraint is introduced as the fourth term. It is used to maintain a straight bar path so the effect of grip width can be analysed independently. This term is further explained in Stage 2 (Chapter 7).

The weighting matrix is defined as

$$W = \text{diag}(w_{\text{shoulder,yaw}}, w_{\text{shoulder,pitch}}, w_{\text{elbow}}, w_{\text{wrist}}),$$

which allows penalising specific joint torques which will be useful for investigating Research Questions 1 and 3. Once again, all possible joints and DoF are included but will not be used in all models.

### 5.2.6 Initial Guess

For the initial guess, the joint angles were linearly interpolated between the start and end positions for each degree of freedom using:

$$\theta = \text{linspace}(\theta_i, \theta_f, N + 1),$$

where  $\theta_i$  and  $\theta_f$  are the initial and final joint angles, respectively. This provides a straight-line approximation of motion for the solver to refine. For the grip width tests, the shoulder yaw angle was initially set to zero, allowing the solver to adjust it dynamically and determine the optimal grip width during optimisation. For all tests, the initial guess for joint angular velocities is set to zero.

# Chapter 6

## Stage 1: 2D Arm Motion

The design and development of the model and trajectory optimisation framework followed an iterative process. Each iteration modified some or all of the variable components to conduct the different tests. For each test, an initial iteration was developed to obtain results. The results are discussed and compared to literature to validate the design and ensure its suitability for clinical application. If the results were inaccurate, the variable components were refined in another iteration before proceeding to the next test.

This is an iterative design process where tests are conducted sequentially. The variable components listed below are assumed to remain the same as in the previous test unless otherwise specified in the current test:

- Model Design
- Anthropometric Parameters
- Boundary Conditions
- Control and Path Constraints
- Objective Function Design
- Initial Guess

The collocation error measures how well the discretized trajectory satisfies the continuous dynamics. Small errors indicate a dynamically consistent trajectory, while larger errors suggest insufficient discretization or incomplete solver convergence. The largest collocation error is on the order of  $10^{-8}$ , confirming all tests are accurate and reliable.

Please note: Only the figures relevant for analysis are shown in this chapter. All additional figures for each test can be found in Appendix C.

## 6.1 Test A1.1

Find bar path with narrow grip width and constant elbow flare.

### 6.1.1 Iteration 1: Problem Formulation

#### Model A Design

Pitch, yaw, and roll correspond to rotations about the  $y$ -,  $z$ -, and  $x$ -axes, respectively. The joint angles are defined as  $\theta_1$  for shoulder pitch,  $\theta_2$  for elbow pitch, and  $\theta_3$  for wrist pitch.  $\theta_1$  is measured relative to the global  $x$ -axis, while  $\theta_2$  and  $\theta_3$  are measured relative to the preceding link, as shown in Figure 6.1. The local coordinate system for each link is defined with the  $z$ -axis (red) and  $x$ -axis (pink) located at the joint, as shown in Figure 6.2. In this model all joints rotate about the  $y$ -axis (blue), which is not visible in the figure but points out of the page.

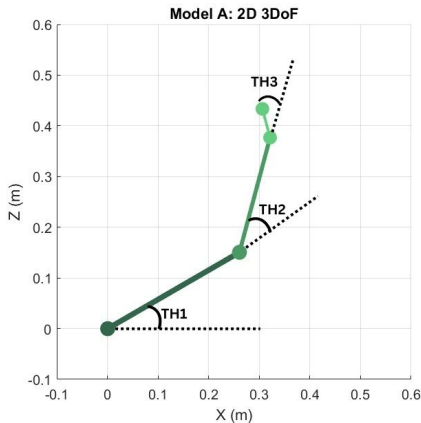


Figure 6.1: Joint angles defined for shoulder, elbow, and wrist.

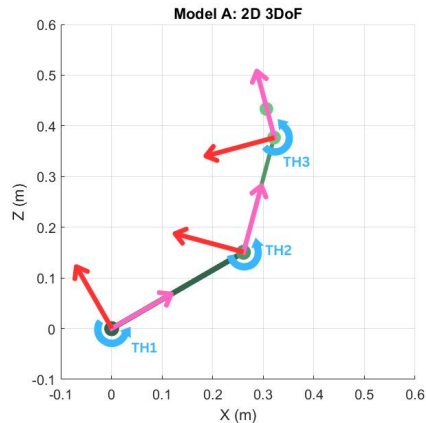


Figure 6.2: Local coordinate axes for each link.

#### Anthropometric Parameters

Total body mass of  $M = 67.8 \text{ kg}$ .

$$\begin{aligned} \text{Link 1 (Upper Arm): } & m_1 = 0.030695 M, \quad L_1 = 0.3012 \text{ m}, \\ \text{Link 2 (Forearm): } & m_2 = 0.017035 M, \quad L_2 = 0.2342 \text{ m}, \\ \text{Link 3 (Hand): } & m_3 = 0.008065 M, \quad L_3 = 0.0586 \text{ m}. \end{aligned}$$

## 6.1. TEST A1.1

Moments of inertia were estimated using the slender-rod approximation,  $I = \frac{1}{12}mL^2$ .

### Boundary Conditions

The boundary conditions for the trajectory optimisation are defined as follows:

Initial:

$$\theta_1 = -\frac{\pi}{8}, \quad \dot{\theta}_1 = 0, \quad \theta_2 = \frac{5\pi}{8}, \quad \dot{\theta}_2 = 0, \quad \theta_3 = 0, \quad \dot{\theta}_3 = 0.$$

Final:

$$\theta_1 = \frac{\pi}{2}, \quad \dot{\theta}_1 = 0, \quad \theta_2 = 0, \quad \dot{\theta}_2 = 0, \quad \theta_3 = 0, \quad \dot{\theta}_3 = 0.$$

### Control and Path Constraints

Joint velocities were limited to 2 m/s and torques to 40 Nm. The joints were constrained to the following ranges of motion:

$$\begin{aligned} -\frac{\pi}{8} &\leq \text{shoulder} \leq \frac{\pi}{2}, \\ 0 &\leq \text{elbow} \leq \pi, \\ -\frac{\pi}{2} &\leq \text{wrist} \leq \frac{\pi}{2}. \end{aligned}$$

To prevent the hand from moving behind the head, the horizontal position is constrained as

$$x_{\text{hand}} \geq 0.$$

### Objective Function Design

The objective function, as previously described, is:

$$J = J + \frac{\Delta t}{6} (u_k^\top W u_k + 4u_m^\top W u_m + u_{k+1}^\top W u_{k+1}) + \lambda_1 \|u_{k+1} - u_k\|^2 + \lambda_2 (\dot{\theta}_{1,k}^2 + \dot{\theta}_{2,k}^2 + \dot{\theta}_{3,k}^2)$$

For this test there is equal shoulder and elbow protection so the weighting matrix is

defined as:

$$W = \text{diag}(w_{\text{shoulder}} = 1, w_{\text{elbow}} = 1, w_{\text{wrist}} = 1),$$

## Initial Guess

The initial guess for joint angles  $(\theta_1, \theta_2, \theta_3)$  is a straight-line interpolation between the initial and final values:

$$\theta = \text{linspace}(\theta_i, \theta_f, N + 1)$$

The initial guess for joint angular velocities is set to zero.

### 6.1.2 Iteration 1: Results and Discussion

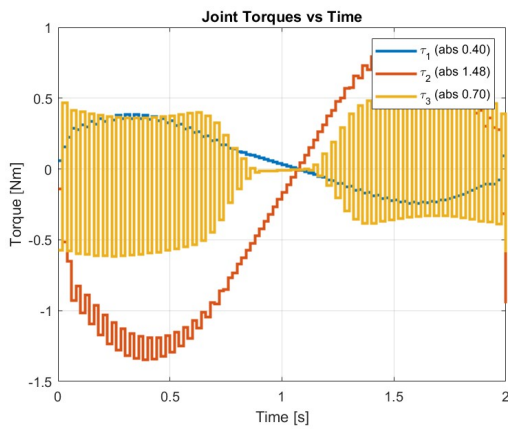


Figure 6.3: Computed joint torques for shoulder, elbow, and wrist.

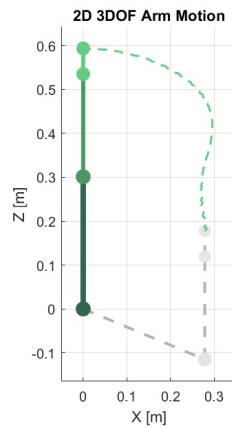


Figure 6.4: Bar path for Test A1.1.

The shoulder and elbow torques appear reasonable throughout the lift. However, the wrist torque exhibits significant volatility seen in Figure 6.3. This is reflected in the bar path seen in Figure 6.4. Attempts to reduce the wrist's range of motion led to solver convergence issues. Consequently, the wrist and hand were removed in the subsequent iteration. This simplification is justified, as the wrist is expected to remain stationary during the lift.

### 6.1.3 Iteration 2: Problem Formulation

#### Model A Design

The design of Model A is nearly identical to the previous iteration, with the wrist and hand removed. The joint angles for the shoulder and elbow are shown in Figure 6.5, while the local coordinate axes for each link are illustrated in Figure 6.6.

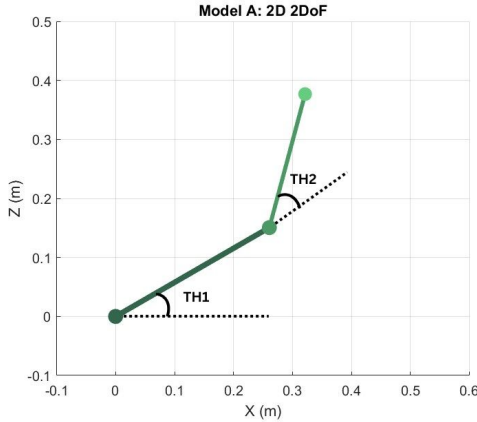


Figure 6.5: Joint angles defined for shoulder and elbow.

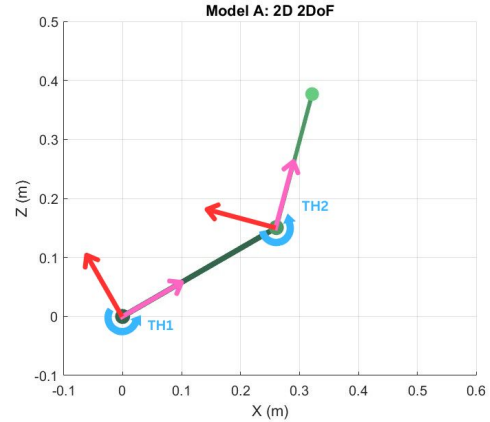


Figure 6.6: Local coordinate axes for each link.

#### Anthropometric Parameters

Total body mass:  $M = 67.8 \text{ kg}$ .

$$\text{Link 1 (Upper Arm): } m_1 = 0.030695 M, \quad L_1 = 0.3012 \text{ m},$$

$$\text{Link 2 (Forearm): } m_2 = 0.017035 M, \quad L_2 = 0.2342 \text{ m}.$$

Moments of inertia were estimated using the slender-rod approximation,  $I = \frac{1}{12}mL^2$ .

#### Boundary Conditions

Initial:

$$\theta_1 = -\frac{\pi}{8}, \quad \dot{\theta}_1 = 0, \quad \theta_2 = \frac{5\pi}{8}, \quad \dot{\theta}_2 = 0.$$

Final:

$$\theta_1 = \frac{\pi}{2}, \quad \dot{\theta}_1 = 0, \quad \theta_2 = 0, \quad \dot{\theta}_2 = 0.$$

## Control and Path Constraints

Joint velocities were limited to 2 m/s and torques to 40 Nm. The joints were limited to the following ranges of motion:

$$\begin{aligned} -\frac{\pi}{8} &\leq \text{shoulder} \leq \frac{\pi}{2}, \\ 0 &\leq \text{elbow} \leq \pi. \end{aligned}$$

To prevent the hand from moving behind the head, the horizontal position is constrained as

$$x_{\text{hand}} \geq 0.$$

## Objective Function Design

The objective function is:

$$J = J + \frac{\Delta t}{6} (u_k^\top W u_k + 4u_m^\top W u_m + u_{k+1}^\top W u_{k+1}) + \lambda_1 \|u_{k+1} - u_k\|^2 + \lambda_2 (\dot{\theta}_{1,k}^2 + \dot{\theta}_{2,k}^2)$$

Weighting matrix:

$$W = \text{diag}(w_{\text{shoulder}} = 1, w_{\text{elbow}} = 1).$$

## Initial Guess

The initial guess for joint angles  $(\theta_1, \theta_2)$  is a straight-line interpolation:

$$\theta = \text{linspace}(\theta_i, \theta_f, N + 1)$$

Initial joint angular velocities are set to zero.

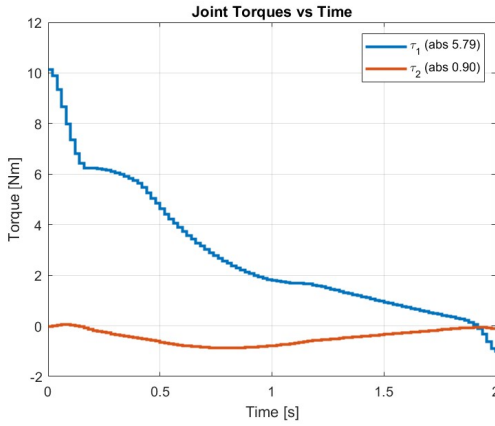


Figure 6.7: Computed joint torques for shoulder and elbow.

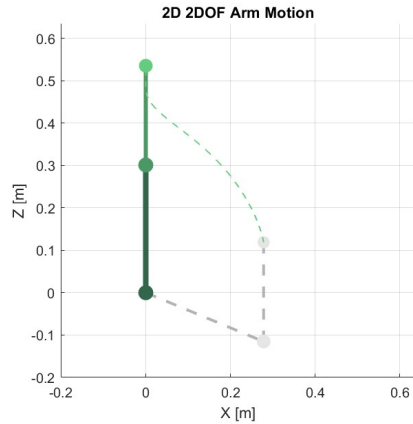


Figure 6.8: Bar path for Test A1.1.

### 6.1.4 Iteration 2: Results and Discussion

The shoulder and elbow torques, shown in Figure 6.7, remain within reasonable limits throughout the lift, with absolute torque efforts of  $t_1 = 5.79$  and  $t_2 = 0.90$ . The bar path shown in Figure 6.8 is relatively straight with a slight J-curve, which aligns with literature findings: a straight path helps protect the elbow and a curved path protects the shoulder. The observed trajectory represents a compromise between these two objectives as the shoulder and elbow are equally protected in this test.

## 6.2 Test A1.2

Find bar path when protecting the shoulder with narrow grip width and constant elbow flare.

### 6.2.1 Problem Formulation

#### Objective Function Design

The objective function is:

$$J = J + \frac{\Delta t}{6} (u_k^\top W u_k + 4u_m^\top W u_m + u_{k+1}^\top W u_{k+1}) + \lambda_1 \|u_{k+1} - u_k\|^2 + \lambda_2 (\dot{\theta}_{1,k}^2 + \dot{\theta}_{2,k}^2)$$

The weighting matrix includes a heavier penalty for shoulder torque:

$$W = \text{diag} (w_{\text{shoulder}} = 10, w_{\text{elbow}} = 1) .$$

### 6.2.2 Results and Discussion

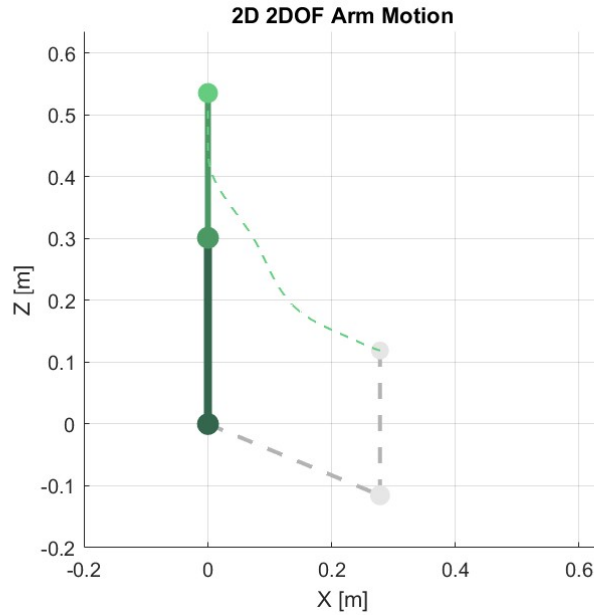


Figure 6.9: Bar path for Test A1.2.

In the previous test, where the shoulder and elbow are equally protected, the absolute torque efforts were  $t_1 = 5.79$  and  $t_2 = 0.90$ . In this test the absolute torque efforts are  $t_1 = 5.11$  and  $t_2 = 1.16$ . The shoulder torque decreases as expected while the elbow torque increases. The bar path in Figure 6.9 follows a typical J-curve, consistent with literature findings that such a path reduces shoulder loading by moving the bar closer to the joint early in the lift.

## 6.3 Test A1.3

Find bar path when protecting the elbow with narrow grip width and constant elbow flare.

### 6.3.1 Problem Formulation

#### Objective Function Design

The objective function is:

$$J = J + \frac{\Delta t}{6} (u_k^\top W u_k + 4u_m^\top W u_m + u_{k+1}^\top W u_{k+1}) + \lambda_1 \|u_{k+1} - u_k\|^2 + \lambda_2 (\dot{\theta}_{1,k}^2 + \dot{\theta}_{2,k}^2)$$

The weighting matrix includes a heavier penalty for elbow torque:

$$W = \text{diag}(w_{\text{shoulder}} = 1, w_{\text{elbow}} = 10).$$

### 6.3.2 Results and Discussion

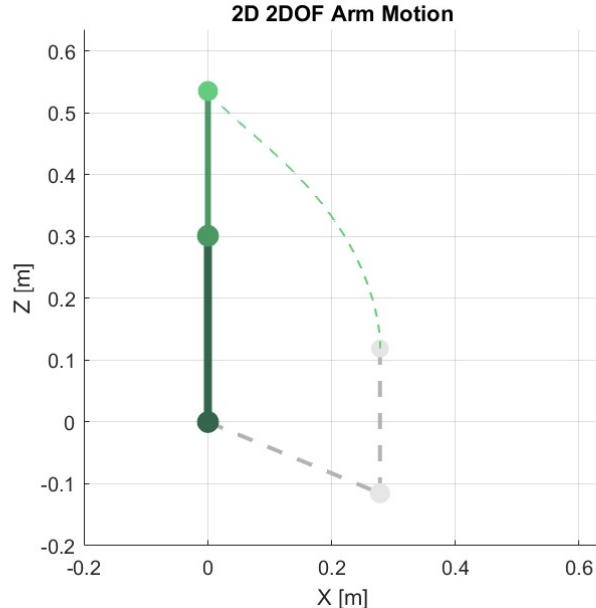


Figure 6.10: Bar path for Test A1.3.

In Test A1.1, where the shoulder and elbow are equally protected, the absolute torque efforts were  $t_1 = 5.79$  and  $t_2 = 0.90$ . In this test, the absolute torque efforts are  $t_1 = 5.90$  and  $t_2 = 0.61$ . The elbow torque decreases as expected while the shoulder torque increases. The bar path in Figure 6.10 follows a straight line, consistent with literature findings that such a path reduces elbow torque by limiting elbow motion and emphasizing shoulder-driven movement.

## 6.4 Test A2.1

Find bar path variation for different brachial indices with narrow grip width and constant elbow flare.

### 6.4.1 Problem Formulation

#### Anthropometric Parameters

Total body mass:  $M = 67.8 \text{ kg}$ . To test different brachial indices,  $L_1$  is varied while  $L_2$  remains constant.

Link 1 (Upper Arm):  $m_1 = 0.030695 M$ ,  $L_1 = L_{1,\text{mean}} + [-2, -1, 0, 1, 2] \cdot L_{1,\text{std}} \text{ m}$ ,

Link 2 (Forearm):  $m_2 = 0.017035 M$ ,  $L_2 = 0.2342 \text{ m}$ .

where  $L_{1,\text{mean}} = 0.3012 \text{ m}$  and  $L_{1,\text{std}} = 0.0166 \text{ m}$ . Moments of inertia were estimated using the slender-rod approximation,  $I = \frac{1}{12}mL^2$ .

#### Objective Function Design

The objective function is:

$$J = J + \frac{\Delta t}{6} (u_k^\top W u_k + 4u_m^\top W u_m + u_{k+1}^\top W u_{k+1}) + \lambda_1 \|u_{k+1} - u_k\|^2 + \lambda_2 (\dot{\theta}_{1,k}^2 + \dot{\theta}_{2,k}^2)$$

The weighting matrix with equal protection for shoulder and elbow torque:

$$W = \text{diag}(w_{\text{shoulder}} = 1, w_{\text{elbow}} = 1).$$

### 6.4.2 Results and Discussion

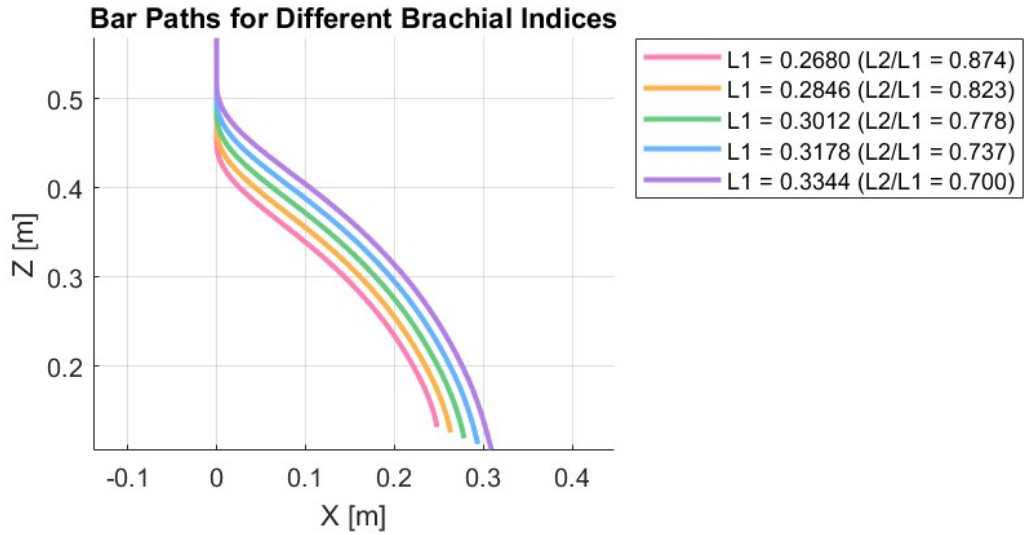


Figure 6.11: Bar paths of different brachial indices for Test A2.1.

As the brachial index increases, the absolute shoulder torque effort rises from  $t_{\text{pink}} = 5.22$  to  $t_{\text{purple}} = 6.38$ , while the absolute elbow torque effort increases more modestly from  $t_{\text{pink}} = 0.87$  to  $t_{\text{purple}} = 0.93$ . This indicates that, for the same lift, a longer upper arm demands greater torque effort. These results support findings in the literature that a longer upper arm is negatively correlated with performance. As shown in Figure 6.11, all bar paths are relatively straight with a slight J-curve shape. This consistent shape indicates that variations in body proportions have minimal effect on the overall bar path shape.

# Chapter 7

## Stage 2: 3D Arm Motion

Stage 2 builds upon Stage 1, extending the model and trajectory optimisation framework to include shoulder yaw for grip width analysis. The same iterative design process described in Stage 1 was followed, with updates made only to the relevant variable components for each test.

### 7.1 Test B1.1

Find bar path with narrow grip width and constant elbow flare.

#### 7.1.1 Problem Formulation

##### Model B Design

The joint angles are defined as  $\theta_1$  for shoulder yaw,  $\theta_2$  for shoulder pitch, and  $\theta_3$  for elbow pitch.  $\theta_1$  and  $\theta_2$  are measured relative to the global axes and  $\theta_3$  is measured relative to the preceding link, as shown in Figure 7.1 and 7.2. The local coordinate system for each link is defined with the  $x$ -axis (pink),  $y$ -axis (blue), and  $z$ -axis (red), positioned at each joint, as illustrated in Figure 7.3.  $\theta_1$  rotates about the  $z$ -axis, while  $\theta_2$  and  $\theta_3$  rotate about the  $y$ -axis.

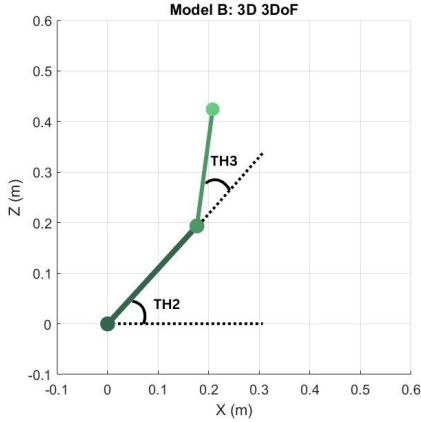


Figure 7.1: Joint angles for shoulder pitch and elbow pitch in the  $z$ - $x$  plane.

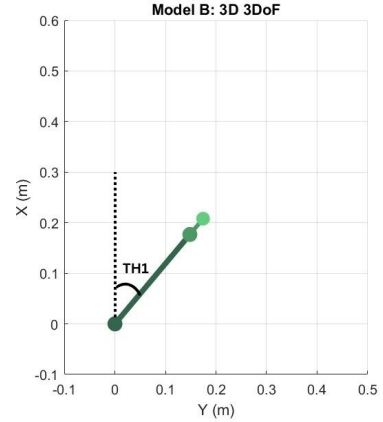


Figure 7.2: Joint angle for shoulder yaw in the  $x$ - $y$  plane.

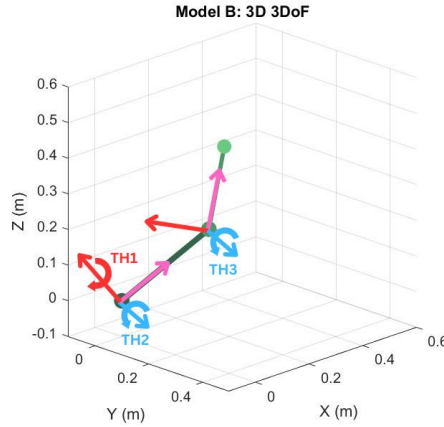


Figure 7.3: Local coordinate axes for each link.

## Anthropometric Parameters

Total body mass:  $M = 67.8 \text{ kg}$ .

Link 1 (Upper Arm):  $m_1 = 0.030695 M$ ,  $L_1 = 0.3012 \text{ m}$ ,

Link 2 (Forearm):  $m_2 = 0.017035 M$ ,  $L_2 = 0.2342 \text{ m}$ .

Moments of inertia were estimated using the slender-rod approximation,  $I = \frac{1}{12}mL^2$ .

The biacromial diameter is 0.35306 m. Grip widths were calculated as percentages of the biacromial diameter, where 100% represents a narrow grip and 180% represents a wide grip.

## Boundary Conditions

For a narrow grip width,  $\alpha$  represents the grip width angle at **100%** of the biacromial diameter.

Initial:

$$\theta_1 = \alpha, \quad \dot{\theta}_1 = 0, \quad \theta_2 = -\frac{\pi}{8}, \quad \dot{\theta}_2 = 0, \quad \theta_3 = \frac{5\pi}{8}, \quad \dot{\theta}_3 = 0.$$

Final:

$$\dot{\theta}_1 = 0, \quad \theta_2 = \frac{\pi}{2}, \quad \dot{\theta}_2 = 0, \quad \theta_3 = 0, \quad \dot{\theta}_3 = 0.$$

## Control and Path Constraints

Joint velocities were limited to 2 m/s and torques to 40 Nm. The joints were limited to the following ranges of motion:

$$\begin{aligned} 0 &\leq \text{shoulder yaw} \leq \frac{\pi}{2}, \\ -\frac{\pi}{8} &\leq \text{shoulder pitch} \leq \frac{\pi}{2}, \\ 0 &\leq \text{elbow pitch} \leq \pi. \end{aligned}$$

To prevent the hand from moving behind the head, the hand position is constrained as

$$x_{\text{hand}} \geq 0.$$

## Objective Function Design

The objective function is:

$$J = J + \frac{\Delta t}{6} (u_k^\top W u_k + 4u_m^\top W u_m + u_{k+1}^\top W u_{k+1}) + \lambda_1 \|u_{k+1} - u_k\|^2 + \lambda_2 (\dot{\theta}_{1,k}^2 + \dot{\theta}_{2,k}^2)$$

The weighting matrix with equal protection for shoulder and elbow torque:

$$W = \text{diag}(w_{\text{shoulder yaw}} = 1, w_{\text{shoulder pitch}} = 1, w_{\text{elbow pitch}} = 1).$$

## Initial Guess

The initial guess for joint angles  $(\theta_1, \theta_2, \theta_3)$  is a straight-line interpolation:

$$\theta = \text{linspace}(\theta_i, \theta_f, N + 1)$$

$\theta_f$  for shoulder yaw is not defined so it is roughly estimated to be  $\theta_i/2$  for the initial guess. Initial joint angular velocities are set to zero.

### 7.1.2 Results and Discussion

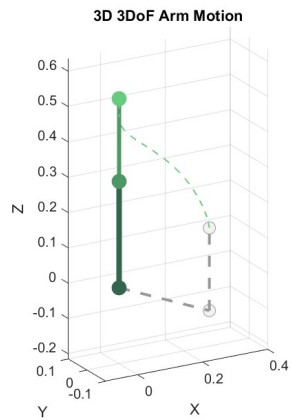


Figure 7.4: Bar path for Test B1.1.

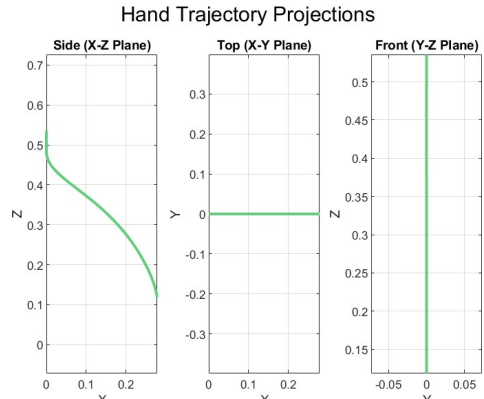


Figure 7.5: Hand trajectory projections in each plane.

The absolute torque efforts are  $t_1 = 0$ ,  $t_2 = 5.78$ , and  $t_3 = 0.90$  which match the results obtained for the 2D model in Test A1.1. The 3D bar path is shown in Figure 7.4 and the hand trajectory projections in Figure 7.5 provide a clear visualisation of the motion in each plane. The bar path follows a relatively straight trajectory with a slight J-curve, consistent with literature findings and Test A1.1 results. These results confirm that the 3D model successfully replicates the 2D model's behaviour, validating its implementation and accuracy.

## 7.2 Test B1.2

Find bar path when protecting the shoulder with narrow grip width and constant elbow flare.

### 7.2.1 Problem Formulation

#### Objective Function Design

The objective function is:

$$J = J + \frac{\Delta t}{6} (u_k^\top W u_k + 4u_m^\top W u_m + u_{k+1}^\top W u_{k+1}) + \lambda_1 \|u_{k+1} - u_k\|^2 + \lambda_2 (\dot{\theta}_{1,k}^2 + \dot{\theta}_{2,k}^2)$$

Weighting matrix includes a heavier penalty for shoulder torques:

$$W = \text{diag}(w_{\text{shoulder yaw}} = 5, w_{\text{shoulder pitch}} = 5, w_{\text{elbow pitch}} = 1).$$

### 7.2.2 Results and Discussion

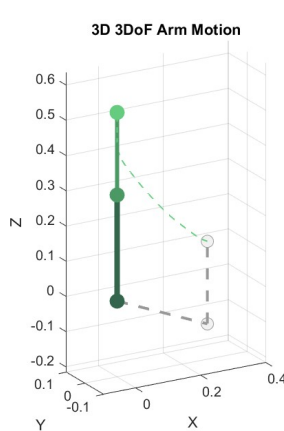


Figure 7.6: Bar path for Test B1.2.

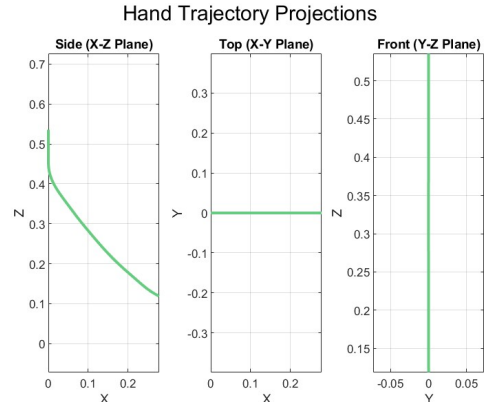


Figure 7.7: Hand trajectory projections in each plane.

In the previous test, where the shoulder and elbow are equally protected, the absolute torque efforts were  $t_1 = 0$ ,  $t_2 = 5.78$ , and  $t_3 = 0.90$ . In this test, the absolute torque efforts are  $t_1 = 0$ ,  $t_2 = 5.22$ , and  $t_3 = 1.11$  which match the results obtained for the 2D model in Test A1.2. The shoulder torque decreases as expected while the elbow torque

increases. The bar path seen in Figure 7.6 and Figure 7.7 follows a typical J-curve, consistent with literature findings and Test A1.2 results. These results confirm that the 3D model successfully replicates the 2D model's behaviour.

## 7.3 Test B1.3

Find bar path when protecting the elbow with narrow grip width and constant elbow flare.

### 7.3.1 Problem Formulation

#### Objective Function Design

The objective function is:

$$J = J + \frac{\Delta t}{6} (u_k^\top W u_k + 4u_m^\top W u_m + u_{k+1}^\top W u_{k+1}) + \lambda_1 \|u_{k+1} - u_k\|^2 + \lambda_2 (\dot{\theta}_{1,k}^2 + \dot{\theta}_{2,k}^2)$$

Weighting matrix includes a heavier penalty for elbow torque:

$$W = \text{diag}(w_{\text{shoulder yaw}} = 1, w_{\text{shoulder pitch}} = 1, w_{\text{elbow pitch}} = 5).$$

### 7.3.2 Results and Discussion

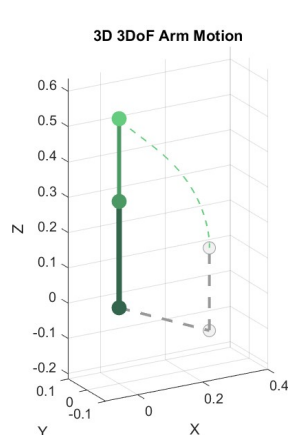


Figure 7.8: Bar path for Test B1.3.

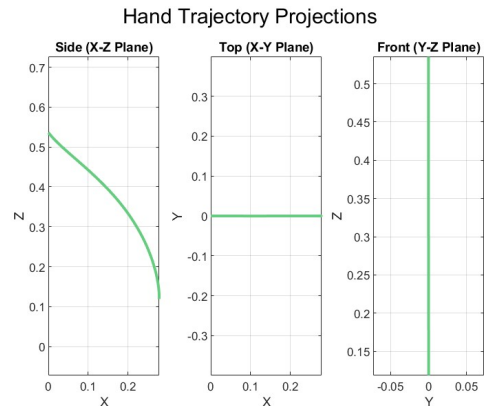


Figure 7.9: Hand trajectory projections in each plane.

In Test B1.1, where the shoulder and elbow are equally protected, the absolute torque efforts were  $t_1 = 0$ ,  $t_2 = 5.78$ , and  $t_3 = 0.90$ . In this test, the absolute torque efforts are  $t_1 = 0$ ,  $t_2 = 5.89$ , and  $t_3 = 0.60$  which match the results obtained for the 2D model in Test A1.3. The elbow torque decreases as expected while the shoulder torque increases. The bar path seen in Figure 7.6 and Figure 7.7 follows a typical straight line, consistent with literature findings and Test A1.3 results. These results confirm that the 3D model successfully replicates the 2D model's behaviour.

## 7.4 Test B1.4

Find bar path with wide grip width and constant elbow flare.

### 7.4.1 Iteration 1: Problem Formulation

#### Boundary Conditions

For a wide grip width,  $\alpha$  represents the grip width angle at **180%** of the biacromial diameter.

Initial:

$$\theta_1 = \alpha, \quad \dot{\theta}_1 = 0, \quad \theta_2 = -\frac{\pi}{8}, \quad \dot{\theta}_2 = 0, \quad \theta_3 = \frac{5\pi}{8}, \quad \dot{\theta}_3 = 0.$$

Final:

$$\dot{\theta}_1 = 0, \quad \theta_2 = \frac{\pi}{2}, \quad \dot{\theta}_2 = 0, \quad \theta_3 = 0, \quad \dot{\theta}_3 = 0.$$

#### Objective Function Design

The objective function is:

$$J = J + \frac{\Delta t}{6} (u_k^\top W u_k + 4u_m^\top W u_m + u_{k+1}^\top W u_{k+1}) + \lambda_1 \|u_{k+1} - u_k\|^2 + \lambda_2 (\dot{\theta}_{1,k}^2 + \dot{\theta}_{2,k}^2)$$

The weighting matrix with equal penalties for shoulder and elbow torque:

$$W = \text{diag}(w_{\text{shoulder yaw}} = 1, w_{\text{shoulder pitch}} = 1, w_{\text{elbow pitch}} = 1).$$

### 7.4.2 Iteration 1: Results and Discussion

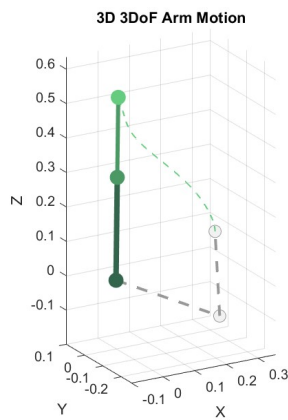


Figure 7.10: Bar path for Test B1.4.

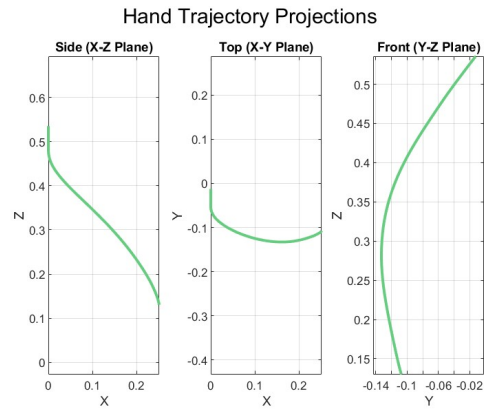


Figure 7.11: Hand trajectory projections in each plane.

A clear issue is immediately evident: the  $y$ -position of the hand changes significantly as seen in Figure C.18. This is incorrect, as the hand should remain fixed in the  $y$ -plane to represent the grip width on the bar, which does not change throughout the lift. To address this, a constraint enforcing a constant  $y$ -position is introduced in the subsequent iteration.

### 7.4.3 Iteration 2: Problem Formulation

#### Control and Path Constraints

Joint velocities were limited to 2 m/s and torques to 40 Nm. The joints were limited to the following ranges of motion:

$$\begin{aligned} 0 &\leq \text{shoulder yaw} \leq \frac{\pi}{2}, \\ -\frac{\pi}{8} &\leq \text{shoulder pitch} \leq \frac{\pi}{2}, \\ 0 &\leq \text{elbow pitch} \leq \pi. \end{aligned}$$

To prevent the hand from moving behind the head, the hand position is constrained as

$$x_{\text{hand}} \geq 0.$$

To keep the grip width on the bar constant and to allow convergence, a soft constraint is added as

$$y_{\text{hand}} - y_{\text{initial hand}} \leq 1e-2.$$

#### 7.4.4 Iteration 2: Results and Discussion

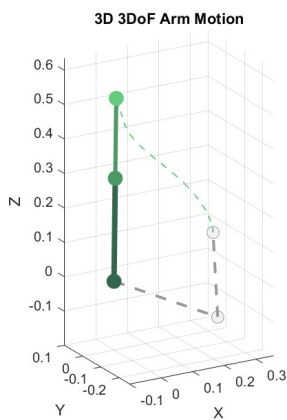


Figure 7.12: Bar path for Test B1.4.

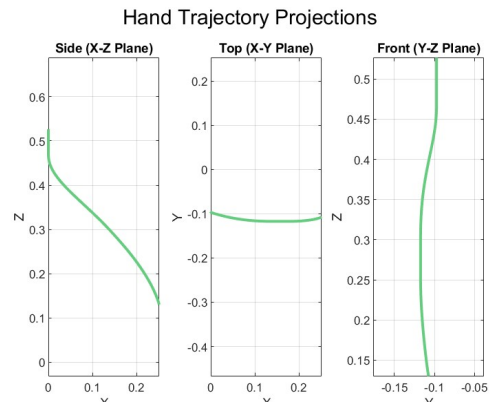


Figure 7.13: Hand trajectory projections in each plane.

The  $y$ -position of the bar remains relatively constant indicating that the grip width is maintained throughout the movement. In Test B1.1, where the shoulder and elbow are equally protected and a narrow grip width was used, the absolute torque efforts were  $t_1 = 0$ ,  $t_2 = 5.78$ , and  $t_3 = 0.90$ . In this test, the absolute torque efforts are  $t_1 = 2.53$ ,  $t_2 = 5.32$ , and  $t_3 = 0.88$ . The elbow torque remains approximately the same and the total shoulder torque increases. This is consistent with literature reporting that wider grip widths increase shoulder stress. The bar path, shown in Figures 7.12 and 7.13, follows a relatively straight trajectory with a slight J-curve which is the same shape as the bar path with a narrow grip width, as expected.

## 7.5 Test B1.5

Find bar path when protecting the shoulder with wide grip width and constant elbow flare.

### 7.5.1 Problem Formulation

#### Objective Function Design

The objective function is:

$$J = J + \frac{\Delta t}{6} (u_k^\top W u_k + 4u_m^\top W u_m + u_{k+1}^\top W u_{k+1}) + \lambda_1 \|u_{k+1} - u_k\|^2 + \lambda_2 (\dot{\theta}_{1,k}^2 + \dot{\theta}_{2,k}^2)$$

The weighting matrix with heavier penalties for shoulder torque:

$$W = \text{diag}(w_{\text{shoulder yaw}} = 5, w_{\text{shoulder pitch}} = 5, w_{\text{elbow pitch}} = 1).$$

### 7.5.2 Results and Discussion

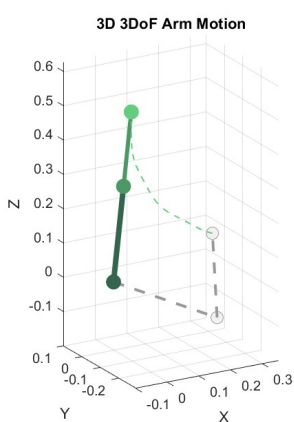


Figure 7.14: Bar path for Test B1.5.

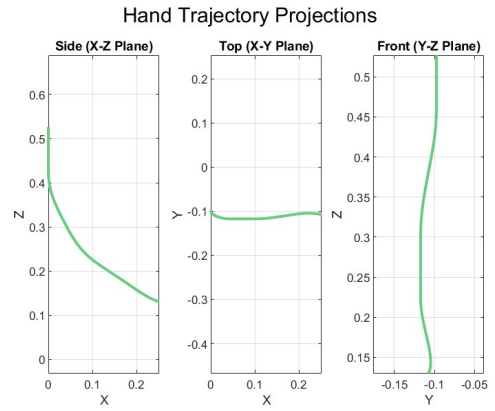


Figure 7.15: Hand trajectory projections in each plane.

In Test B1.2, where the shoulder is protected and a narrow grip width was used, the absolute torque efforts were  $t_1 = 0$ ,  $t_2 = 5.22$ , and  $t_3 = 1.11$ . In this test, the absolute torque efforts are  $t_1 = 2.83$ ,  $t_2 = 4.58$ , and  $t_3 = 1.05$ . The total shoulder torque increases from Test B1.2. This is consistent with literature reporting that wider grip widths increase shoulder stress. The bar path, shown in Figures 7.12 and 7.13, follows a J-curve which is the same shape as the bar path with a narrow grip width, as expected. In Test B1.4 where the shoulder and elbow are equally protected and a wide grip width was used, the absolute torque efforts were  $t_1 = 2.53$ ,  $t_2 = 5.32$ , and  $t_3 = 0.88$ . In this test, the total shoulder torque decreases from Test B1.4, as expected.

## 7.6 Test B1.6

Find bar path when protecting the elbow with wide grip width and constant elbow flare.

### 7.6.1 Problem Formulation

#### Objective Function Design

The objective function is:

$$J = J + \frac{\Delta t}{6} (u_k^\top W u_k + 4u_m^\top W u_m + u_{k+1}^\top W u_{k+1}) + \lambda_1 \|u_{k+1} - u_k\|^2 + \lambda_2 (\dot{\theta}_{1,k}^2 + \dot{\theta}_{2,k}^2)$$

The weighting matrix with heavier penalties for elbow torque:

$$W = \text{diag}(w_{\text{shoulder yaw}} = 1, w_{\text{shoulder pitch}} = 1, w_{\text{elbow pitch}} = 5).$$

### 7.6.2 Results and Discussion

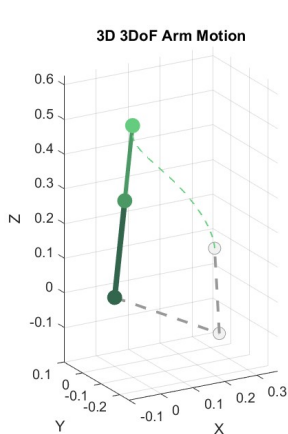


Figure 7.16: Bar path for Test B1.6.

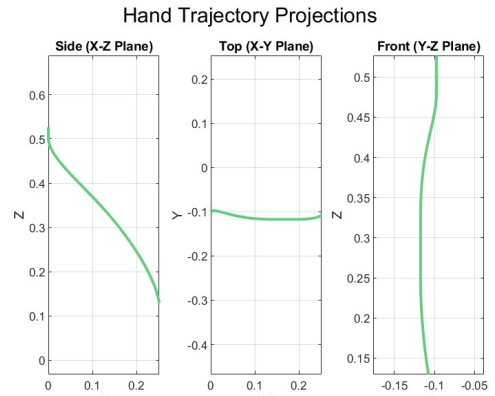


Figure 7.17: Hand trajectory projections in each plane.

In Test B1.3, where the elbow is protected and a narrow grip width was used, the absolute torque efforts were  $t_1 = 0$ ,  $t_2 = 5.89$ , and  $t_3 = 0.60$ . In this test, the absolute torque efforts are  $t_1 = 2.46$ ,  $t_2 = 5.33$ , and  $t_3 = 0.77$ . The total shoulder torque increases from Test B1.3. This is consistent with literature reporting that wider grip widths increase shoulder stress. The bar path, shown in Figures 7.12 and 7.13, follows a straight line

which is the same shape as the bar path with a narrow grip width, as expected. In Test B1.4 where the shoulder and elbow are equally protected and a wide grip width was used, the absolute torque efforts were  $t_1 = 2.53$ ,  $t_2 = 5.32$ , and  $t_3 = 0.88$ . In this test, the total elbow torque decreases from Test B1.4, as expected.

## 7.7 Test B2.1

Find bar path variation for different brachial indices with narrow grip width and constant elbow flare.

### 7.7.1 Problem Formulation

#### Anthropometric Parameters

Total body mass:  $M = 67.8$  kg. To test different brachial indices,  $L_1$  is varied while  $L_2$  remains constant.

Link 1 (Upper Arm):  $m_1 = 0.030695 M$ ,  $L_1 = L_{1,\text{mean}} + [-2, -1, 0, 1, 2] \cdot L_{1,\text{std}}$  m,

Link 2 (Forearm):  $m_2 = 0.017035 M$ ,  $L_2 = 0.2342$  m.

where  $L_{1,\text{mean}} = 0.3012$  m and  $L_{1,\text{std}} = 0.0166$  m. Moments of inertia were estimated using the slender-rod approximation,  $I = \frac{1}{12}mL^2$ .

#### Boundary Conditions

For a narrow grip width,  $\alpha$  represents the grip width angle at **100%** of the biacromial diameter.

Initial:

$$\theta_1 = \alpha, \quad \dot{\theta}_1 = 0, \quad \theta_2 = -\frac{\pi}{8}, \quad \dot{\theta}_2 = 0, \quad \theta_3 = \frac{5\pi}{8}, \quad \dot{\theta}_3 = 0.$$

Final:

$$\dot{\theta}_1 = 0, \quad \theta_2 = \frac{\pi}{2}, \quad \dot{\theta}_2 = 0, \quad \theta_3 = 0, \quad \dot{\theta}_3 = 0.$$

## Objective Function Design

The objective function is:

$$J = J + \frac{\Delta t}{6} (u_k^\top W u_k + 4u_m^\top W u_m + u_{k+1}^\top W u_{k+1}) + \lambda_1 \|u_{k+1} - u_k\|^2 + \lambda_2 (\dot{\theta}_{1,k}^2 + \dot{\theta}_{2,k}^2)$$

The weighting matrix with equal penalties for shoulder and elbow torque:

$$W = \text{diag}(w_{\text{shoulder yaw}} = 1, w_{\text{shoulder pitch}} = 1, w_{\text{elbow pitch}} = 1).$$

## 7.7.2 Results and Discussion

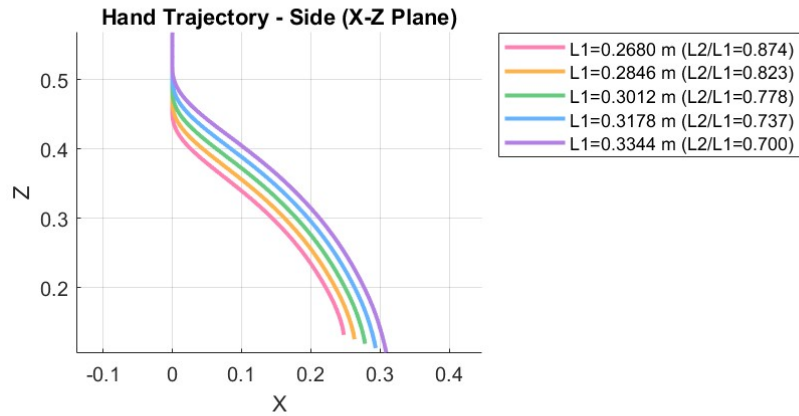


Figure 7.18: Bar paths of different brachial indices for Test B2.1.

The shoulder yaw torque is on the order of  $10^{-3}$  and is therefore considered negligible. As the brachial index increases, the absolute shoulder pitch torque effort rises from  $t_{\text{pink}} = 5.21$  to  $t_{\text{purple}} = 6.36$ , while the absolute elbow pitch torque effort increases more modestly from  $t_{\text{pink}} = 0.87$  to  $t_{\text{purple}} = 0.93$ . These values match the results obtained for the 2D model in Test A2.1. Again, this shows that a longer upper arm requires greater torque for the same lift, aligning with literature linking longer arms to reduced performance. As seen in Figure 7.18, all bar paths remain mostly straight with a slight J-curve, indicating the brachial index has little effect on bar path shape.

## 7.8 Test B2.2

Find bar path variation for different brachial indices with wide grip width and constant elbow flare.

### 7.8.1 Problem Formulation

#### Boundary Conditions

For a wide grip width,  $\alpha$  represents the grip width angle at **180%** of the biacromial diameter.

Initial:

$$\theta_1 = \alpha, \quad \dot{\theta}_1 = 0, \quad \theta_2 = -\frac{\pi}{8}, \quad \dot{\theta}_2 = 0, \quad \theta_3 = \frac{5\pi}{8}, \quad \dot{\theta}_3 = 0.$$

Final:

$$\dot{\theta}_1 = 0, \quad \theta_2 = \frac{\pi}{2}, \quad \dot{\theta}_2 = 0, \quad \theta_3 = 0, \quad \dot{\theta}_3 = 0.$$

### 7.8.2 Results and Discussion

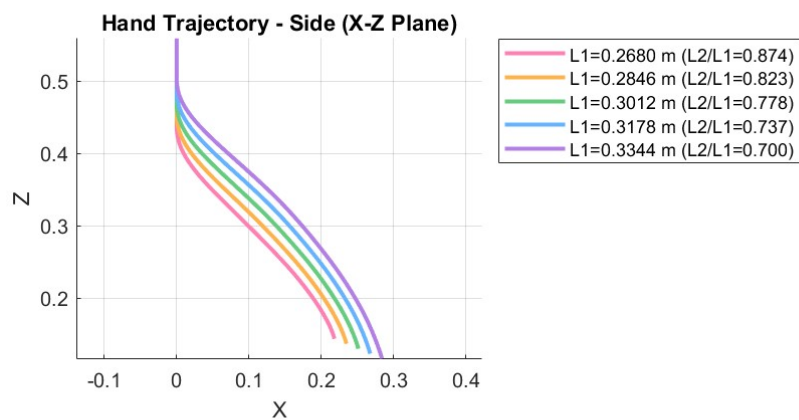


Figure 7.19: Bar paths of different brachial indices for Test B2.2.

As the brachial index increases, the absolute shoulder yaw torque effort rises from  $t_{\text{pink}} = 2.33$  to  $t_{\text{purple}} = 2.70$ , the absolute shoulder pitch torque effort rises from  $t_{\text{pink}} = 4.75$  to  $t_{\text{purple}} = 5.91$  and the absolute elbow pitch torque effort increases more modestly from  $t_{\text{pink}} = 0.85$  to  $t_{\text{purple}} = 0.91$ . Again, this shows that a longer upper arm increases torque demand, supporting literature linking it to lower performance. Figure C.46 shows that the bar paths remain straight with a slight J-curve, indicating the brachial index has minimal influence on bar path shape even with a wide grip width.

## 7.9 Test B3.1

Find grip width for a straight bar path with constant elbow flare.

### 7.9.1 Problem Formulation

#### Anthropometric Parameters

Total body mass:  $M = 67.8 \text{ kg}$ .

Link 1 (Upper Arm):  $m_1 = 0.030695 M, L_1 = 0.3012 \text{ m}$ ,

Link 2 (Forearm):  $m_2 = 0.017035 M, L_2 = 0.2342 \text{ m}$ .

Moments of inertia were estimated using the slender-rod approximation,  $I = \frac{1}{12}mL^2$ . The biacromial diameter is  $0.35306 \text{ m}$  and is used together with the optimal shoulder yaw angles to calculate the grip width.

#### Boundary Conditions

$\alpha$  represents the grip width angle chosen by the solver.

Initial:

$$\theta_1 = \alpha, \quad \dot{\theta}_1 = 0, \quad \theta_2 = -\frac{\pi}{8}, \quad \dot{\theta}_2 = 0, \quad \theta_3 = \frac{5\pi}{8}, \quad \dot{\theta}_3 = 0.$$

Final:

$$\dot{\theta}_1 = 0, \quad \theta_2 = \frac{\pi}{2}, \quad \dot{\theta}_2 = 0, \quad \theta_3 = 0, \quad \dot{\theta}_3 = 0.$$

## Objective Function Design

An additional term is introduced to encourage a constant bar path,  $((x_{\text{hand}} - x_{\text{ref}}(k))^2 + (z_{\text{hand}} - z_{\text{ref}}(k))^2)$ , allowing the effect of grip width to be isolated and analysed.  $x_{\text{ref}}$  and  $z_{\text{ref}}$  are the reference coordinates for a straight bar path. The new objective function is:

$$\begin{aligned} J = J &+ \frac{\Delta t}{6} (u_k^\top W u_k + 4u_m^\top W u_m + u_{k+1}^\top W u_{k+1}) \\ &+ \lambda_1 \|u_{k+1} - u_k\|^2 + \lambda_2 (\dot{\theta}_{1,k}^2 + \dot{\theta}_{2,k}^2) + ((x_{\text{hand}} - x_{\text{ref}}(k))^2 + (z_{\text{hand}} - z_{\text{ref}}(k))^2) \end{aligned}$$

The weighting matrix with equal penalties for shoulder and elbow torque:

$$W = \text{diag}(w_{\text{shoulder yaw}} = 1, w_{\text{shoulder pitch}} = 1, w_{\text{elbow pitch}} = 1).$$

## Initial Guess

The initial guess for joint angles ( $\theta_2, \theta_3$ ) is a straight-line interpolation:

$$\theta = \text{linspace}(\theta_i, \theta_f, N + 1)$$

The initial guess for shoulder yaw ( $\theta_1$ ) and the joint angular velocities are set to zero.

## 7.9.2 Results and Discussion

Table 7.1: Bench press joint angles and grip width for Test B3.1.

Parameter	Value
Initial angle, $\theta_i$	19.95°
Final angle, $\theta_f$	6.67°
Grip width (%)	138.44

The absolute torque efforts are  $t_1 = 1.64$ ,  $t_2 = 5.68$ , and  $t_3 = 0.90$ . Table 7.1 shows the optimal grip width determined for this test is 138.44%. This average grip width aligns with literature recommendations to protect both shoulder and elbow joints.

## 7.10 Test B3.2

Find grip width when protecting the shoulder for a straight bar path with constant elbow flare.

### 7.10.1 Problem Formulation

#### Objective Function Design

The objective function is:

$$\begin{aligned} J = J + \frac{\Delta t}{6} & (u_k^\top W u_k + 4u_m^\top W u_m + u_{k+1}^\top W u_{k+1}) \\ & + \lambda_1 \|u_{k+1} - u_k\|^2 + \lambda_2 (\dot{\theta}_{1,k}^2 + \dot{\theta}_{2,k}^2) + ((x_{\text{hand}} - x_{\text{ref}}(k))^2 + (z_{\text{hand}} - z_{\text{ref}}(k))^2) \end{aligned}$$

The weighting matrix includes a heavier penalty for shoulder yaw torque:

$$W = \text{diag}(w_{\text{shoulder yaw}} = 5, w_{\text{shoulder pitch}} = 1, w_{\text{elbow pitch}} = 1).$$

Shoulder pitch is already regulated by Term 4 of the objective function.

### 7.10.2 Results and Discussion

Table 7.2: Bench press joint angles and grip width for Test B3.2.

Parameter	Value
Initial angle, $\theta_i$	3.17°
Final angle, $\theta_f$	0.18°
Grip width (%)	127.17

In the previous test, where both shoulder and elbow joints are equally protected, the absolute torque efforts were  $t_1 = 1.64$ ,  $t_2 = 5.68$ , and  $t_3 = 0.90$ . In this test, the absolute torque efforts are  $t_1 = 0.06$ ,  $t_2 = 5.87$ , and  $t_3 = 0.92$ . The total shoulder torque decreased as expected while the elbow torque increased. The grip width in the previous test, was

138.44%. Table 7.2 shows the optimal grip width for this test is 127.17%. This aligns with literature recommendations to use narrow grip widths to protect the shoulder joint.

## 7.11 Test B3.3

Find grip width when protecting the elbow for a straight bar path with constant elbow flare.

### 7.11.1 Problem Formulation

#### Objective Function Design

The objective function is:

$$\begin{aligned} J = & J + \frac{\Delta t}{6} (u_k^\top W u_k + 4u_m^\top W u_m + u_{k+1}^\top W u_{k+1}) \\ & + \lambda_1 \|u_{k+1} - u_k\|^2 + \lambda_2 (\dot{\theta}_{1,k}^2 + \dot{\theta}_{2,k}^2) + ((x_{\text{hand}} - x_{\text{ref}}(k))^2 + (z_{\text{hand}} - z_{\text{ref}}(k))^2) \end{aligned}$$

The weighting matrix includes a heavier penalty for elbow torque:

$$W = \text{diag}(w_{\text{shoulder yaw}} = 1, w_{\text{shoulder pitch}} = 1, w_{\text{elbow pitch}} = 5).$$

### 7.11.2 Results and Discussion

Table 7.3: Bench press joint angles and grip width for Test B3.3.

Parameter	Value
Initial angle, $\theta_i$	66.03°
Final angle, $\theta_f$	20.02°
Grip width (%)	161.01

In Test B3.1, where both shoulder and elbow joints are equally protected, the absolute torque efforts were  $t_1 = 1.64$ ,  $t_2 = 5.68$ , and  $t_3 = 0.90$ . In this test, the absolute torque efforts are  $t_1 = 4.13$ ,  $t_2 = 4.51$ , and  $t_3 = 0.80$ . The elbow torque decreased as expected

while the total shoulder torque increased. The grip width in Test B3.1, was 138.44%. Table 7.3 shows the optimal grip width for this test is 161.01%. This aligns with literature recommendations to use wide grip widths to protect the elbow joint.

## 7.12 Test B4.1

Find grip width variation for different brachial indices with a straight bar path and constant elbow flare.

### 7.12.1 Problem Formulation

#### Anthropometric Parameters

Total body mass:  $M = 67.8 \text{ kg}$ . To test different brachial indices,  $L_1$  is varied while  $L_2$  remains constant.

$$\begin{aligned} \text{Link 1 (Upper Arm): } & m_1 = 0.030695 M, \quad L_1 = L_{1,\text{mean}} + [-2, -1, 0, 1, 2] \cdot L_{1,\text{std}} \text{ m}, \\ \text{Link 2 (Forearm): } & m_2 = 0.017035 M, \quad L_2 = 0.2342 \text{ m}. \end{aligned}$$

where  $L_{1,\text{mean}} = 0.3012 \text{ m}$  and  $L_{1,\text{std}} = 0.0166 \text{ m}$ . Moments of inertia were estimated using the slender-rod approximation,  $I = \frac{1}{12}mL^2$ .

#### Objective Function Design

The objective function is:

$$J = J + \frac{\Delta t}{6} (u_k^\top W u_k + 4u_m^\top W u_m + u_{k+1}^\top W u_{k+1}) + \lambda_1 \|u_{k+1} - u_k\|^2 + \lambda_2 (\dot{\theta}_{1,k}^2 + \dot{\theta}_{2,k}^2)$$

The weighting matrix with equal penalties for shoulder and elbow torque:

$$W = \text{diag}(w_{\text{shoulder yaw}} = 1, w_{\text{shoulder pitch}} = 1, w_{\text{elbow pitch}} = 1).$$

### 7.12.2 Results and Discussion

Table 7.4: Bench press joint angles and grip width of varying brachial indices for Test B4.1.

Parameter	0.8739	0.8229	0.7776	0.7369	0.7004
Initial angle, $\theta_i$ ( $^{\circ}$ )	23.10 $^{\circ}$	21.57 $^{\circ}$	19.95 $^{\circ}$	64.96 $^{\circ}$	71.87 $^{\circ}$
Final angle, $\theta_f$ ( $^{\circ}$ )	6.86 $^{\circ}$	6.83 $^{\circ}$	6.67 $^{\circ}$	20.88 $^{\circ}$	23.05 $^{\circ}$
Grip width (%)	138.76	138.69	138.44	162.67	166.58

The results in Table 7.4 show that grip width remains relatively consistent for larger brachial indices, with values of 138.76%, 138.69%, and 138.44%. However, as the brachial index decreases, the required grip width increases substantially to 162.67% and 166.58%. This trend indicates that individuals with longer upper arms must adopt wider grips to maintain comparable bar paths and minimise joint effort during the lift. The change in grip widths between higher and lower brachial indices suggests that variations in limb proportions significantly influence the optimal grip width.

# Chapter 8

## Clinical Application

The developed model and trajectory optimisation framework were found to be accurate and consistent with findings reported in the literature. Beyond its research value, it has practical applications for gym-goers, trainers, and medical professionals seeking to optimise lifting technique. To illustrate this, two hypothetical test subjects, referred to as Josh and Lee, were evaluated. Each was asked to provide their weight, biacromial diameter, upper arm length, forearm length, and any history of shoulder or elbow pain or injury. Using these inputs, their corresponding grip widths and bar paths were determined to demonstrate how individual body proportions and joint conditions influence optimal bench press form.

### 8.1 Test Subject: Josh

Participant Josh, weighing 74.5 kg, reported an upper arm length of 31 cm, forearm length of 27 cm, and a biacromial diameter of 47 cm. He noted experiencing shoulder discomfort but had no prior injuries.

#### 8.1.1 Problem Formulation

The application test uses Model B, a 3D two link arm with 3DoF as described in Stage 2. The trajectory optimisation framework remains the same except for the variable components listed below.

#### Anthropometric Parameters

Total body mass:  $M = 74.5 \text{ kg}$ .

$$\text{Link 1 (Upper Arm): } m_1 = 0.030695 M, \quad L_1 = 0.31 \text{ m},$$

$$\text{Link 2 (Forearm): } m_2 = 0.017035 M, \quad L_2 = 0.27 \text{ m}.$$

## 8.1. TEST SUBJECT: JOSH

Moments of inertia were estimated using the slender-rod approximation,  $I = \frac{1}{12}mL^2$ . The biacromial diameter is 0.47 m and is used together with the optimal shoulder yaw angles to calculate the grip width.

### Objective Function Design

The straight line soft constraint is removed so that both bar path and grip width can be determined. The objective function is:

$$J = J + \frac{\Delta t}{6} (u_k^\top W u_k + 4u_m^\top W u_m + u_{k+1}^\top W u_{k+1}) + \lambda_1 \|u_{k+1} - u_k\|^2 + \lambda_2 (\dot{\theta}_{1,k}^2 + \dot{\theta}_{2,k}^2)$$

Weighting matrix includes a heavier penalty for shoulder torques:

$$W = \text{diag}(w_{\text{shoulder yaw}} = 5, w_{\text{shoulder pitch}} = 5, w_{\text{elbow pitch}} = 1).$$

### 8.1.2 Results and Discussion

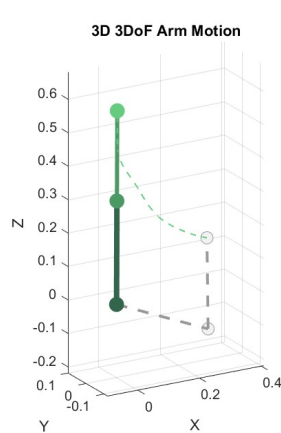


Figure 8.1: Bar path during the lift.

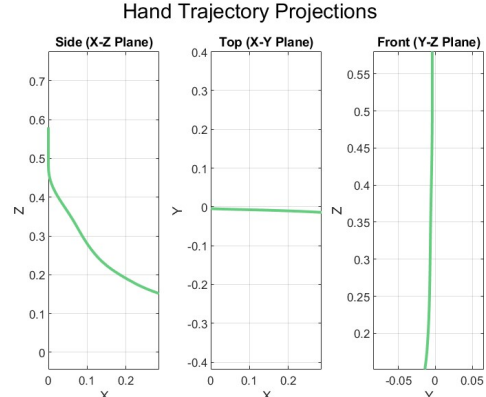


Figure 8.2: Hand trajectory projections in each plane.

Table 8.1: Bench press joint angles and grip width

Parameter	Value
Initial angle, $\theta_i$	$3.92^\circ$
Final angle, $\theta_f$	$0.41^\circ$
Grip width (%)	127.08

The absolute torque efforts are  $t_1 = 0.12$ ,  $t_2 = 5.82$ , and  $t_3 = 1.39$ . Figure 8.1 and Figure 8.2 show that the bar path follows a characteristic J-curve, which aligns with recommendations in the literature for minimising shoulder stress during the bench press. Table 8.1 indicates a grip width of 127.08%, consistent with studies suggesting that narrower grip widths reduce shoulder joint loading. Josh's smaller brachial index of 0.8710 further supports this result, as individuals with longer upper arm length typically benefit from narrower grips.

## 8.2 Test Subject: Lee

In contrast, participant Lee, weighing 62.7 kg, reported an upper arm length of 27 cm, forearm length of 22 cm, and a biacromial diameter of 35 cm. Lee reported no current pain but had a history of an elbow injury.

### 8.2.1 Problem Formulation

#### Anthropometric Parameters

Total body mass:  $M = 62.7$  kg.

$$\begin{aligned} \text{Link 1 (Upper Arm): } & m_1 = 0.030695 M, \quad L_1 = 0.27 \text{ m}, \\ \text{Link 2 (Forearm): } & m_2 = 0.017035 M, \quad L_2 = 0.22 \text{ m}. \end{aligned}$$

Moments of inertia were estimated using the slender-rod approximation,  $I = \frac{1}{12}mL^2$ . The biacromial diameter is 0.35 m and is used together with the optimal shoulder yaw angles to calculate the grip width.

#### Objective Function Design

The objective function is:

$$J = J + \frac{\Delta t}{6} (u_k^\top W u_k + 4u_m^\top W u_m + u_{k+1}^\top W u_{k+1}) + \lambda_1 \|u_{k+1} - u_k\|^2 + \lambda_2 (\dot{\theta}_{1,k}^2 + \dot{\theta}_{2,k}^2)$$

Weighting matrix includes a heavier penalty for elbow torques:

$$W = \text{diag} (w_{\text{shoulder yaw}} = 1, w_{\text{shoulder pitch}} = 1, w_{\text{elbow pitch}} = 5).$$

### 8.2.2 Results and Discussion

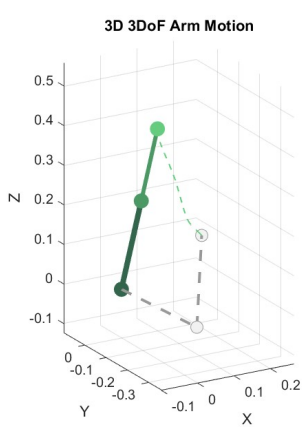


Figure 8.3: Bar path during the lift.

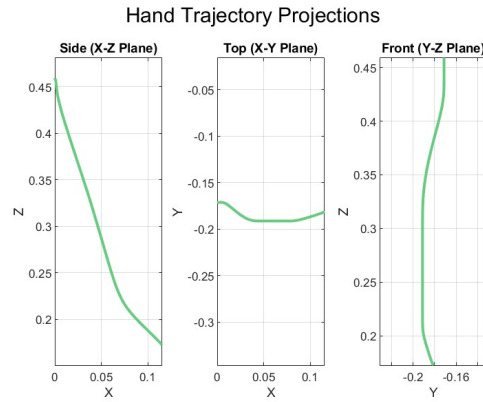


Figure 8.4: Hand trajectory projections in each plane.

Table 8.2: Bench press joint angles and grip width

Parameter	Value
Initial angle, $\theta_i$	77.29°
Final angle, $\theta_f$	20.46°
Grip width (%)	159.76

The absolute torque efforts are  $t_1 = 3.47$ ,  $t_2 = 3.47$ , and  $t_3 = 0.65$ . Figure 8.3 and Figure 8.4 show that the bar path follows a relatively straight line, which aligns with recommendations in the literature, although a slight J-curve is still present. Table 8.2 indicates an optimal grip width of 159.76%, consistent with studies suggesting that wider grip widths reduce elbow joint loading. Lee's brachial index of 0.8148 is just smaller than average so a smaller grip width is recommended. These results show when considering the bar path, grip width and brachial index the optimal solution may differ from expectations.

# Chapter 9

## Conclusion

An investigation into the fundamental biomechanics of the bench press, alongside a review of current human body modelling techniques and trajectory optimisation methods, established a strong theoretical foundation for this study. Research questions were formulated to guide the analysis, and a series of tests were conducted to address each one. From the results obtained in the Stage 1 and Stage 2 test, the four research questions were successfully answered, demonstrating the reliability of the developed model and trajectory optimisation framework. Subsequently, clinical application example tests were performed to illustrate the practical relevance of the model. The final conclusions drawn from each research question, as well as the clinical application, are presented below. Finally, recommendations are made for future work.

### 9.1 Question 1

Question 1: How does the **bar path** change when protecting the shoulder versus the elbow (with grip width and elbow flare held constant)?

The bar path is a straight line with a slight J-curve when shoulder and elbow are equally protected, a J-curve when the shoulder is protected and a straight line when the elbow is protected. The same bar path shapes were seen when a narrow grip and a wide grip were simulated. This matches with the bar path recommendations in the literature, demonstrating the reliability of the developed model and trajectory optimisation framework for determining bar paths with different joint requirements.

### 9.2 Question 2

Question 2: How does the **bar path** vary for different brachial indices (with grip width and elbow flare held constant)?

The bar path shape did not change with different brachial indices. Although it was observed that a longer upper arm requires greater torque to perform the same movement. These trends were seen for both the narrow and wide grip simulations. These results support findings in the literature that a longer upper arm is negatively correlated with performance. It was concluded that the model and trajectory optimisation framework are reliable for determining bar paths for various brachial indices.

## 9.3 Question 3

Question 3: How does **grip width** change when protecting the shoulder versus the elbow (with bar path and elbow flare held constant)?

An average grip width was optimal when shoulder and elbow are equally protected, a narrow grip width when the shoulder is protected and a wide grip width when the elbow is protected. This matches with the grip width recommendations in the literature, demonstrating the reliability of the developed model and trajectory optimisation framework for determining grip widths depending on joint requirements.

## 9.4 Question 4

Question 4: How does **grip width** vary for different brachial indices (with bar path and elbow flare held constant)?

A narrow grip width was optimal for large brachial indices and a wide grip width was optimal for smaller brachial indices. It was theorised that for larger upper arms the grip width increased to maintain comparable bar paths and minimise joint effort during the lift. Therefore, the model and trajectory optimisation framework are reliable for determining grip widths for various brachial indices.

## 9.5 Clinical Application

To demonstrate the practical relevance of the model, two test subjects, referred to as Josh and Lee, were evaluated. They provided their anthropometric information and reported

any existing joint pain or previous injuries. The results from their individual tests revealed a combination of intuitive and less intuitive outcomes. The intuitive findings aligned with existing research, showing that specific bar paths or grip widths are preferable based on joint conditions and brachial index. However, the less intuitive results highlight the model's capability to identify optimal solutions that minimise joint effort, which may require balancing between ideal bar paths and grip widths depending on the individual's anatomy and joint condition. This demonstrates the model's practical relevance, as it supports the idea that every individual possesses a unique optimal bench press form.

## 9.6 Recommendations

- **Improve the Skeletal Model:** The skeletal system should be expanded to make the model more realistic. Moving to a 3D 4DOF model by adding another DoF to the shoulder joint would allow for the study of elbow flare and its impact on joint torque and bar path, addressing Questions 5 and 6. Adding the wrist and hand to form a three-link arm would also help analyse wrist motion and strain, important for preventing injuries and improving lift efficiency.
- **Improve the Model Design:** The model could be improved by including muscles and their activation patterns. This would allow investigation into both muscle growth and injury risk, linking performance with safety. A more realistic model could also show how different muscles work together during various lifting techniques.
- **Expand the Research:** The optimisation framework used in this study could be applied to other exercises. A good next step would be to study the dumbbell bench press. Future work could also explore exercises like the shoulder press, incline bench press, and chest fly to better understand upper-body movement strategies.
- **Commercial Use:** This research has strong practical and commercial potential. Clinical tests could be done to compare model predictions with real lifting data. A mobile app could be developed using video tracking to help users compare their form to their ideal form and get real-time feedback. Another idea is an adaptive Smith machine that adjusts the bar's path to match each lifter's ideal motion.

# Bibliography

- [1] B. Carroll and D. C. C. Liebenson, “The bench press: The most misunderstood lift in strength & conditioning,” *Journal of Bodywork & Movement Therapies*, vol. 21, no. 1, pp. 227–229, January 2017. [Online]. Available: <https://api.semanticscholar.org/CorpusID:245577564>
- [2] H. A. E.-M. El-Gazzar, “Bench press exercise: the greatest functionally and biomechanically drill,” *Journal of Applied Sports Science*, vol. 14, no. 1, June 2024. [Online]. Available: <https://pubmed.ncbi.nlm.nih.gov/31567719/>
- [3] E. L. Kristiansen, S. Larsen, and R. van den Tillaar, “The acute effect of accentuated eccentric overloading upon the kinematics and myoelectric activity in the eccentric and concentric phase of a traditional bench press,” *Sports*, vol. 10, 2021. [Online]. Available: <https://api.semanticscholar.org/CorpusID:245577564>
- [4] M. A. Bernstorff, N. Schumann, A. Finke, T. A. Schildhauer, and M. Königshausen, “Popular gym fitness sport: An analysis of 1387 recreational athletes regarding prone to pain exercises and the corresponding localisations,” *Sports*, vol. 12, 2023. [Online]. Available: <https://api.semanticscholar.org/CorpusID:266660278>
- [5] D. A. Bonilla, L. A. Cardozo, J. M. Vélez-Gutiérrez, A. Arévalo-Rodríguez, S. Vargas-Molina, J. R. Stout, R. B. Kreider, and J. L. Petro, “Exercise selection and common injuries in fitness centers: A systematic integrative review and practical recommendations,” *International Journal of Environmental Research and Public Health*, vol. 19, 2022. [Online]. Available: <https://api.semanticscholar.org/CorpusID:252855846>
- [6] S. Bartolomei, E. Caroli, V. Coloretti, G. Rosaci, M. Cortesi, and G. Coratella, “Flat-back vs. arched-back bench press: Examining the different techniques performed by power athletes,” *J Strength Cond Res*, vol. 38, no. 7, pp. 1200–1205, July 1 2024, epub 2024 Mar 29.

- [7] L. Mausehund, A. Werkhausen, J. Bartsch, and T. Krosshaug, “Understanding bench press biomechanics – the necessity of measuring lateral barbell forces,” *Journal of Strength and Conditioning Research*, vol. 36, no. 10, pp. 2685–2695, October 1 2022, epub 2021 Feb 4. [Online]. Available: <https://pubmed.ncbi.nlm.nih.gov/33555823/>
- [8] B. Wood, S. W. Cummings, R. H. Crompton, and C. Tangen, “Human muscle system,” Encyclopedia Britannica, July 31 2025, accessed 26 September 2025. [Online]. Available: <https://www.britannica.com/science/human-muscle-system>
- [9] D. Rodríguez-Ridao, J. A. Antequera-Vique, I. Martín-Fuentes, and J. M. Muyor, “Effect of five bench inclinations on the electromyographic activity of the pectoralis major, anterior deltoid, and triceps brachii during the bench press exercise,” *International Journal of Environmental Research and Public Health*, vol. 17, 2020. [Online]. Available: <https://api.semanticscholar.org/CorpusID:222351955>
- [10] J. Padulo, G. Laffaye, A. Chaouachi, and K. Chamari, “Bench press exercise: the key points,” *Journal of Sports Medicine and Physical Fitness*, vol. 55, no. 6, pp. 604–608, June 2015, epub 2014 May 13. [Online]. Available: <https://pubmed.ncbi.nlm.nih.gov/24823345/>
- [11] Y.-H. Chang, Y.-C. Chou, Y.-C. Chang, K.-H. Tan, and M.-H. Wu, “The effects of high-intensity power training versus traditional resistance training on exercise performance,” *International Journal of Environmental Research and Public Health*, vol. 19, 2022. [Online]. Available: <https://api.semanticscholar.org/CorpusID:251263818>
- [12] D. L. Marques, H. P. Neiva, D. A. Marinho, I. Pires, C. Nunes, and M. C. Marques, “Estimating the relative load from movement velocity in the seated chest press exercise in older adults,” *PLOS ONE*, vol. 18, 2023. [Online]. Available: <https://api.semanticscholar.org/CorpusID:258484574>
- [13] S. O. Tjøsvoll, P. J. Mork, V. M. Iversen, M. B. Rise, and M. S. Fimland, “Periodized resistance training for persistent non-specific low back pain: a mixed methods feasibility study,” *BMC Sports Science, Medicine and Rehabilitation*, vol. 12, 2020. [Online]. Available: <https://api.semanticscholar.org/CorpusID:218540297>
- [14] G. Bonaspetti, G. Dib, and F. Azzola, “Body builder’s shoulder: Posterior labrum periosteal sleeve avulsion (polpsa) and glenoid posterior rim stress fracture due to intense bench pressing,” *Case Reports in Orthopedics*, vol. 2022, 2022. [Online]. Available: <https://api.semanticscholar.org/CorpusID:246304342>

## BIBLIOGRAPHY

- [15] R. G. Lockie and M. R. Moreno, “The close-grip bench press,” *Strength and Conditioning Journal*, vol. 39, no. 4, pp. 30–35, 2017. [Online]. Available: [https://www.researchgate.net/publication/318289674\\_The\\_Close-Grip\\_Bench\\_Press](https://www.researchgate.net/publication/318289674_The_Close-Grip_Bench_Press)
- [16] L. D. Vecchio, “The health and performance benefits of the squat, deadlift and bench press,” 2018. [Online]. Available: <https://api.semanticscholar.org/CorpusID:4645911>
- [17] M. J. Duffey, “A biomechanical analysis of the bench press,” Ph.D. dissertation, The Pennsylvania State University, 200?, ph.D. dissertation. [Online]. Available: <https://etda.libraries.psu.edu/catalog/8894>
- [18] X. Roy, K. Arseneault, and P. Sercia, “The effect of 12 variations of the bench press exercise on the emg activity of three heads of the pectoralis major,” *IUSCA Journal*, 2020. [Online]. Available: <https://api.semanticscholar.org/CorpusID:236905830>
- [19] S. Larsen, O. Gomo, and R. van den Tillaar, “A biomechanical analysis of wide, medium, and narrow grip width effects on kinematics, horizontal kinetics, and muscle activity on the sticking region in recreationally trained males during 1-rm bench pressing,” *Frontiers in Sports and Active Living*, vol. 2, 2021. [Online]. Available: <https://api.semanticscholar.org/CorpusID:231667334>
- [20] M. Reya, J. karabot, B. Cvetianin, and N. arabon, “Factors underlying bench press performance in elite competitive powerlifters,” *Journal of Strength and Conditioning Research*, vol. 35, pp. 2179 – 2186, 2019. [Online]. Available: <https://api.semanticscholar.org/CorpusID:85514521>
- [21] A. Reimann, R. Beyer, R. Mumm, and C. Scheffler, “Reference tables with centiles of limb to body height ratios of healthy human adults for assessing potential thalidomide embryopathy.” *Anthropologischer Anzeiger; Bericht über die biologisch-anthropologische Literatur*, 2019. [Online]. Available: <https://api.semanticscholar.org/CorpusID:76667083>
- [22] S. Pecolt, A. Błażejewski, T. Królikowski, and D. Katafiasz, “Multi-segment, spatial biomechanical model of a human body,” *Procedia Computer Science*, vol. 207, pp. 272–281, 2022, knowledge-Based and Intelligent Information Engineering Systems: Proceedings of the 26th International Conference KES2022. [Online]. Available: <https://www.sciencedirect.com/science/article/pii/S1877050922009334>
- [23] M. Eltayeb, “Biomechanical model for musculoskeletal simulation,” 08 2023, pp. 187–193. [Online]. Available: [https://www.researchgate.net/publication/373043147\\_Biomechanical\\_model\\_for\\_musculoskeletal\\_simulation#:~:text=Biomechanical%20model%20for%20musculoskeletal%20simulation](https://www.researchgate.net/publication/373043147_Biomechanical_model_for_musculoskeletal_simulation#:~:text=Biomechanical%20model%20for%20musculoskeletal%20simulation)

text=Musculoskeletal%20modeling%20is%20a%20technique,remains%20costly%20and%20time%2Dconsuming.

- [24] I. Roupa, M. R. da Silva, F. Marques, S. B. Gonçalves, P. Flores, and M. T. da Silva, “On the modeling of biomechanical systems for human movement analysis: A narrative review,” *Archives of Computational Methods in Engineering*, vol. 29, no. 7, pp. 4915–4958, 2022. [Online]. Available: <https://link.springer.com/article/10.1007/s11831-022-09757-0>
- [25] R. Haratian, “Motion capture sensing technologies and techniques: A sensor agnostic approach to address wearability challenges,” *Sensing and Imaging*, vol. 23, 2022. [Online]. Available: <https://api.semanticscholar.org/CorpusID:255067446>
- [26] C. Latella, “Human whole-body dynamics estimation for enhancing physical human-robot interaction,” *ArXiv*, vol. abs/1912.01136, 2019. [Online]. Available: <https://api.semanticscholar.org/CorpusID:208548366>
- [27] A. Biscarini, A. Calandra, and S. Contemori, “Three-dimensional mechanical modeling of the barbell bench press exercise: Unveiling the biomechanical function of the triceps brachii,” *Proceedings of the Institution of Mechanical Engineers, Part P: Journal of Sports Engineering and Technology*, vol. 234, pp. 245 – 256, 2020. [Online]. Available: <https://api.semanticscholar.org/CorpusID:221013679>
- [28] S.-H. Lee, E. Sifakis, and D. Terzopoulos, “Comprehensive biomechanical modeling and simulation of the upper body,” *ACM Trans. Graph.*, vol. 28, no. 4, Sep. 2009. [Online]. Available: <https://doi.org/10.1145/1559755.1559756>
- [29] J. A. C. Ambrósio and A. Kecskeméthy, “Multibody dynamics of biomechanical models for human motion via optimization,” in *Computational Methods in Applied Sciences*, ser. Computational Methods in Applied Sciences, J. C. G. Orden, J. M. Goicolea, and J. Cuadrado, Eds., 2007, vol. 4, pp. 245–272. [Online]. Available: [https://www.academia.edu/17930204/Multibody\\_Dynamics\\_of\\_Biomechanical\\_Models\\_for\\_Human\\_Motion\\_via\\_Optimization](https://www.academia.edu/17930204/Multibody_Dynamics_of_Biomechanical_Models_for_Human_Motion_via_Optimization)
- [30] M. S. Daoud, Y. Y. Ghadi, and H. M. AlMimi, “Optimization of the application software in biomechanics and their contribution to the biological field,” *Journal of Engineering Science and Technology Review*, 2019. [Online]. Available: <https://api.semanticscholar.org/CorpusID:150339383>
- [31] A. Seth, J. L. Hicks, T. K. Uchida, A. Habib, C. L. Dembia, J. J. Dunne, C. F. Ong, M. S. DeMers, A. Rajagopal, M. Millard, S. R. Hamner, E. M. Arnold, J. R. Yong, S. K. Lakshmikanth, M. A. Sherman, J. P. Ku, and S. L. Delp, “Opensim: Simulating musculoskeletal dynamics and neuromuscular control to study human

- and animal movement,” *PLoS Computational Biology*, vol. 14, 2018. [Online]. Available: <https://api.semanticscholar.org/CorpusID:51722068>
- [32] N. Fahse, M. Millard, F. Kempfer, S. Maier, M. Roller, and J. Fehr, “Dynamic human body models in vehicle safety: An overview,” *GAMM-Mitteilungen*, vol. 46, 2023. [Online]. Available: <https://api.semanticscholar.org/CorpusID:257232960>
- [33] P. M. Bush, S. Gaines, F. T. Gammoh, and S. Wooden, “A comparison of software tools for occupational biomechanics and ergonomic research,” 2012. [Online]. Available: <https://api.semanticscholar.org/CorpusID:5541676>
- [34] G. E. Loeb and R. Davoodi, “Musculoskeletal mechanics and modeling,” *Scholarpedia*, vol. 11, p. 12389, 2016. [Online]. Available: <https://api.semanticscholar.org/CorpusID:30380162>
- [35] M. Posa, C. Cantu, and R. Tedrake, “A direct method for trajectory optimization of rigid bodies through contact,” *The International Journal of Robotics Research*, vol. 33, pp. 69 – 81, 2014. [Online]. Available: <https://api.semanticscholar.org/CorpusID:6532910>
- [36] M. Posa, S. Kuindersma, and R. Tedrake, “Optimization and stabilization of trajectories for constrained dynamical systems,” *2016 IEEE International Conference on Robotics and Automation (ICRA)*, pp. 1366–1373, 2016. [Online]. Available: <https://api.semanticscholar.org/CorpusID:1879547>
- [37] M. Kelly, “An introduction to trajectory optimization: How to do your own direct collocation,” *SIAM Rev.*, vol. 59, pp. 849–904, 2017. [Online]. Available: <https://api.semanticscholar.org/CorpusID:33541404>
- [38] O. von Stryk and R. Bulirsch, “Direct and indirect methods for trajectory optimization,” *Annals of Operations Research*, vol. 37, pp. 357–373, 1992. [Online]. Available: <https://api.semanticscholar.org/CorpusID:42262624>
- [39] S. L. Nejadian, M. Rostami, and F. Towhidkhah, “Optimization of barbell trajectory during the snatch lift technique by using optimal control theory,” *American Journal of Applied Sciences*, vol. 5, pp. 524–531, 2008. [Online]. Available: <https://api.semanticscholar.org/CorpusID:43973138>
- [40] M. H. Jon and U. Rim, “Dynamic analysis and optimization of snatch lift based on barbell trajectory and on an anthropometric model comprised of six links,” *Engineering Reports*, vol. 6, 2023. [Online]. Available: <https://api.semanticscholar.org/CorpusID:265182460>

## BIBLIOGRAPHY

- [41] H. D. las Casas, N. Chambers, H. Richter, and K. E. Sparks, “Real-time trajectory optimization in robot-assisted exercise and rehabilitation,” *ArXiv*, vol. abs/2104.11273, 2021. [Online]. Available: <https://api.semanticscholar.org/CorpusID:233388130>
- [42] Maplesoft, “Robot manipulators: Position, orientation and coordinate transformations,” [https://www.maplesoft.com/content/EngineeringFundamentals/13/MapleDocument\\_13/Position,%20Orientation%20and%20Coordinate%20Transformations.pdf](https://www.maplesoft.com/content/EngineeringFundamentals/13/MapleDocument_13/Position,%20Orientation%20and%20Coordinate%20Transformations.pdf), n.d., accessed: October 15, 2025.
- [43] J. Andersson, J. Gillis, G. Horn, J. B. Rawlings, and M. Diehl, “Casadi - a software framework for nonlinear optimization and optimal control: Documentation,” <https://web.casadi.org/docs/>, 2018, accessed: 25 October 2025.
- [44] SciPy Developers, “Scipy documentation,” <https://docs.scipy.org/doc/scipy/>, 2025, accessed: 26 October 2025.
- [45] T. M. Inc., “fmincon – find minimum of constrained nonlinear multivariable function,” <https://www.mathworks.com/help/optim/ug/fmincon.html>, 2025, accessed: 26 October 2025.
- [46] T. Puoane, K. Steyn, D. Bradshaw, R. Laubscher, J. Fourie, V. Lambert, and N. Mbananga, “Obesity in south africa: the south african demographic and health survey,” *Obesity research*, vol. 10, no. 10, pp. 1038–1048, 2002.
- [47] R. Drillis, R. Contini, and M. Bluestein, “Body segment parameters,” *Artif. limbs*, vol. 8, no. 1, pp. 44–66, 1964.
- [48] H. W. Stoudt, “Skinfolds, body girths, biacromial diameter, and selected anthropometric indices of adults, united states, 1960-1962,” 1970.
- [49] J. C. Galloway and G. F. Koshland, “General coordination of shoulder, elbow and wrist dynamics during multijoint arm movements,” *Experimental Brain Research*, vol. 142, no. 2, pp. 163–180, January 2002, epub 2001 Dec 6. [Online]. Available: <https://pubmed.ncbi.nlm.nih.gov/11807572/>

# Appendix A

## Graduate Attributes

GA	Requirement	Justification and Section in the Report
1	Problem Solving	The project applies an advanced robotics technique, trajectory optimisation, to a biomechanics research problem. It integrates knowledge of nonlinear control, mathematics, and human motion analysis to formulate and solve a complex problem. The problem is introduced in Chapter 1, literature is analysed in Chapter 2, and conclusions are presented in Chapter 9.
4	Investigations, Experiments, and Data Analysis	Experimental-style testing was performed to analyse bench press kinematics and joint torques. The investigations and data analysis are presented in Chapter 6, Chapter 7, and Chapter 8.
5	Use of Engineering Tools	MATLAB and CasADi were used for modelling, simulation, and optimisation. These tools enabled the formulation and solution of nonlinear optimal control problems. The choice of tools is discussed in Chapter 5, Subsection 5.1.1, and their application is demonstrated throughout Chapter 6, Chapter 7, and Chapter 8.
6	Professional and Technical Communication (Long Report)	The project is presented as a 15 000-word technical report with figures, tables, and equations that effectively communicate results. The report adheres to academic and professional writing standards, was prepared in L <sup>A</sup> T <sub>E</sub> X, and all figures are either referenced or generated using MATLAB.
8	Individual Work	I worked independently throughout the project, meeting weekly with my supervisor for feedback. All design, modelling, and analysis were self-conducted. Evidence of this independent contribution is reflected throughout the report.
9	Independent Learning Ability	I demonstrated independent learning by extending beyond taught coursework, developing advanced trajectory optimisation and biomechanics knowledge through literature review (Chapter 2) and self-study, where I learnt the foundational theory discussed in Chapter 3.



## Appendix B

# Ethics Clearance

## B.1 Ethics Pre-screening Questionnaire Outcome Letter



---

### PRE-SCREENING QUESTIONNAIRE OUTCOME LETTER

STU-EBE-2025-PSQ001953

2025/08/20

Dear Liyana Singh,

Your Ethics pre-screening questionnaire (PSQ) has been evaluated by your departmental ethics representative. Based on the information supplied in your PSQ, it has been determined that you do not need to make a full ethics application for the research project in question.

You may proceed with your research project titled:

Advanced BroScience: Investigating Lifting Technique with Trajectory Optimization

Please note that should aspect(s) of your current project change, you should submit a new PSQ in order to determine whether the changed aspects increase the ethical risks of your project. It may be the case that project changes could require a full ethics application and review process.

Regards,

Faculty Research Ethics Committee

# Appendix C

## Additional Information

### C.1 GitHub Link

The MATLAB code can be found on my GitHub: [https://github.com/LiyanaSingh/EEE4022S\\_AdvancedBroScience\\_SNGLIY001](https://github.com/LiyanaSingh/EEE4022S_AdvancedBroScience_SNGLIY001)

### C.2 Stage 1 Figures

#### C.2.1 Test A1.1

##### Iteration 1

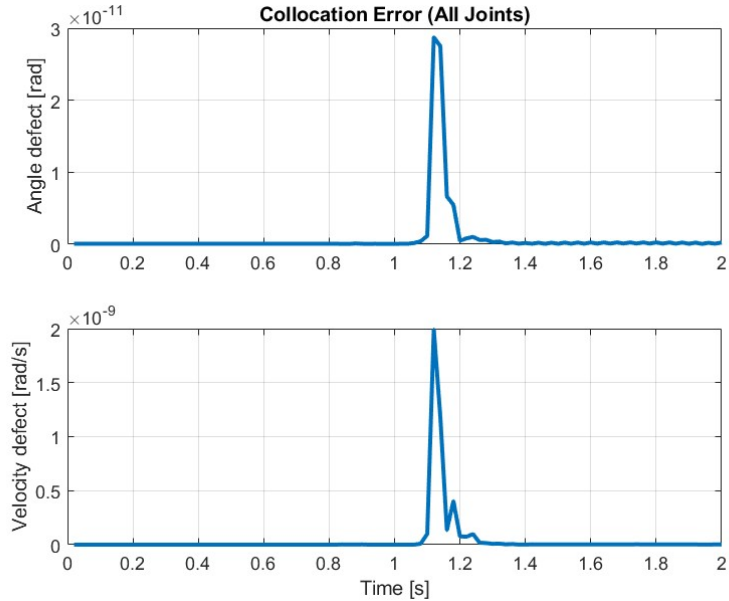


Figure C.1: Collocation error for the trajectory optimisation.

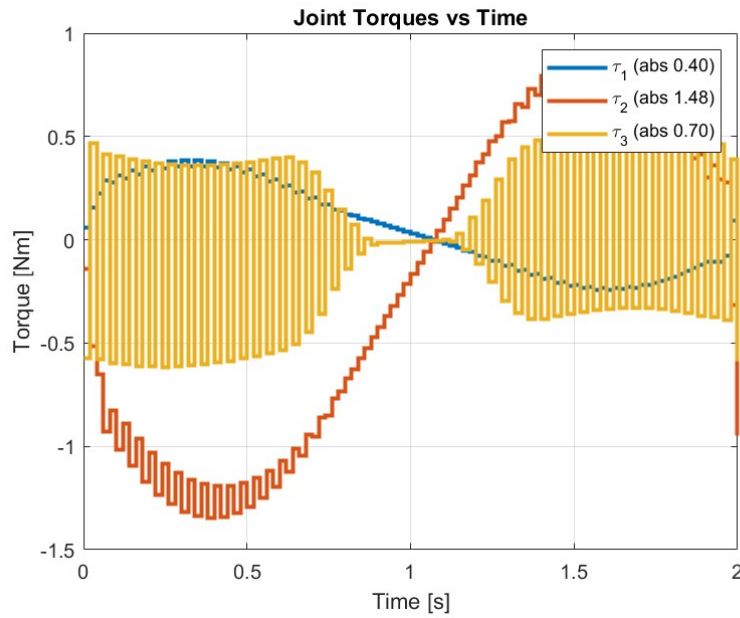


Figure C.2: Computed joint torques for shoulder, elbow, and wrist.

## Iteration 2

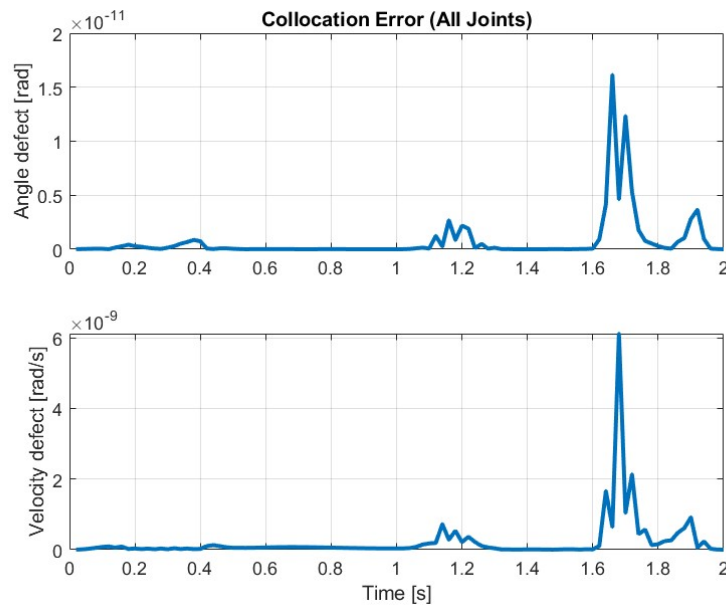


Figure C.3: Collocation error for the trajectory optimisation.

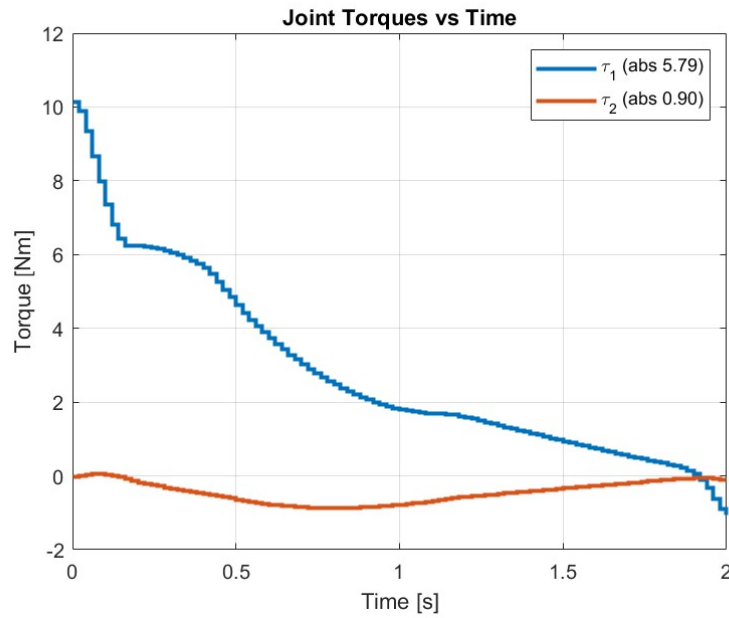


Figure C.4: Computed joint torques for shoulder and elbow.

### C.2.2 Test A1.2

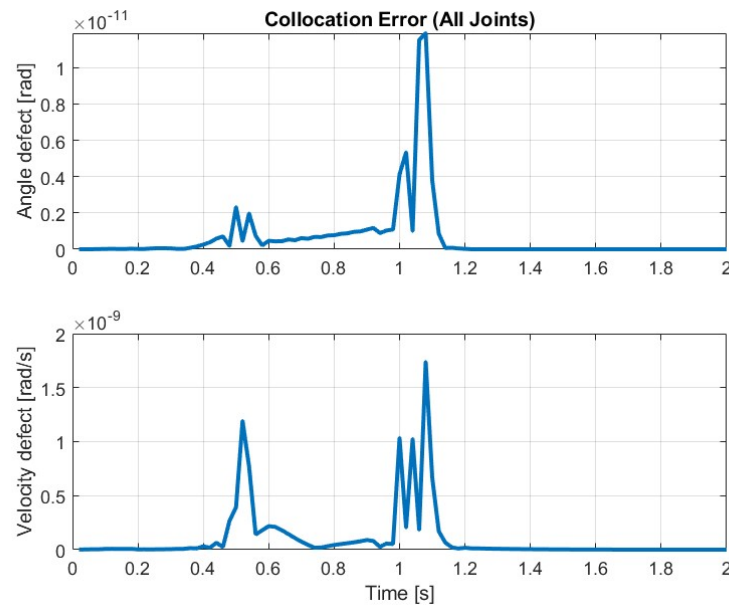


Figure C.5: Collocation error for the trajectory optimisation.

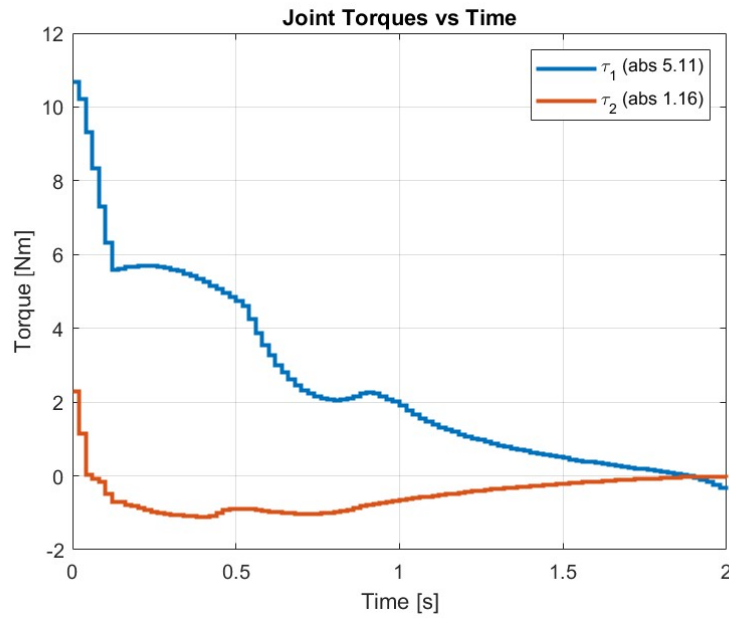


Figure C.6: Computed joint torques for shoulder and elbow.

### C.2.3 Test A1.3

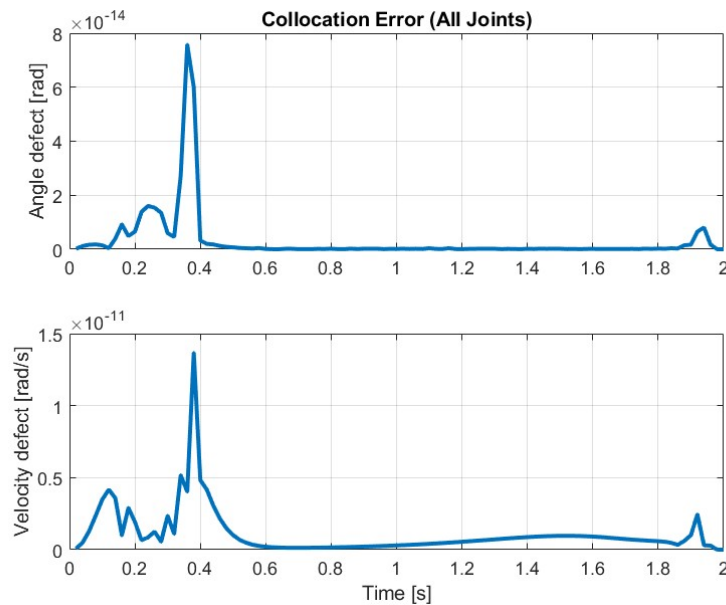


Figure C.7: Collocation error for the trajectory optimisation.

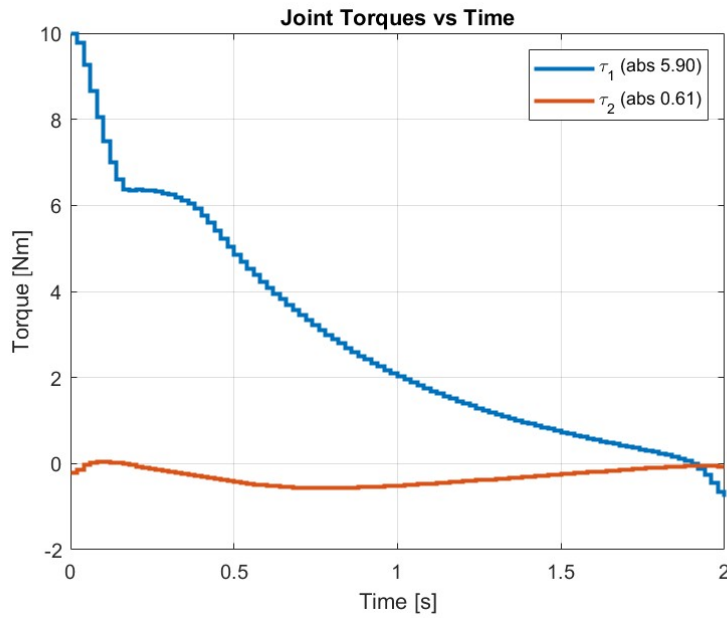


Figure C.8: Computed joint torques for shoulder and elbow.

#### C.2.4 Test A2.1

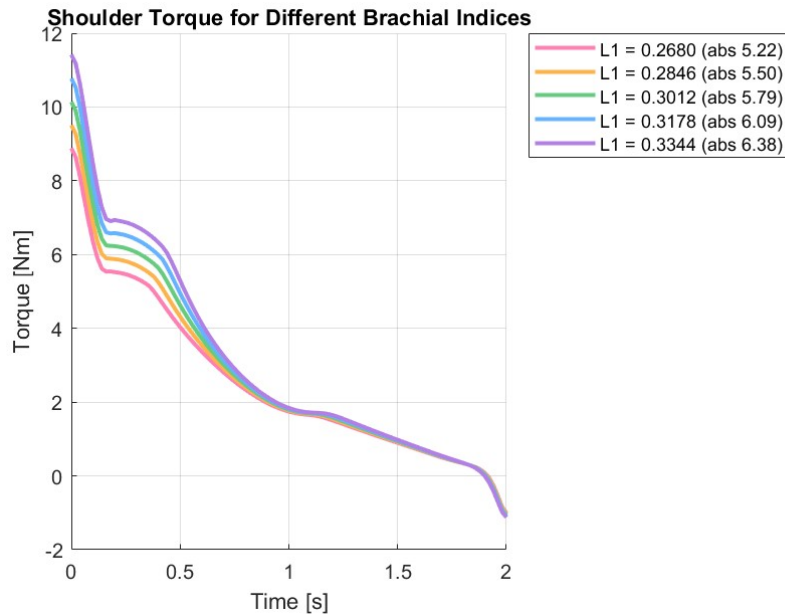


Figure C.9: Shoulder torque profiles for different brachial index values.

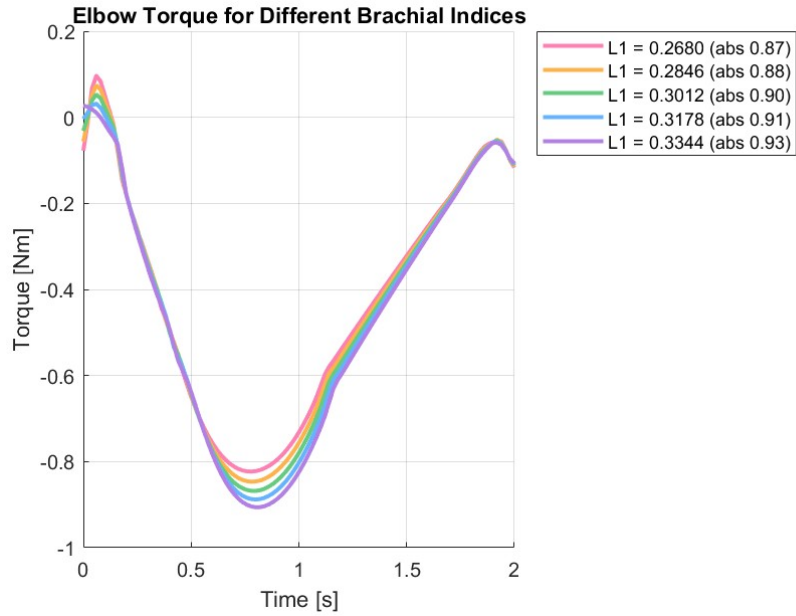


Figure C.10: Elbow torque profiles for different brachial index values.

## C.3 Stage 2 Figures

### C.3.1 Test B1.1

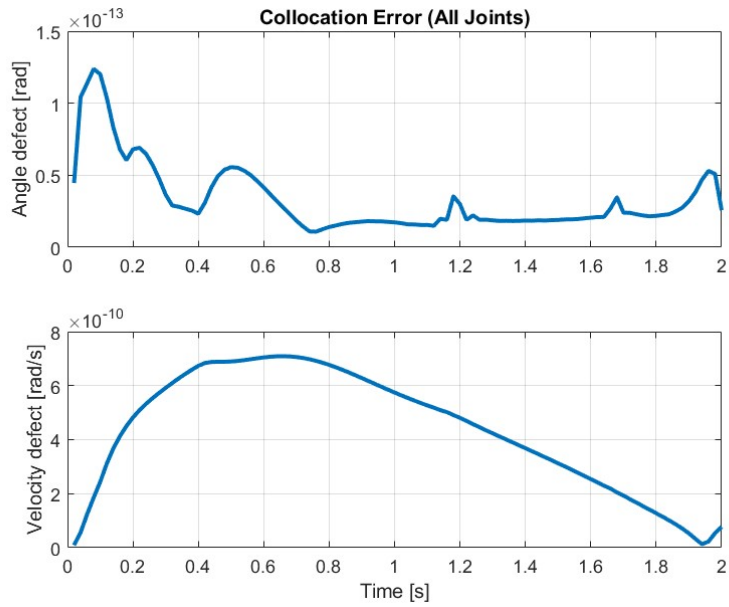


Figure C.11: Collocation error for the trajectory optimisation.

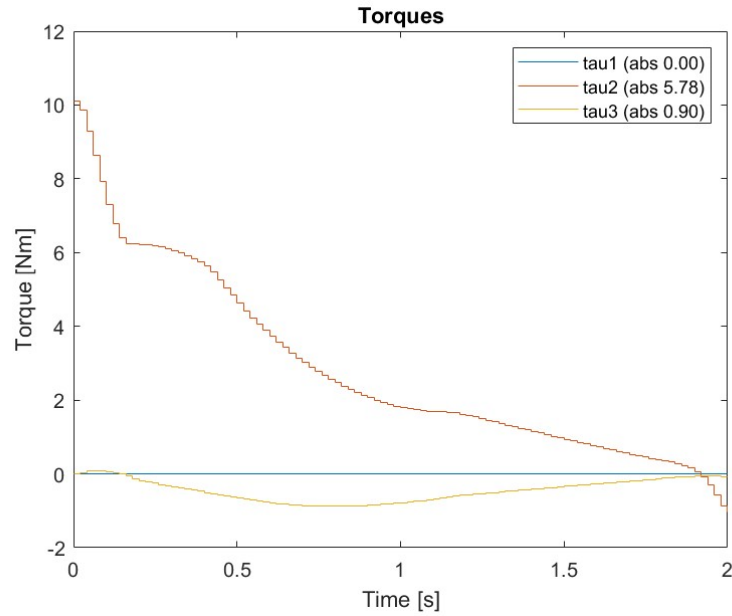


Figure C.12: Computed joint torques for shoulder yaw, shoulder pitch, and elbow pitch.

### C.3.2 Test B1.2

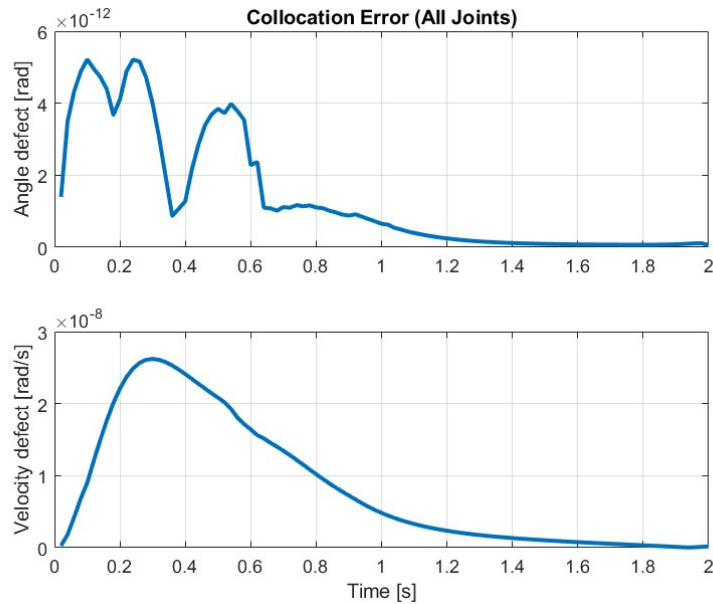


Figure C.13: Collocation error for the trajectory optimisation.

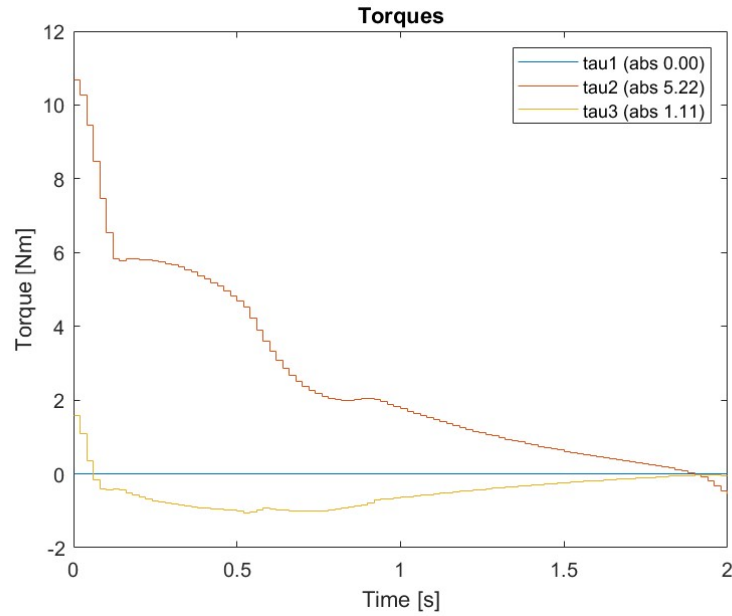


Figure C.14: Computed joint torques for shoulder yaw, shoulder pitch, and elbow pitch.

### C.3.3 Test B1.3

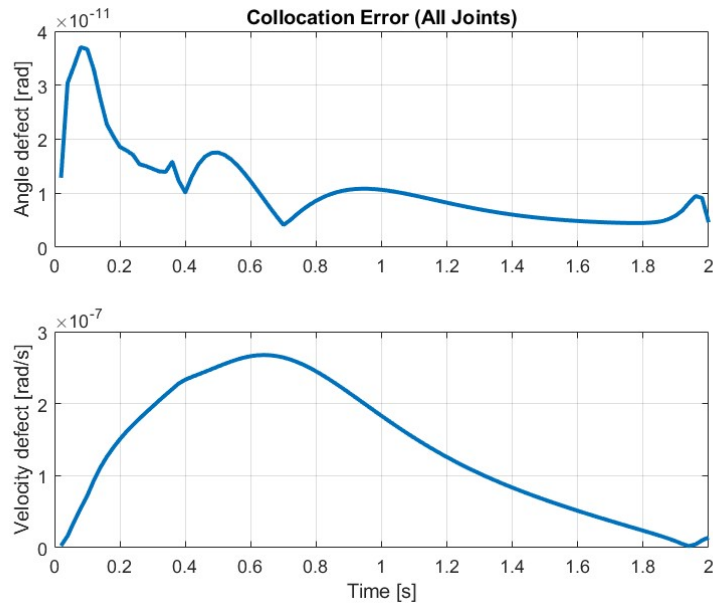


Figure C.15: Collocation error for the trajectory optimisation.

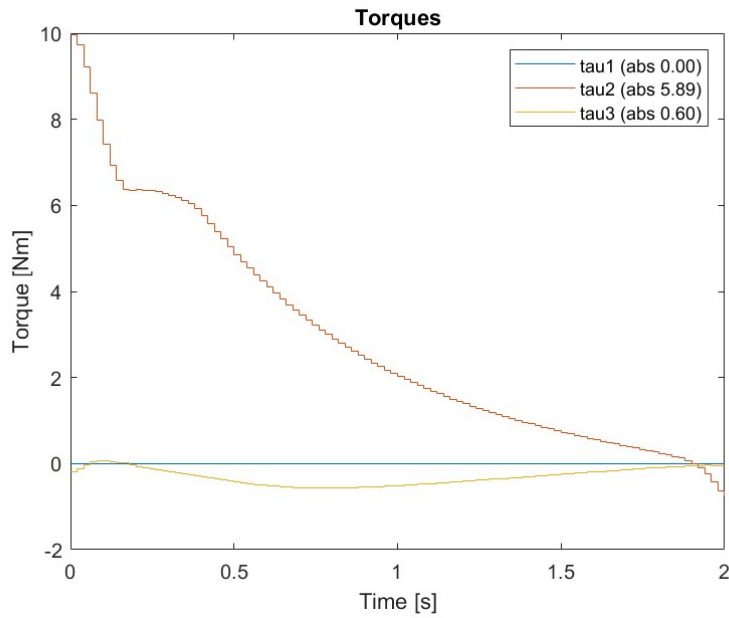


Figure C.16: Computed joint torques for shoulder yaw, shoulder pitch, and elbow pitch.

#### C.3.4 Test B1.4

#### C.3.5 Iteration 1

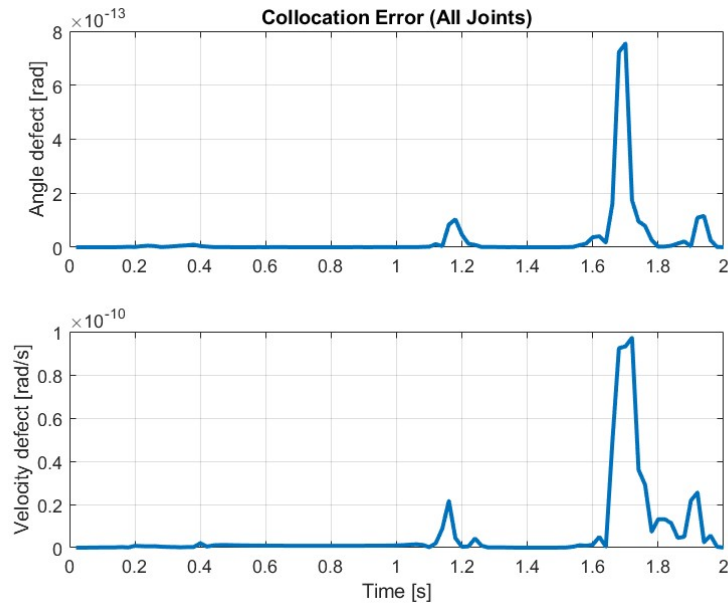


Figure C.17: Collocation error for the trajectory optimisation.

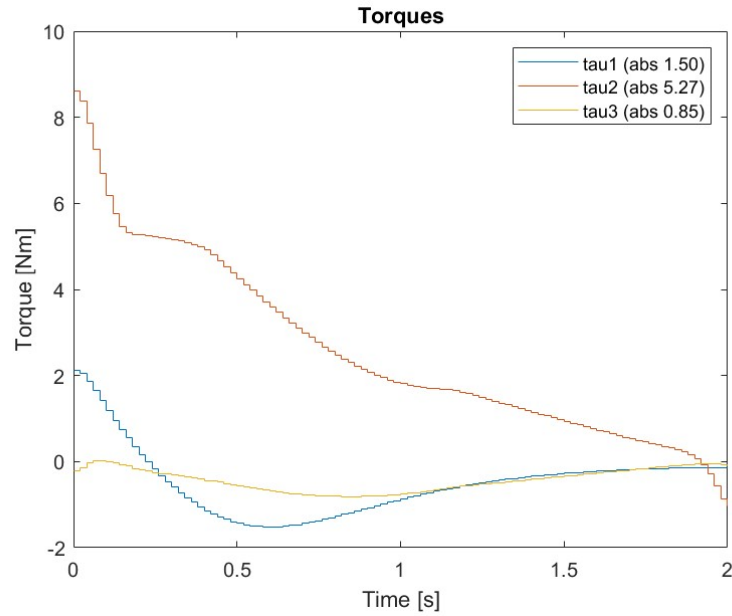


Figure C.18: Computed joint torques for shoulder yaw, shoulder pitch, and elbow pitch.

### C.3.6 Iteration 2

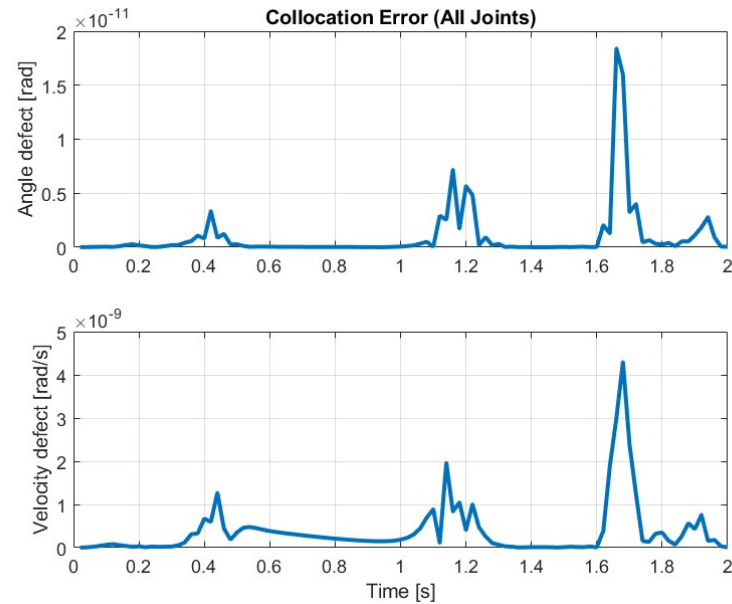


Figure C.19: Collocation error for the trajectory optimisation.

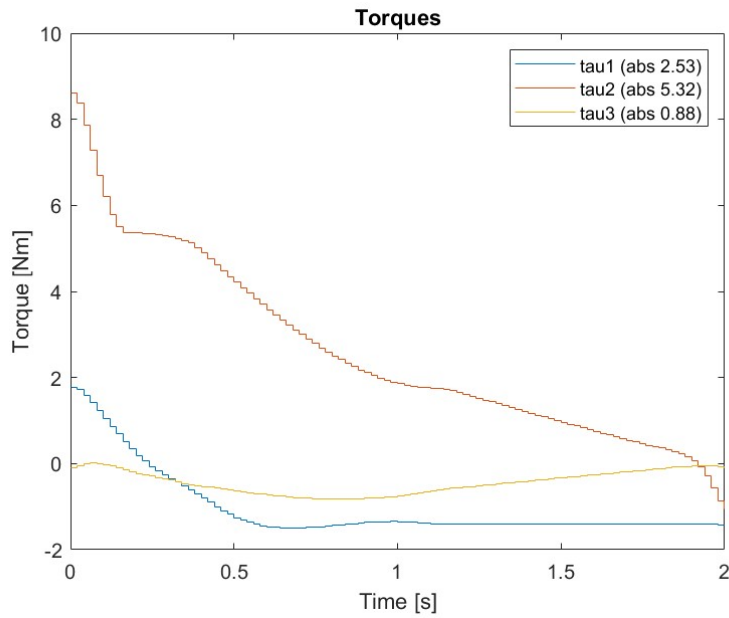


Figure C.20: Computed joint torques for shoulder yaw, shoulder pitch, and elbow pitch.

### C.3.7 Test B1.5

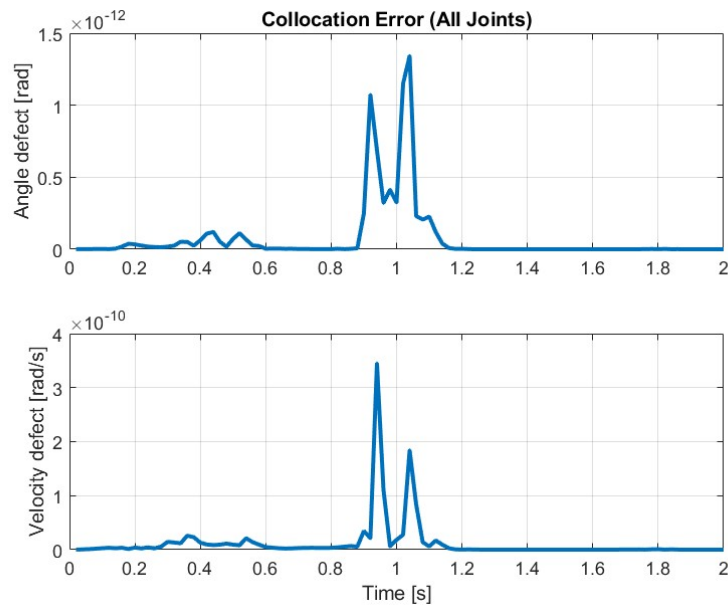


Figure C.21: Collocation error for the trajectory optimisation.

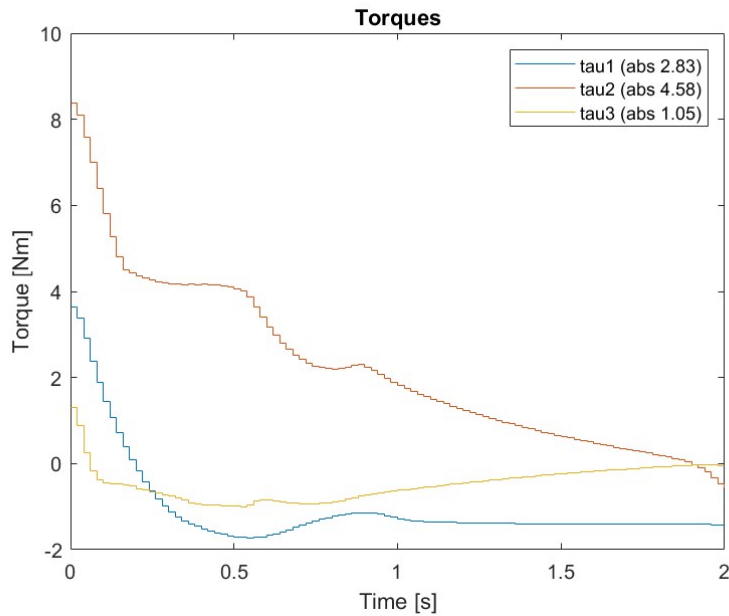


Figure C.22: Computed joint torques for shoulder yaw, shoulder pitch, and elbow pitch.

### C.3.8 Test B1.6

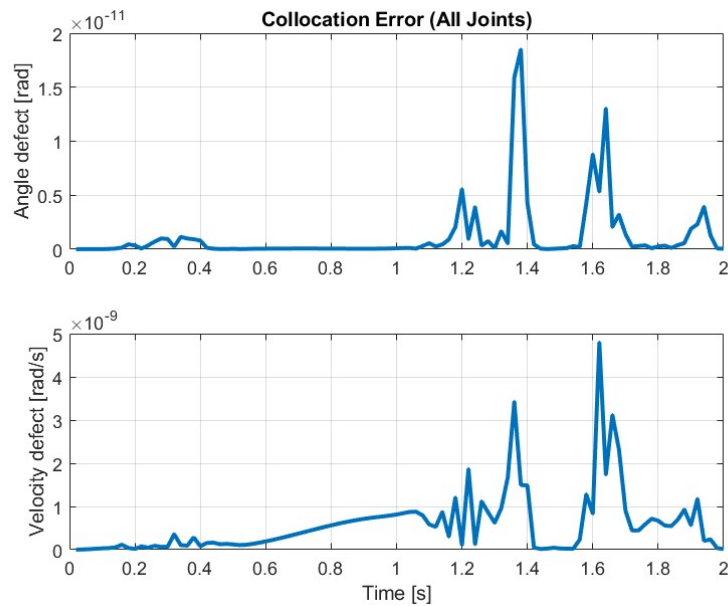


Figure C.23: Collocation error for the trajectory optimisation.

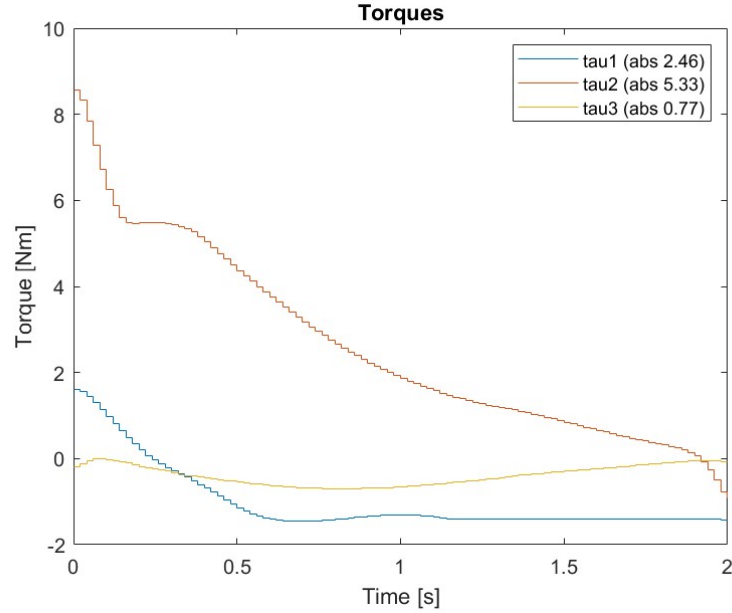


Figure C.24: Computed joint torques for shoulder yaw, shoulder pitch, and elbow pitch.

### C.3.9 Test B2.1

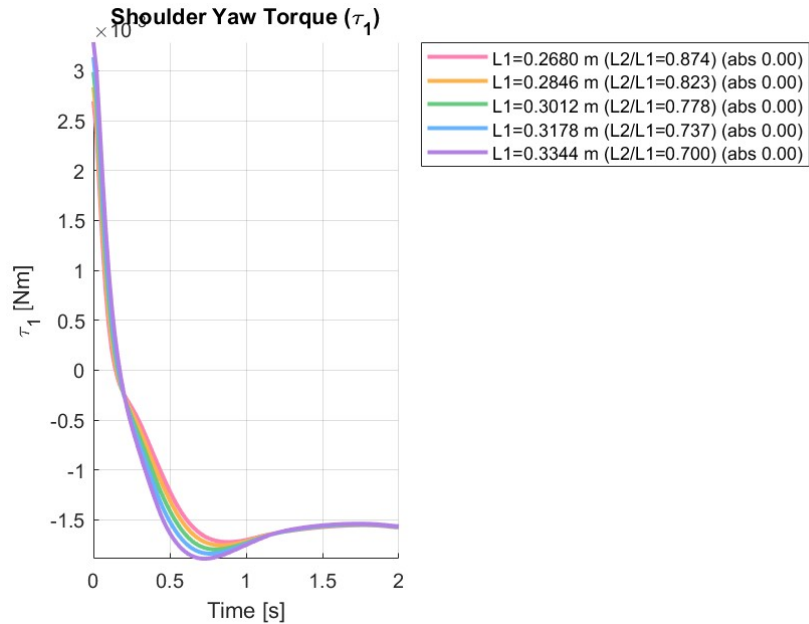


Figure C.25: Shoulder yaw torque profile for different brachial index values.

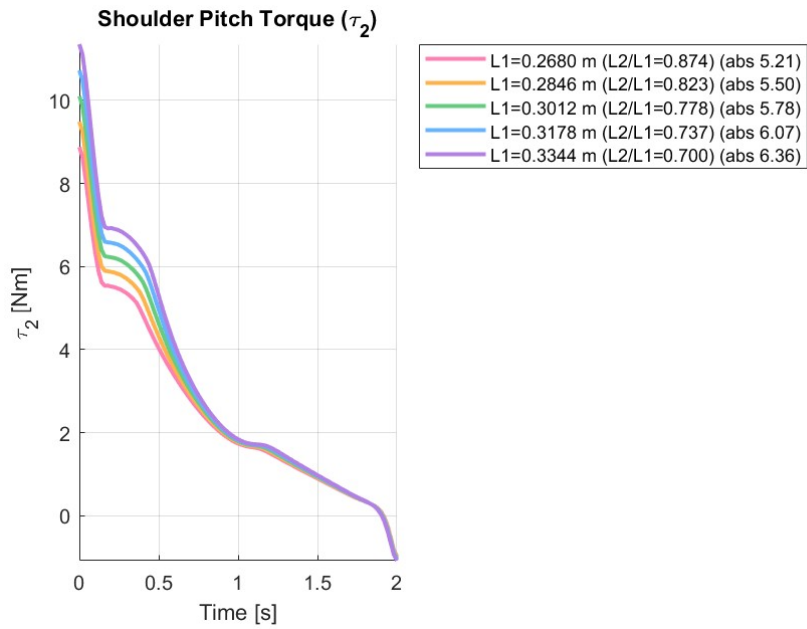


Figure C.26: Shoulder pitch torque profile for different brachial index values.

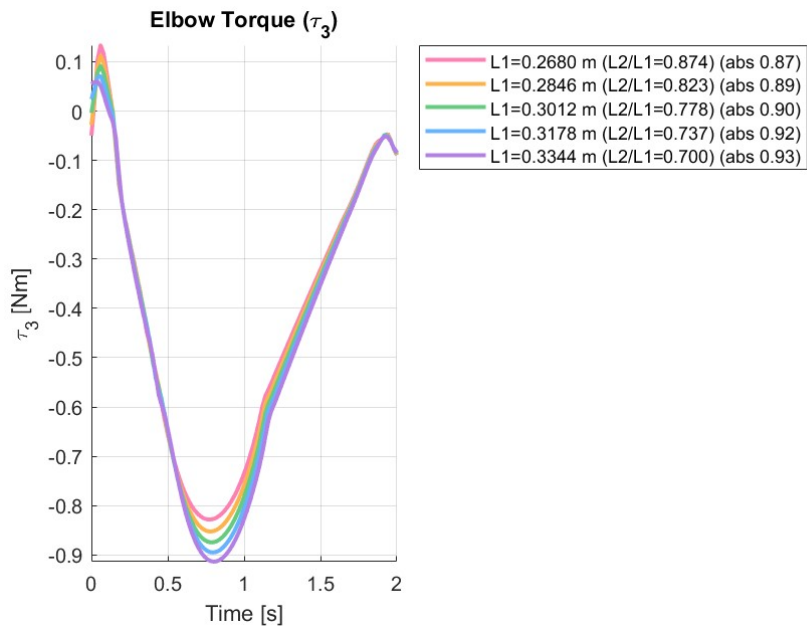


Figure C.27: Elbow pitch torque profile for different brachial index values.

## C.3.10 Test B2.2

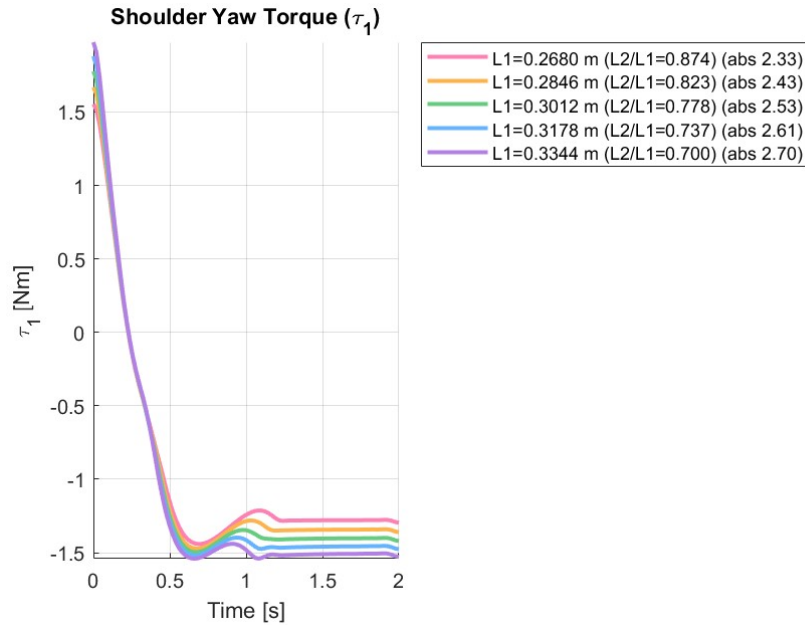


Figure C.28: Shoulder yaw torque profile for different brachial index values.

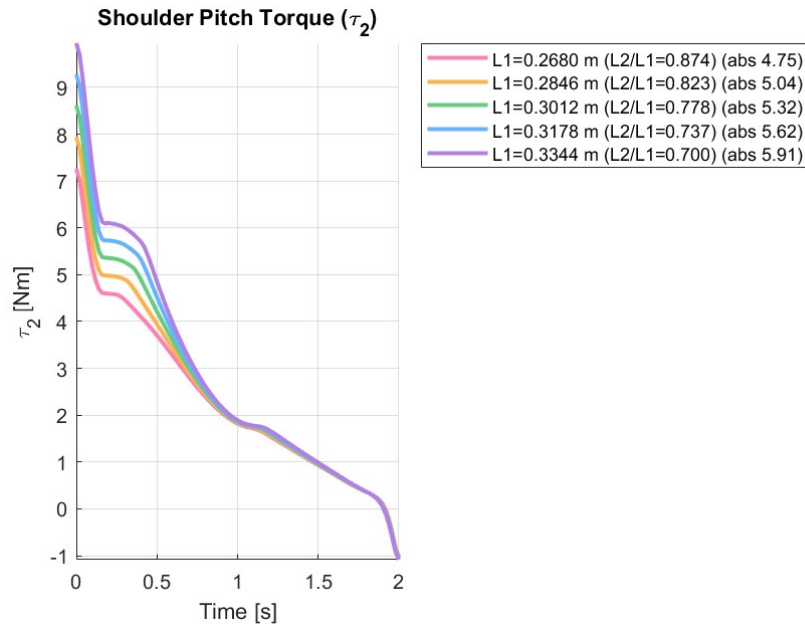


Figure C.29: Shoulder pitch torque profile for different brachial index values.

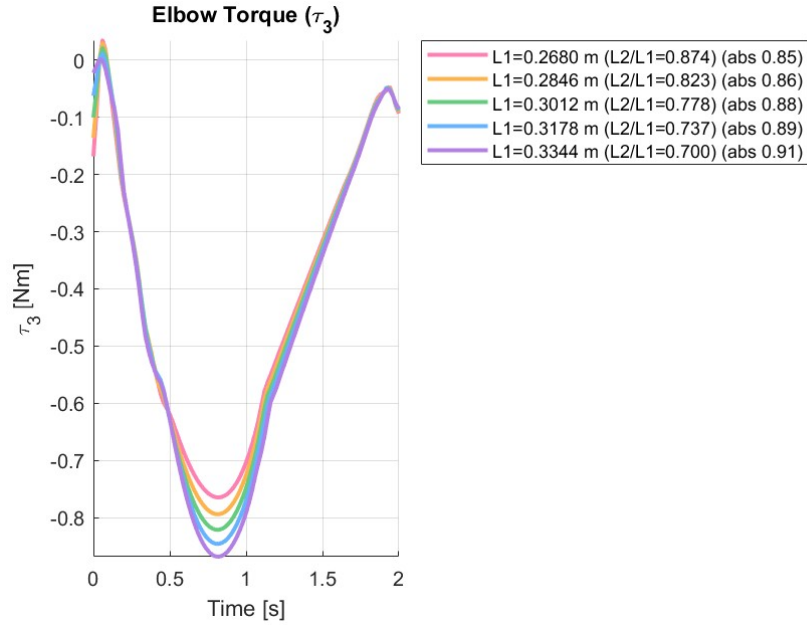


Figure C.30: Elbow pitch torque profile for different brachial index values.

### C.3.11 Test B3.1

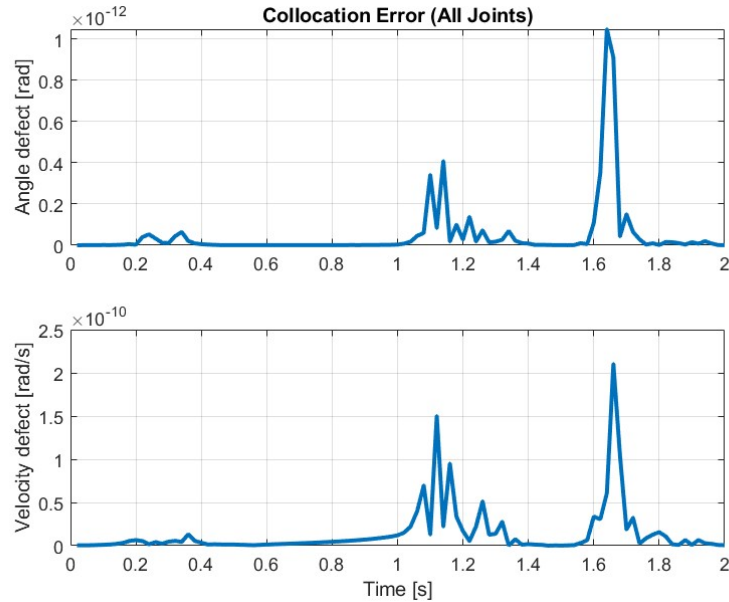


Figure C.31: Collocation error for the trajectory optimisation.

### C.3. STAGE 2 FIGURES

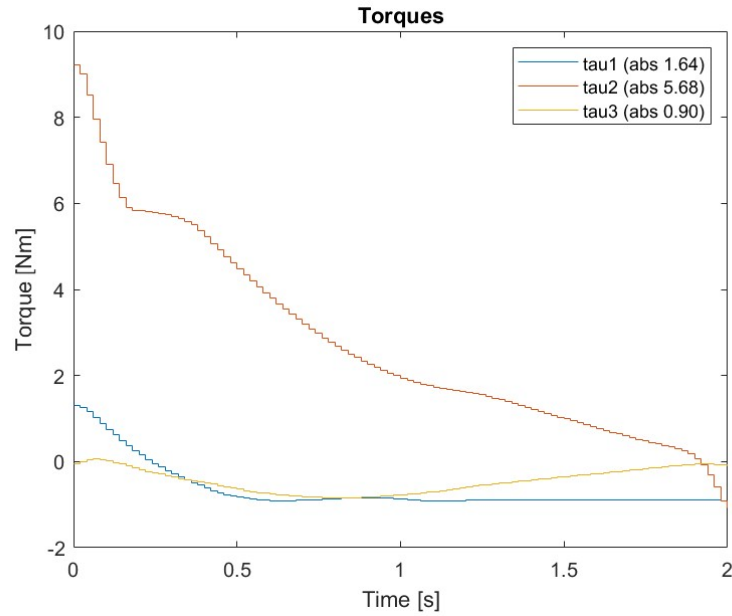


Figure C.32: Computed joint torques for shoulder yaw, shoulder pitch, and elbow pitch.

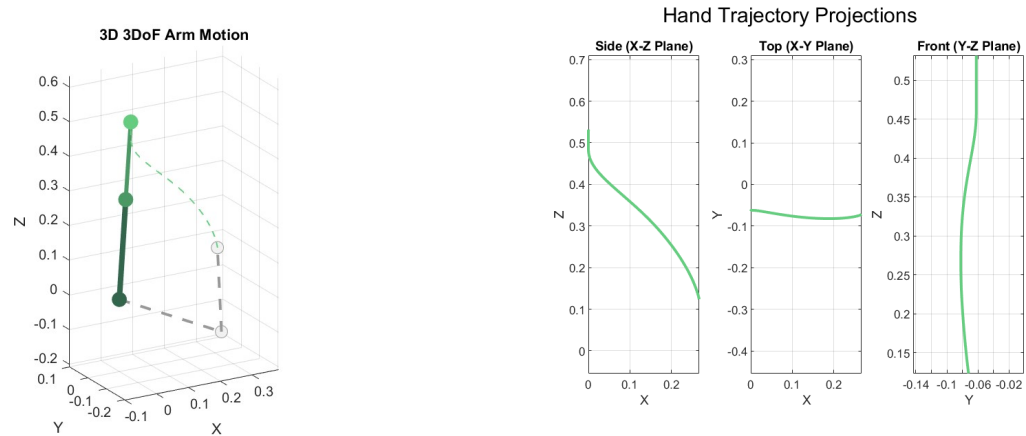


Figure C.33: Bar path during the lift.

Figure C.34: Hand trajectory projections in each plane.

## C.3.12 Test B3.2

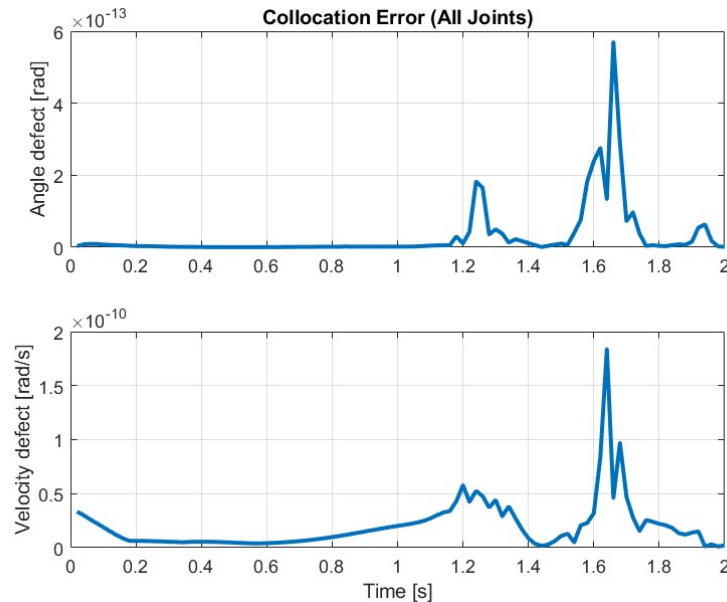


Figure C.35: Collocation error for the trajectory optimisation.

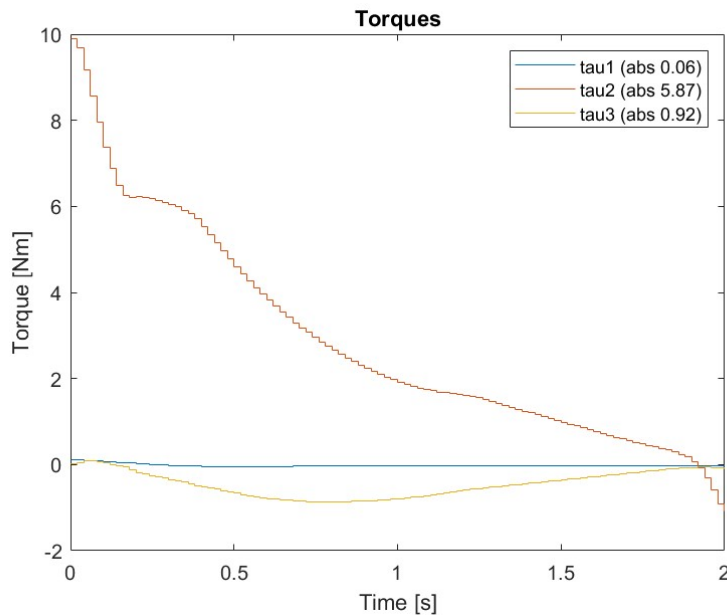


Figure C.36: Computed joint torques for shoulder yaw, shoulder pitch, and elbow pitch.

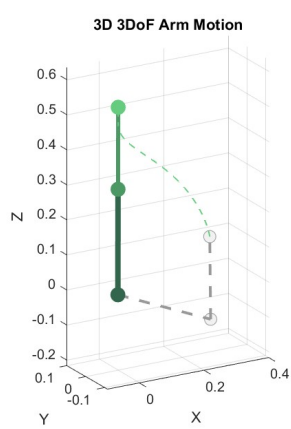


Figure C.37: Bar path during the lift.

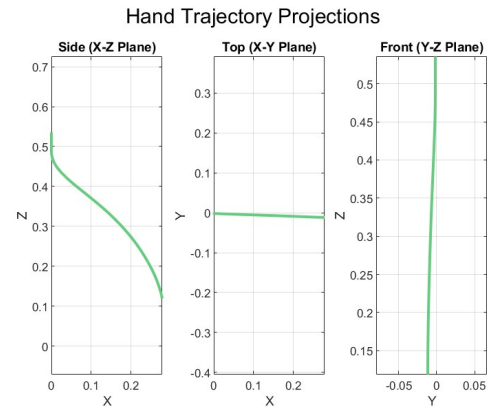


Figure C.38: Hand trajectory projections in each plane.

### C.3.13 Test B3.3

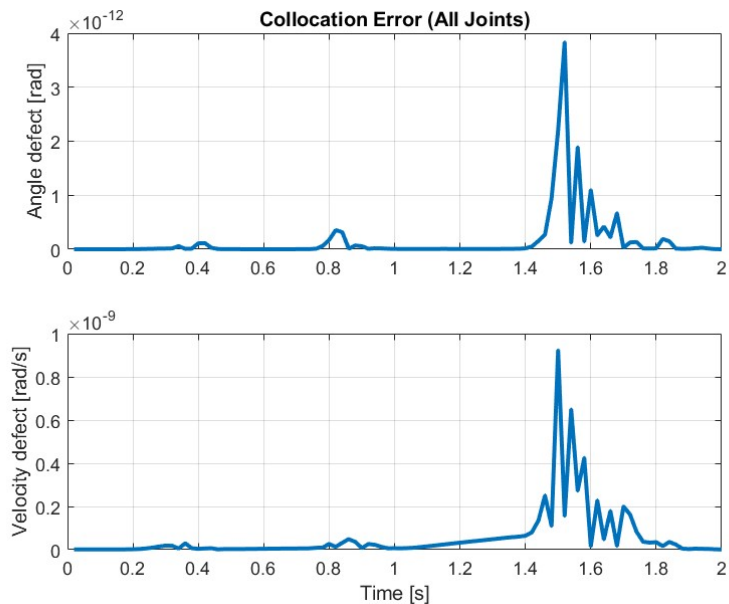


Figure C.39: Collocation error for the trajectory optimisation.

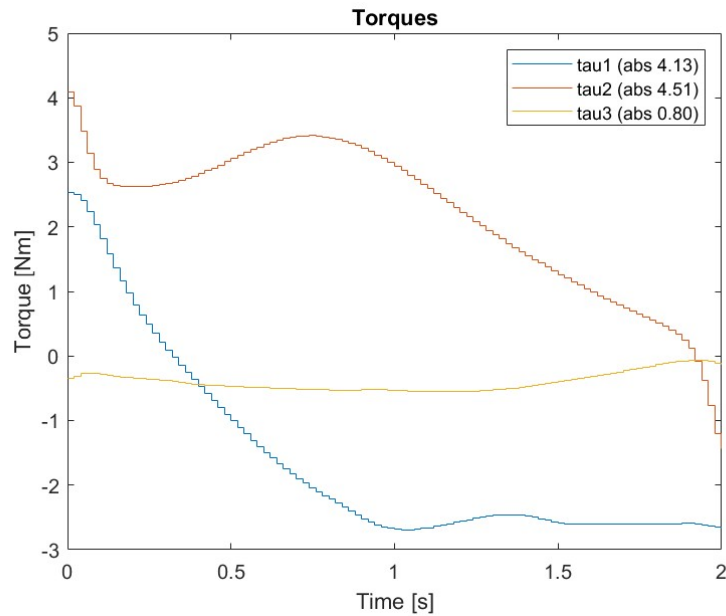


Figure C.40: Computed joint torques for shoulder yaw, shoulder pitch, and elbow pitch.

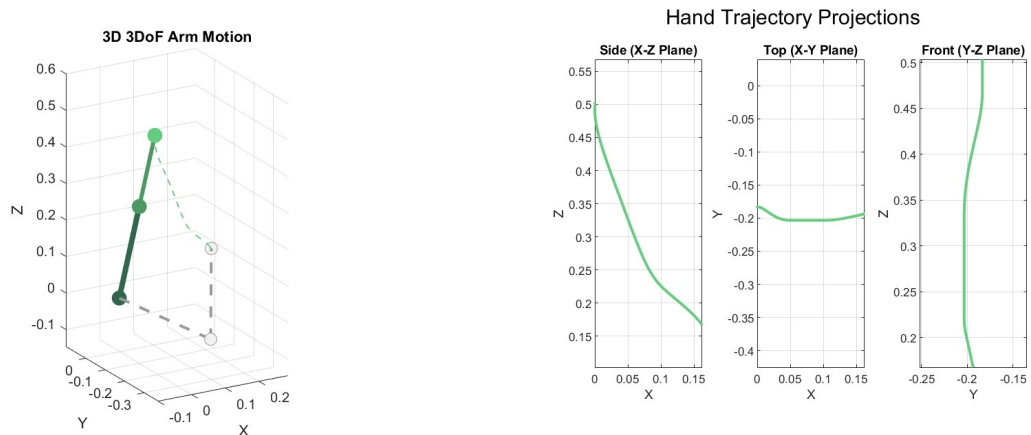


Figure C.41: Bar path during the lift.

Figure C.42: Hand trajectory projections in each plane.

## C.3.14 Test B4.1

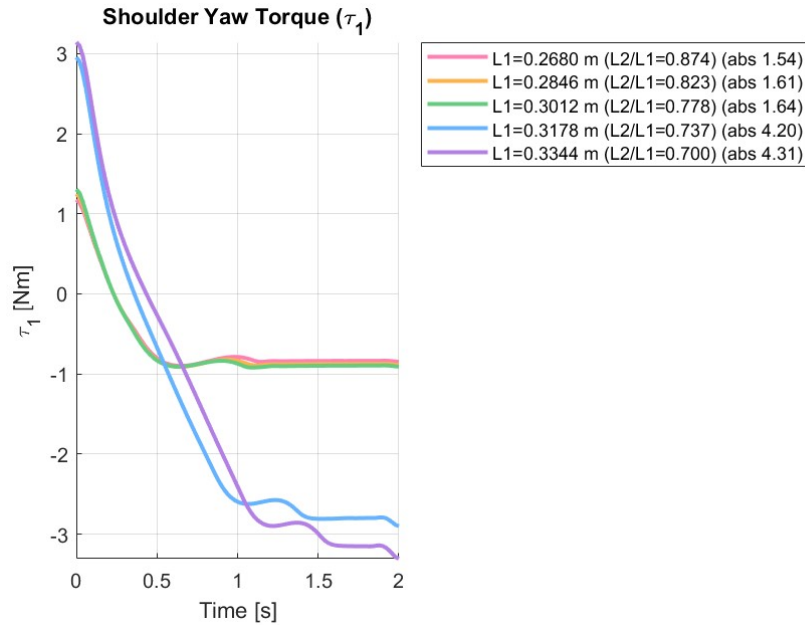


Figure C.43: Shoulder yaw torque profile for different brachial index values.

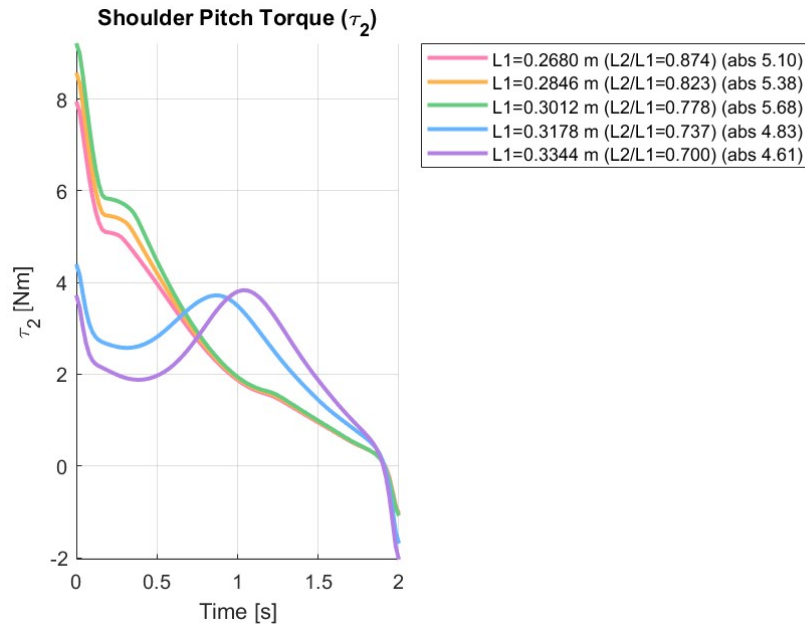


Figure C.44: Shoulder pitch torque profile for different brachial index values.

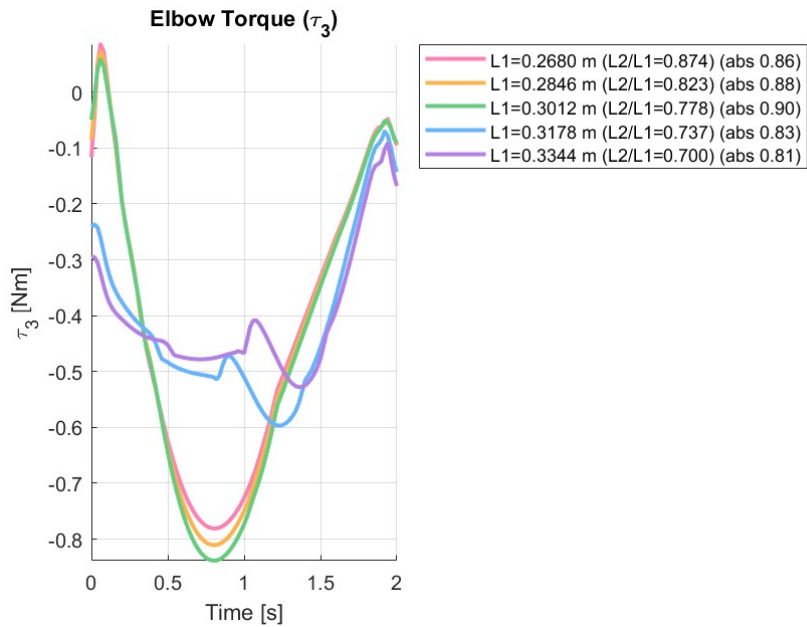


Figure C.45: Elbow pitch torque profile for different brachial index values.

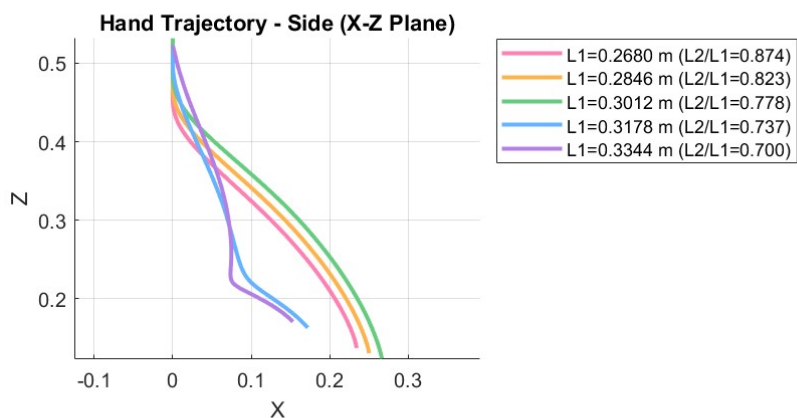


Figure C.46: Bar paths for different brachial index values.